UNIVERSITAT
POLITÈCNICA
DE VALÈNCIA

A new index for detecting and avoiding Type II singularities for the control of non-redundant parallel robots

PhD. Dissertation

Author: José Luis Pulloquinga Zapata

Advisors: Ángel Valera Fernández
Vicente Mata Amela

Valencia, April 2023

Fundings and Grants

This research was partially funded by Fondo Europeo de Desarrollo Regional (PID2021-125694OB-I00) and cofounded by Vicerrectorado de Investigación de la Universitat Politècnica de València (PAID-11-21).

The author received a scholarship from the grant Programa de Ayudas de Investigación y Desarrollo de la Universitat Politècnica de València (PAID-01-19).

The research stay of the author at University of Rome Tor Vergata was funded by the grant Programa de Ayudas para movilidad de estudiantes de doctorado de la Universitat Politècnica de València en 2022 from Spain and by Erasmus+ Student Mobility for Traineeship 2020.

Acknowledgements

La elaboración de esta tesis ha significado una etapa muy importante en mi vida. Llegar a la finalización de la tesis no hubiese sido posible sin la ayuda de varias personas a las quiero agradecer.

En primer lugar, quiero agradecer a Vicente Mata Amela y Ángel Valera Fernandez, directores de la presente Tesis Doctoral, por todo su apoyo profesional y personal. He disfrutado trabajar con ustedes estos cuatro años de doctorado, admiro mucho la forma calmada y proactiva con la que afrontan todos los problemas que se les presentan. Sin su apoyo no hubiese podido conseguir el contrato predoctoral que financio mis estudios de doctorado.

Quiero mostrar mi gratitud a los profesores Alvaro Page, Marina Vallés, Antonio Besa, Francisco José Valero, Miguel Díaz y Fernando Castillo, por compartir conmigo su valiosa experiencia profesional y personal. También quiero reconocer la enorme labor de María Amparo Guerrero, gracias a tu ayuda se pudieron completar todos los trámites y gestiones administrativas. No puede faltar mi agradecimiento a Fede por todas las veces que resolvió los problemas relacionados con los ordenadores del laboratorio de robótica.

I would like to thank all the members of the COMPMECH research group for making me feel part of the team during my stay in Bilbao. Thanks to professors Oscar Altuzarra, Victor Petuya and Alfonso Hernández for their professionalism, help and kindness. I also want to thank the research group LARM^2 for sharing their knowledge during my stay in Rome. All the work carried out during my research stays is an essential part of this thesis.

Quiero agradecer al profesor Iván Zambrano y a todo su equipo de trabajo de la Escuela Politécnica Nacional en Ecuador por permitirme colaborar en su proyecto de investigación para la rehabilitación robótica de miembro inferior. De manera especial quiero agradecerle al Profesor Patricio Cruz por toda su ayuda y por motivarme a iniciar mi carrera como investigador. Sus consejos me han servido mucho en la travesía del doctorado.

Gracias a mis compañeros de doctorado Pau y Rafa por toda su ayuda, por su amistad y por hacer del doctorado una experiencia divertida. Ambos son unos genios y sobre todo unas personas excepcionales. Gracias a Jesús, Javi y Daniel por permitirme colaborar en el desarrollo de sus trabajos de fin de curso. Todos ustedes han hecho que atesore cada momento en el laboratorio de robótica.

También quiero agradecer a todos mis amigos que de una forma u otra me han mantenido motivado durante estos años de doctorado. Gracias Nelly, William, Cesar, Anny, Sergio, Jhoel, Jesús, Eli, Pablo, Pedro, Cris, Lili, Nuria, Pableins, Lau y Alina, atesoraré con mucho cariño todos los momentos que compartimos. En especial quiero agradecer a mis amigos Sergio y Jhoel que durante mis primeros años en Valencia nunca me dejaron solo.

Por otro lado, quiero agradecer a mis padres Sonia y Sixto, y a mi hermana Mary, por apoyarme y ayudarme a seguir mis metas a pesar del dolor que les causa mi ausencia. Quiero agradecerles por toda su confianza y su amor infinito. Sonia y Sixto son unos padres estupendos, aunque quisiera no podría quejarme; siempre nos han impulsado, a mi hermana y a mí, a ser buenas personas y a perseguir nuestros sueños. Mary quiero agradecerte por el cuidado y amor que les has dado a mis padres en mi ausencia.

Quiero agradecerle a Maryna todo su amor, comprensión y apoyo infinito durante los momentos más difíciles del doctorado. Quiero que sepas que eres la mejor del mundo porque a pesar de todo el estrés, mis ausencias por el trabajo y los malos momentos que se generaron durante las estancias, siempre me has apoyado y creído en mí. Nunca dejes de brillar porque la vida es más bonita contigo.

Finalmente, quiero agradecer a todas las personas que saben que de una forma u otra participaron en esta aventura llamada doctorado.

Está tesis esta dedicada a:

A mis padres, Sonia y Sixto, quienes me dieron todo su amor y me enseñaron que con esfuerzo y dedicación todo es posible.

A mi hermanita, Mary, quien me motiva a ser mejor persona cada día.

A mi novia, Maryna, quien me da todo su amor, apoyo y comprensión.

A la persona que a pesar del miedo a fallar sigue intentando: yo.

Y, finalmente, a toda mi familia por su cariño incondicional.

Abstract

Parallel Robots (PR)s are mechanisms where the end-effector is linked to the base or fixed platform by at least two open kinematics chains. The closed-chain architecture provides PRs with high payload and high accuracy, making them suitable for a variety of applications including human-robot interaction. In contrast, the main drawback of non-redundant PR is the presence of singularities within the workspace (Type II singularities). In proximity to a Type II singularity, a non-redundant PR loses control over the movements of the end-effector. The loss of control represents a major risk for users, especially in robotic rehabilitation. In the last decades, PRs have become popular in lower-limb rehabilitation because of the increment in the number of people living with physical limitations mainly associated with the ageing of the world's population. Thus, this thesis is about the detection and avoidance of Type II singularities to ensure complete control of a non-redundant PR developed for knee rehabilitation and diagnosis, named 3U$\underline{\text{P}}$S+R$\underline{\text{P}}$U for its configuration.

In the literature, there are several indices for detecting and measuring the closeness to a singular configuration based on analytical and geometrical methods. However, some of these indices have no physical meaning and they are unable to identify the actuators responsible for the loss of control. The first contribution of this thesis is the development of two novel indices to detect and measure the proximity to a Type II singularity capable of identifying the pair of actuators responsible for the singularity. The two indices are the angles between the linear ($\Theta_{i,j}$) and the angular ($\Omega_{i,j}$) components of two i, j normalised Output Twist Screws (OTSs). A normalised OTS represents the direction of the motion imposed by an actuator to the end-effector, consider-

ing the other actuators being locked. A Type II singularity is detected when the angles $\Theta_{i,j} = \Omega_{i,j} = 0$ and its closeness is measured by the minimum $\Theta_{i,j}$ ($min\Theta$) and minimum $\Omega_{i,j}$ ($min\Omega$) for planar and spatial cases, respectively. The effectiveness of the indices $\Theta_{i,j}$ and $\Omega_{i,j}$ is evaluated from a theoretical and experimental perspective. The case studies are the 3U$\underline{P}$S+R$\underline{P}$U and a five bars mechanism. Along the same line, an experimental procedure is proposed for setting a proper limit of closeness to a Type II singularity. The limit of singularity closeness of an arbitrary index is set by the progressive approach of the PR to a Type II singularity and measuring the last controllable pose.

Subsequently, two novel deterministic algorithms for releasing and avoiding Type II singularities based on $min\Theta$ and $min\Omega$ are developed for non-redundant PRs. The $min\Theta$ and $min\Omega$ are used to identify the two actuators to move for release or prevent the PR from the singularity. These algorithms require an accurate measuring of the pose reached by the end-effector and the reference pose for the actuators. The release and avoidance algorithms are set by the sample time of the controller and the average working velocity of the robot.

The algorithm to release a PR from a singular configuration is successfully applied in a vision-based hybrid controller for the 3U$\underline{P}$S+R$\underline{P}$U PR. The hybrid controller uses a photogrammetry system to measure the pose of the robot because of the degeneration of the kinematic model in the vicinity of a singularity. The Type II singularity avoidance algorithm is applied to offline and online free-singularity trajectory planning for a five-bar mechanism and the 3U$\underline{P}$S+R$\underline{P}$U PR. These applications verify the low computation cost and the minimum deviation introduced in the original trajectory for both novel algorithms.

The direct implementation of a force/position controller in the 3U$\underline{P}$S+R$\underline{P}$U PR is unsafe because the patient could unintentionally drive the PR to a Type II singularity. Therefore, this thesis concludes by presenting a novel force/position controller complemented with the Type II singularity avoidance algorithm. The complemented controller is evaluated during patient-active exercises in a mannequin leg and an uninjured human limb. The results show that the novel combined controller keeps the 3U$\underline{P}$S+R$\underline{P}$U PR far from singular configurations with a minimum deviation on the original trajectory. Hence, this thesis enables the 3U$\underline{P}$S+R$\underline{P}$U PR for the safe rehabilitation of injured lower limbs.

Resumen

Los robots paralelos (PR por sus siglas en ingles) son mecanismos donde el efector final está unido a la base o plataforma fija, mediante al menos dos cadenas cinemáticas abiertas. La arquitectura de cadenas cerradas dota a los PR de una gran capacidad de carga y alta precisión, lo que los hace adecuados para diversas aplicaciones, entre ellas la interacción persona-robot. En cambio, el principal inconveniente de un PR no redundante es la presencia de singularidades dentro del espacio de trabajo (singularidades Tipo II). En las proximidades de una singularidad Tipo II, un PR no redundante pierde el control sobre los movimientos del efector final. La pérdida de control representa un riesgo importante para los usuarios, especialmente en rehabilitación robótica. En las últimas décadas, los PR se han popularizado en la rehabilitación de miembros inferiores debido al aumento del número de personas que viven con limitaciones físicas, asociadas principalmente al envejecimiento de la población mundial. Así, esta tesis trata sobre la detección y evasión de singularidades de Tipo II para asegurar total control de un PR no redundante desarrollado para la rehabilitación y diagnóstico de rodilla, denominado 3U<u>P</u>S+R<u>P</u>U por su arquitectura.

En la literatura, existen varios índices para detectar y medir la cercanía a una singularidad basados en métodos analíticos y geométricos. Sin embargo, algunos de estos índices carecen de significado físico y son incapaces de identificar los actuadores responsables de la pérdida de control. La primera contribución de esta tesis es el desarrollo de dos novedosos índices para detectar y medir la proximidad a una singularidad de Tipo II, capaces de identificar el par de actuadores responsables de la singularidad. Los dos índices son los ángulos en-

tre los componentes lineal ($\Theta_{i,j}$) y angular ($\Omega_{i,j}$) de dos Twist Screw de Salida (OTS por sus siglas en ingles) normalizados i, j. Un OTS normalizado representa la dirección del movimiento impuesto por un actuador al efector final, considerando que los demás actuadores están bloqueados. Una singularidad Tipo II es detectada cuando $\Theta_{i,j} = \Omega_{i,j} = 0$ y su proximidad se mide mediante los minimos ángulos $\Theta_{i,j}$ ($min\Theta$) y $\Omega_{i,j}$ ($min\Omega$) para los casos plano y espacial, respectivamente. La eficacia de los índices $\Theta_{i,j}$ y $\Omega_{i,j}$ se evalua de forma teórica y experimental. Los casos de estudio son el robot 3U$\underline{P}$S+R$\underline{P}$U y un mecanismo de cinco barras. En la misma línea, se propone un procedimiento experimental para el adecuado establecimiento del límite de cercanía a una singularidad de Tipo II. El límite de proximidad a la singularidad de un índice arbitrario se establece mediante la aproximación progresiva del PR a una singularidad y la medición de la última posición controlable.

Posteriormente, se desarrollan dos nuevos algoritmos deterministas para liberar y evitar una singularidad de Tipo II basados en $min\Theta$ y $min\Omega$ para PR no redundantes. $min\Theta$ y $min\Omega$ se utilizan para identificar los dos actuadores a mover para liberar o evitar el PR de una singularidad. Estos algoritmos requieren una medición precisa de la pose alcanzada por el efector final y la pose de referencia para los actuadores. Los algoritmos de liberación y evasión se establecen mediante el tiempo de muestreo del controlador y la velocidad de trabajo media del robot. El algoritmo para liberar un PR de una configuración singular se aplica con éxito en un controlador híbrido basado en visión artificial para el PR 3U$\underline{P}$S+R$\underline{P}$U. El controlador híbrido utiliza un sistema de fotogrametría para medir la pose del robot debido a la degeneración del modelo cinemático en las proximidades de una singularidad. El algoritmo de evasión de singularidades Tipo II se aplica a la planificación offline y online de trayectorias no singulares para un mecanismo de cinco barras y el PR 3U$\underline{P}$S+R$\underline{P}$U. Estas aplicaciones verifican el bajo coste computacional y la mínima desviación introducida por los nuevos algoritmos en la trayectoria original.

La implementación directa de un controlador de fuerza/posición en el PR 3U$\underline{P}$S+R$\underline{P}$U es insegura porque el paciente podría llevar involuntariamente al PR a una singularidad. Por lo tanto, esta tesis concluye presentando un novedoso controlador de fuerza/posición complementado con el algoritmo de evitación de singularidades de Tipo II. El nuevo controlador se evalúa durante rehabilitación activa de una pierna de maniquí y una pierna humana no lesionada. Los resultados muestran que el nuevo controlador combinado mantiene el PR 3U$\underline{P}$S+R$\underline{P}$U lejos de configuraciones singulares con una desviación mínima de la trayectoria original. Por lo tanto, esta tesis habilita el 3U$\underline{P}$S+R$\underline{P}$U PR para la rehabilitación segura de miembros inferiores lesionados.

Resum

Els robots paral·lels (PR per les seues sigles en engonals) són mecanismes on l'efector final està unit a la base o plataforma fixa, mitjançant almenys dues cadenes cinemàtiques obertes. L'arquitectura de cadenes tancades dota als PR d'una gran capacitat de càrrega i alta precisió, la qual cosa els fa adequats per a diverses aplicacions, entre elles la interacció persona-robot. En canvi, el principal inconvenient d'un PR no redundant és la presència de singularitats dins de l'espai de treball (singularitats Tipus II). En les proximitats d'una singularitat Tipus II, un PR no redundant perd el control sobre els moviments de l'efector final. La pèrdua de control representa un risc important per als usuaris, especialment en rehabilitació robòtica. En les últimes dècades, els PR s'han popularitzat en la rehabilitació de membres inferiors a causa de l'augment del nombre de persones que viuen amb limitacions físiques, associades principalment a l'envelliment de la població mundial. Així, aquesta tesi tracta sobre la detecció i evació de singularitats de Tipus II per a assegurar total control d'un PR no redundant desenvolupat per a la rehabilitació i diagnòstic de genoll, denominat 3U$\underline{\text{P}}$S+R$\underline{\text{P}}$U per la seua arquitectura.

En la literatura, existeixen diversos índexs per a detectar i mesurar la proximitat a una singularitat basats en mètodes analítics i geomètrics. No obstant això, alguns d'aquests índexs manquen de significat físic i són incapaços d'identificar els actuadors responsables de la pèrdua de control. La primera contribució d'aquesta tesi és el desenvolupament de dos nous índexs per a detectar i mesurar la proximitat a una singularitat de Tipus II, capaços d'identificar el parell d'actuadors responsables de la singularitat. Els dos índexs són els angles entre els components lineal ($\Theta_{i,j}$) i angular ($\Omega_{i,j}$) de dues Twist Screw

d'Eixida (OTS per les seues sigles en engonals) normalitzats i, j. Un OTS normalitzat representa la direcció del moviment imposat per un actuador a l'efector final, considerant que els altres actuadors estan bloquejats. Una singularitat Tipus II és detectada quan $\Theta_{i,j} = \Omega_{i,j} = 0$ i la seua proximitat es mesura mitjançant els minimos angles $\Theta_{i,j}$ ($min\Theta$) i $\Omega_{i,j}$ ($min\Omega$) per als casos pla i espacial, respectivament. L'eficàcia dels índexs $\Theta_{i,j}$ i $\Omega_{i,j}$ es evalua de manera teòrica i experimental. Els casos d'estudi són el robot 3U$\underline{\text{P}}$S+R$\underline{\text{P}}$U i un mecanisme de cinc barres. En la mateixa línia, es proposa un procediment experimental per a l'adequat establiment del límit de proximitat a una singularitat de Tipus II. El límit de proximitat a la singularitat d'un índex arbitrari s'estableix mitjançant l'aproximació progressiva del PR a una singularitat i el mesurament de l'última posició controlable.

Posteriorment, es desenvolupen dos nous algorismes deterministes per a alliberar i evadir una singularitat de Tipus II basats en $min\Theta$ i $min\Omega$ per a PR no redundants. $min\Theta$ i $min\Omega$ s'utilitzen per a identificar els dos actuadors a moure per a alliberar o evadir el PR d'una singularitat. Aquests algorismes requereixen un mesurament precís de la posa aconseguida per l'efector final i la posa de referència per als actuadors. Els algorismes d'alliberament i evasió s'estableixen mitjançant el temps de mostreig del controlador i la velocitat de treball mitjana del robot. L'algorisme per a alliberar un PR d'una configuració singular s'aplica amb èxit en un controlador híbrid basat en visió artificial per al PR 3U$\underline{\text{P}}$S+R$\underline{\text{P}}$U. El controlador híbrid utilitza un sistema de fotogrametria per a mesurar la posa del robot a causa de la degeneració del model cinemàtic en les proximitats d'una singularitat. L'algorisme d'evació de singularitats Tipus II s'aplica a la planificació offline i en línia de trajectòries no singulars per a un mecanisme de cinc barres i el PR 3U$\underline{\text{P}}$S+R$\underline{\text{P}}$U. Aquestes aplicacions verifiquen el baix cost computacional i la mínima desviació introduïda pels nous algorismes en la trajectòria original.

La implementació directa d'un controlador de força/posició en el PR 3U$\underline{\text{P}}$S+R$\underline{\text{P}}$U és insegura perquè el pacient podria portar involuntàriament al PR a una singularitat. Per tant, aquesta tesi conclou presentant un nou controlador de força/posició complementat amb l'algorisme d'evació de singularitats de Tipus II. El nou controlador s'avalua durant la rehabilitació activa d'una cama de maniquí i una cama humana no lesionada. Els resultats mostren que el nou controlador combinat manté el PR 3U$\underline{\text{P}}$S+R$\underline{\text{P}}$U lluny de configuracions singulars amb una desviació mínima de la trajectòria original. Per tant, aquesta tesi habilita el 3U$\underline{\text{P}}$S+R$\underline{\text{P}}$U PR per a la rehabilitació segura dels membres inferiors lesionats.

Contents

List of Figures

List of Tables

Acronyms

3DTS 3D Tracking System.

ACP Assembly change point.

AVR Absolute Variation Rate.

CMO Constrained Multi-Objective.

CT Computed-Torque.

DOF Degree of freedom.

FKP Forward Kinematic Problem.

GTW Good-Transmission Workspace.

IDP Inverse Dynamic Problem.

IHME Institute for Health Metrics and Evaluation.

IKP Inverse Kinematic Problem.

ISA Instantaneous Screw Axis.

ITI Input Transmission Index.

LAB Linear Algebra-Based.

LCoI Local Constraint Index.

LTI Local Transmission Index.

MAE Mean Absolute Error.

MAPE Mean Absolute Percentage Error.

OTI Output Transmission Index.

OTS Output Twist Screw.

PD Proportional-Derivative.

PD+G Proportional-Derivative controller with Gravitational compensation.

PI Proportional-Integral.

PID Proportional-Integral-Derivative.

PKM Parallel Kinematic Machine.

PR Parallel Robot.

ROS2 Robot Operating System 2.

SRA Singularity Release Algorithm.

TI Transmission Index.

TWS Transmission Wrench Screw.

WHO World Health Organization.

Nomenclature

$A(s)$	Admittance mechanical model in Laplace variable s.
$\|a\|$	Absolute value of the scalar a.
$\vec{\Phi}$	Input-output constraint equations of a parallel robot.
$\vec{\Phi}_c$	Constraint equations of a parallel robot.
θ_i	Characteristics angle between $\$_{n_i}$ and $\$_{T_i}$.
κ	Condition number of a matrix.
$\vec{u}$	Control actions generated by a controller.
D	Square matrix that represent the damping of the $I(s)$.
$\dot{q}$	Time derivative of the variable q.
F	Number of degrees of freedom of the end-effector.
$\|\|A\|\|$	Determinant of the matrix A.
$\vec{a} \cdot \vec{b}$	Dot or scalar product between vectors $\vec{a}$ and $\vec{b}$.
e_{pin}	Boolean variable to control the activation of the singularity release algorithm.
$\vec{F}_c$	Forces and moments measured on the DOFs of the end-effector.
$\vec{F}_{ind_i}$	Forces transmitted from the actuator i to the mobile platform.

$\vec{F}_r$	Reference forces and moments for the DOFs of the end-effector.
GCI	Global condition index.
$I(s)$	Impedance mechanical model in Laplace variable s.
λ_i	Input transmission index.
J	Jacobian matrix for the forward kinematic problem.
J_D	Forward Jacobian matrix.
J_I	Inverse Jacobian matrix.
J_O	Overall Jacobian matrix.
K	Square matrix that represent the stiffness of the $I(s)$.
γ	Local transmission index.
M	Square matrix that represent the mass of the $I(s)$.
w	Manipulability index of a robot.
$min\Omega$	Angle $\Omega_{i,j}$ with the minimum value.
$min\Theta$	Angle $\Theta_{i,j}$ with the minimum value.
$\hat{\$}$	Normalised screw.
$\|\vec{a}\|$	Norm of the vector $\vec{a}$.
$\vec{\mu}$	Unit vector.
$\vec{\mu}^*$	Dual part of a normalised screw.
n_T	Number of samples taken from a trajectory.
$\$_{n_i}$	Screw normal to all transmission wrench screws except to i-th.
$\Omega_{i,j}$	Angle between the angular parts of the i and j normalised output twist screws.
η_i	Output transmission index.
$\$_{O_i}$	Output twist screw from the limb i.
∂q	Partial derivative of the variable q.
$P(s)$	An arbitrary pose control law in Laplace variable s.

q_{ij}	Generalised coordinate for the j revolute or prismatic joint in the limb i.
$\vec{q}_{ind}$	Subset of active joints or actuators of a parallel robot.
$\vec{q}_{ind_c}$	Actual location or orientation of the actuators of a parallel robot.
$\vec{q}_{ind_r}$	Reference location or orientation of the actuators of a parallel robot.
$\circ$	Reciprocal product.
${}^f\boldsymbol{R}_m$	Rotation matrix between the f and m reference system.
$\Theta_{i,j}$	Angle between the linear parts of the i and j normalised output twist screws.
$\vec{T}_{ind_i}$	Moments transmitted by the actuator i in a specific point of the mobile platform.
$\$_m$	Twist screw for the linear and angular velocity of the mobile platform.
t_T	Total time for a trajectory.
$\$_{T_i}$	Transmission wrench screw from the limb i.
$\vec{u}$	Control signals for the actuators.
$\vec{u}_F$	Control signals generated by a force controller.
$\vec{u}_X$	Control signals generated by a pose controller.
$\vec{\nu}_m$	Linear velocity in an arbitrary point of the mobile platform.
$\overrightarrow{V\Omega}$	Vector that allocate all possible angles $\Omega_{i,j}$.
$\overrightarrow{V\Theta}$	Vector that allocate all possible angles $\Theta_{i,j}$.
$\vec{\omega}_m$	Angular velocity of the mobile platform.
$W(s)$	An arbitrary force control law in Laplace variable s.
$\vec{X}$	Location and orientation of a parallel robot.
$\vec{X}_c$	Actual location and orientation of a parallel robot.
$\vec{X}_r$	Reference location and orientation of a parallel robot.

Chapter 1

Introduction

This chapter presents the motivation for this thesis and the background of robotic rehabilitation based on parallel manipulators. Next, the objectives and the main contributions of this research are presented. Finally, the structure of the thesis provides a brief description of the contents of each chapter.

1.1 Robotic rehabilitation for lower limb

The ageing of the world's population and non-communicable diseases increase the number of people living with physical, mental or social limitations. World Health Organization (WHO) estimates that 1.3 billion people (16 % of the global population) experience a significant physical or mental impairment that difficult daily activities (WHO, 2022).

Stroke is the most common cause of disability or impairment in the world. In 2019, 86 million survivors of stroke needed rehabilitation (Cieza et al., 2020). According to Institute for Health Metrics and Evaluation (IHME), 14 million survivors of stroke who require rehabilitation live in the European region, of which 460 000 people are from Spain (IHME, 2021). People that survive a stroke, osteoarthritis or spinal cord injuries require physical rehabilitation to treat the impairment in the mobility of the upper or lower limb (Van der Loos et al., 2016). In addition, there is growing evidence that many survivors of COVID-19 will live with various sequelae that require physical rehabilitation (Iqbal et al., 2021; Cieza et al., 2020).

Physical rehabilitation performs repetitive movements on the injured or impaired limb in order to recover the mobility of the patient (Xie, 2016; Díaz et al., 2011). Although physical rehabilitation helps people to treat their disabilities, this process has several limitations (Xie, 2016; Van der Loos et al., 2016). The main limitations are:

- Time-consuming procedure, because the patient and the physiotherapist have to travel to medical centres or rehabilitation clinics for extended periods of time.
- The repetitive movements could be tedious and uninteresting for patients. If the patient becomes demotivated, the voluntary effort exerted by the patient during the rehabilitation declines and so does the velocity of the rehabilitation recovery.
- Physiotherapists only attend to a limited number of patients due to their hands-on assistance during rehabilitation.
- The evaluation of the progress of the patient is subjective because depends on the experience of the physiotherapist.

To overcome the limitations of conventional rehabilitation, robots have been introduced to achieve effective and cost-efficient physical therapy. In 1970, industrial robots were adapted to introduce early prototypes of rehabilitation robots for lower limb therapy (Kolpashchikov et al., 2022; Van der Loos et al., 2016). In 1976, a master/slave pneumatically actuated wearable robot for lower limb therapy of paraplegic patients is introduced (Rabischong and Bel, 1976). The movements of the robot were remotely controlled by a therapist worn with a master sensor suit. In 2000, a driven gait orthosis was combined with a treadmill for the rehabilitation of the lower limb of paraplegic patients (Colombo et al., 2000). It was the first prototype of the commercial rehabilitation system Lokomat. In the same year, a gait trainer without a treadmill was developed to simulate stance and swing movements (Hesse and Uhlenbrock, 2000). The gait trainer positioned a harness-secured patient on two foot plates while the ropes of the harness controlled the vertical and lateral movements of the centre of mass.

Over the past two decades, several robotic systems for lower limb rehabilitation have been developed. Figure 1.1 shows some robotic systems developed for lower limb rehabilitation. AAFO (Blaya and Herr, 2004), LokoHelp (Freivogel et al., 2008), ALEX (Banala et al., 2009), KAFO (Sawicki and Ferris, 2009) and LOPES (Tufekciler et al., 2011) are some examples of treadmill gait training. For the foot plate-based robotic system, some developments are Haptic

Walker (Schmidt et al., 2005), GM5 (Yano et al., 2010) and LLRR (Wu et al., 2016). These robotic systems apply therapy over long periods of time without tiring reducing the workload of physiotherapists. The sensors of the robotic system provide data for an effective evaluation of the recovery status of patients. However, the previous robotic systems are voluminous with high energy consumption, requiring large spaces in medical centres for implementation. In addition, the rehabilitation of a specific human joint in the lower limb is unfeasible.

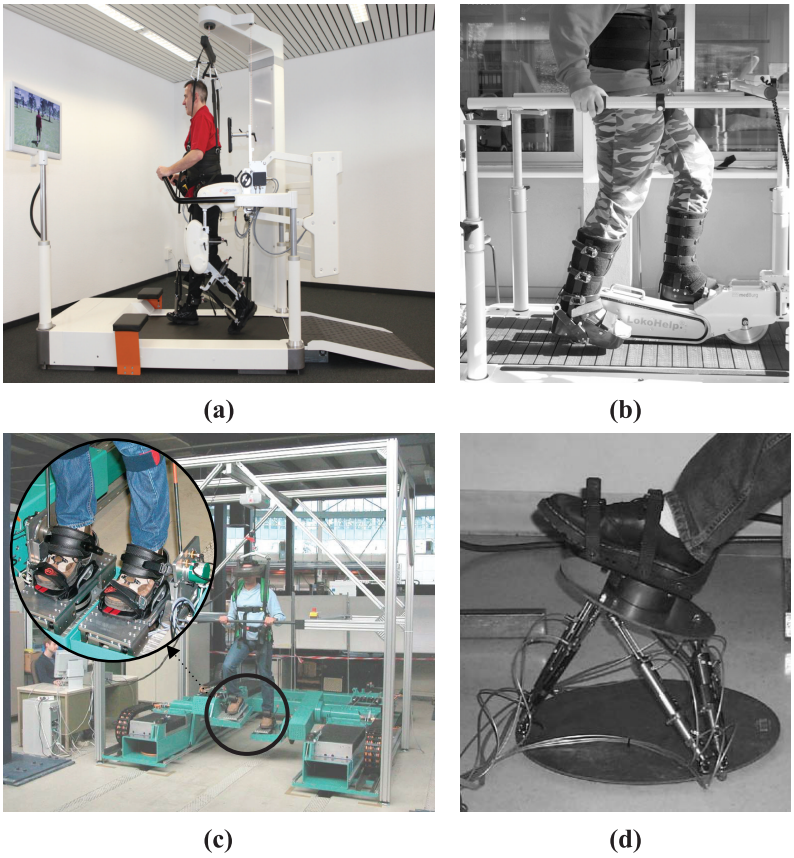

Figure 1.1: Robotic systems for lower limb rehabilitation: (a) Lokomat (Díaz et al., 2011) (b) LokoHelp (Freivogel et al., 2008) (c) Haptic Walker (Schmidt et al., 2005) (d) Rutgers Ankle (Girone et al., 2001).

In 2001, the Rutgers Ankle was developed as the first robotic mechanism to exercise the human ankle without walking (Girone et al., 2001). The Rutgers

Ankle combines a Stewart platform with virtual reality to perform patient-active exercises. The Stewart platform is a closed kinematic chain mechanism with six degrees of freedom (DOFs) controlled by double-acting pneumatic cylinders. Several ankle rehabilitation systems were developed based on closed-chain mechanisms, such as (Saglia et al., 2009, 2013; McDaid et al., 2013; Vallés et al., 2017; Dong et al., 2021). The closed-chain mechanisms were extended to knee rehabilitation in (Rastegarpanah et al., 2016) and (Aginaga et al., 2018). The closed-chain mechanisms or Parallel Robots (PRs) increase their application in robotic rehabilitation because PRs are compact mechanisms that offer high stiffness with high accuracy and excellent load capacity (Taghirad, 2013).

Motion rehabilitation therapies can be divided into patient-passive and patient-active exercises. In the patient-passive exercise, the PR follows a reference trajectory defined by the therapist without considering the patient interaction, i.e., the robot requires a trajectory controller (Saglia et al., 2013). In a patient-active exercise, a PR modifies the motion defined by the therapist according to the forces exerted by the patient (Meng et al., 2015). The control strategies applied to patient-active exercises are admittance control (Kim et al., 2019), hybrid force/position control (Ju et al., 2005), bio-signals based control (Fan and Yin, 2013), and adaptive control (Wu et al., 2018). The admittance control allows a dynamic relationship between the PR position and the patient effort making it one of the most appropriate for lower limb rehabilitation (Meng et al., 2015).

The main advantages of the rehabilitation based on PRs are:

- Improvement of the productivity of the rehabilitation sessions because of the high repeatability of the PRs and the reduction of physical fatigue of the physiotherapist.
- Engaging rehabilitation exercises because the virtual reality could add visual elements to the therapy.
- Several patients could be rehabilitated simultaneously under the supervision of one physiotherapist.
- Objective evaluation of the progress of the patient based on quantitative data provided by the sensors on the PR.

However, PRs present drawbacks regarding the size of their workspace (Taghirad, 2013; Liu and Wang, 2014), and the presence of singularities within the workspace (Altuzarra et al., 2004). The reduced workspace of a PR is coped

by kinematic optimisation of the robot (Wang et al., 2010; Russo et al., 2018; Valero et al., 2020). In a singular configuration within the workspace of a PR, the end-effector could move despite the actuators being locked. Under these conditions, if an external force is applied to the end-effector or mobile platform, the control over the motion of the end-effector is lost. In lower limb rehabilitation, the PR interacts with the leg of the patient. Thus, a PR must ensure complete control over the end-effector despite the presence of singularities during the rehabilitation process.

The singularities within the workspace are faced by adding redundant actuators (Wu et al., 2013; Saafi et al., 2015; Wen et al., 2019), enlargement of the workspace (Arakelian et al., 2008), trajectory planning (Dash et al., 2005; Shiller, 2015; Corinaldi et al., 2018) and control algorithms for singularity crossing or avoidance (Briot and Arakelian, 2008; Agarwal et al., 2016). These methods are detailed in Section 2.6.

Adding actuators involves major changes in the architecture of the PR that increase the complexity of the kinematic modelling. In addition, this option requires methods for online singularities avoidance using redundant actuators that increase the complexity of the control law (Nouri Rahmat Abadi and Carretero, 2022).

The methods for trajectory planning in non-redundant PRs modify an original trajectory to achieve a non-singular one. The controllers for singularity avoidance require online modification of the original trajectory. In patient-passive rehabilitation, significant changes over the trajectory are risky because it is defined by a therapist for a patient with physical impairment. Furthermore, several trajectory planning algorithms require considerable effort to select proper parameters to achieve an accurate singularity-free trajectory (Khoukhi et al., 2009). Analogously, singularity crossing/avoidance controllers are complex to tune for accurate trajectory tracking with effective singularity crossing/avoidance.

The Universitat Politècnica de València has designed, build, and optimised a 4-DOF PR for knee rehabilitation (Vallés et al., 2018; Valero et al., 2020). The 4-DOF PR for knee rehabilitation is named 3U$\underline{\text{P}}$S+R$\underline{\text{P}}$U due to its mechanical architecture. Even after optimizing the workspace of the 3U$\underline{\text{P}}$S+R$\underline{\text{P}}$U, a small percentage of singularities still remains inside the workspace of the robot (Araujo-Gómez et al., 2019). Therefore, PRs applied to robotic rehabilitation requires measuring with accuracy the closeness to a singular configuration within the workspace to prevent reaching it during a rehabilitation procedure.

1.2 Motivation and objectives of the thesis

The singular configurations within the workspace of a non-redundant PRs have been classified and analysed from different methods (Briot and Khalil, 2015). Gosselin and Angeles (1990) define a Forward Kinematic or Type II singularity as a configuration within the workspace where the PR is unable to bear the external forces despite having all the actuators locked. A simple method to detect a Type II singularity is the vanishing of the determinant of the Forward Jacobian matrix ($\|J_D\|$). The Forward Jacobian matrix (J_D) is defined by the time derivatives of the kinematic constraint equations of the PR with respect to the DOF of the end-effector. Due to that a PR could combine translational and angular DOF the J_D has non-homogeneous dimensions. Hence, a physical interpretation of the $\|J_D\|$ becomes complicated (Voglewede and Ebert-Uphoff, 2004; Merlet, 2006). In addition, the $\|J_D\|$ is not able to identify the limbs involved in the Type II singularity.

There are several methods to detect Type II singularities based on Grassmann geometry (Merlet, 1989; Monsarrat and Gosselin, 2001), Grassmann-Cayley algebra (Ben-Horin and Shoham, 2006; Amine et al., 2012) and Screw Theory (Joshi and Tsai, 2002; Voglewede and Ebert-Uphoff, 2004; Liu et al., 2012). However, a PR could lose control in a Type II singularity and its vicinity due to its joint clearances, actuator uncertainties, and manufacturing errors. Thus, defining a proper threshold for the closeness to a Type II singularity is still a challenging problem. The state of the art of singularity analysis and singularity closeness measurement in PR are presented in Section 2.4 and Section 2.5, respectively.

During patient-active rehabilitation exercises, the patient interacts with a robot by using a force/position controller. According to the forces exerted by the patient, a conventional force/position controller freely modifies the trajectory imposed by the therapist within the workspace of the PR. If a Type II singularity appears within the workspace, the patient could unintentionally drive the PR to a singular configuration. Hence, a force/position controller cannot be straightforwardly implemented in a PR.

Force/position control law has been applied to PR after optimising the singularity-free workspace or by constraining the workspace using mechanical stoppers (McDaid et al., 2013; Dong et al., 2021). Agarwal et al. (2016) designed a control scheme to avoid Type II singularities of a planar PR by using artificial potential functions. Hill et al. (2017) combines a Computed-Torque (CT) controller with a virtual-constraint controller to online avoidance of Type II singularities in a planar PR. These approaches present accurate results. However, they

have not been executed with human interaction or extended to non-redundant spatial PRs. In robotic rehabilitation, as the PR interacts with an injured limb or with a constrained mobility limb, ensuring an accurate avoidance of Type II singularities is essential. Therefore, an additional approach is required to handle Type II singularities to make force/position controllers suitable for rehabilitation tasks with a PR.

This thesis aims to contribute to the field of singularity analysis applied to the control of PRs. Specifically, the development of an index for detecting and avoiding Type II singularities for the control of non-redundant PRs. The research is applied to the 3UPS+RPU PR developed in the Universitat Politècnica de València for knee rehabilitation and diagnosis. Based on the current state of the singularity analysis for PRs, the objectives of this thesis are:

- To develop a new Type II singularity index with a physical meaning capable of detecting a singularity and identifying the limbs involved in the singular configuration.
- To apply the developed new index with physical meaning to the measurement of closeness to a Type II singularity. The new index should provide a feasible interpretation of the closeness to a Type II singularity.
- To develop an experimental procedure to set a proper limit of closeness to a Type II singularity that overcomes the limitation of non-modeled effects such as joint clearances. The experimental procedure should be adaptable to different PRs according to their application.
- To develop an algorithm to release a general non-redundant PR from a Type II singularity using the new index to identify the set of actuators that the robot must move to achieve the releasing procedure.
- To develop an algorithm for Type II singularity avoidance with minimum modifications on the original trajectory to make it suitable for patient-active rehabilitation based on PRs. The avoidance algorithm should be able to be combined with different control laws.
- To develop a new force/position controller that overcomes the limitation of the singular configurations by means of the real-time implementation of the new proposed singularity avoidance algorithm. The complemented controller should be applied to the 3UPS+RPU PR to enable it for safe active and passive knee rehabilitation.

1.3 Contribution of the thesis

Takeda and Funabashi (1995) proposed a Transmission Index (TI) to evaluate the dexterity of a 6-DOF PR by calculating the virtual power transmitted from the actuators to the end-effector. The 6-DOF PR was analysed as six single-DOF mechanisms by fixing all actuators of the PR except one. Based on this approach, Wang et al. (2010) defined the Output Transmission Index (OTI) for kinematic performance evaluation of non-redundant PRs. The OTI is the normalised virtual coefficient between the Transmission Wrench Screw (TWS) and the Output Twist Screw (OTS) of each single-DOF mechanism. The OTI was applied to detect Type II singularities in a 4-DOF PR (Xie and Liu, 2016).

An OTS defines the instantaneous motion of the end-effector produced by a single actuator while the others are locked. Wang et al. (2010) shown that at least two OTSs become linear dependent in a Type II singularity. However, the motion decomposition based on OTSs has not been used to detect or measure the closeness to a Type II singularity. This thesis proposes to analyse the parallelism between the linear and angular components between two OTSs to detect and measure the closeness to a Type II singularity. The parallelism between the linear components of two OTSs is measured by the angle $\Theta_{i,j}$, and the angle $\Omega_{i,j}$ measures the parallelism between the angular components of two OTSs. The subindices i, j represent the two limbs under analysis.

In a planar PR with 2-DOF, the motion of the mobile platform or end-effector is controlled by two limbs that generate one angle $\Theta_{i,j}$ and one angle $\Omega_{i,j}$. In the spatial case, the end-effector is controlled by at least three limbs that generate a minimum of three possible angles $\Theta_{i,j}$ and $\Omega_{i,j}$. In a Type II singularity the angles $\Theta_{i,j}$ and $\Omega_{i,j}$ are zero for all possible combinations i, j $(i \neq j)$. However, measuring the closeness to a Type II singularity based on the decrement of all the angles $\Theta_{i,j}$ and $\Omega_{i,j}$ becomes complex. Thus, this thesis proposes measuring the proximity to a Type II singularity based on the minimum angle $\Omega_{i,j}$ $(min\Omega)$ for spatial PRs. The subindices i, j of angle $min\Theta$ identify the two limbs responsible for the singular configuration approach. In the planar case, the closeness to a Type II singularity is measured by the minimum angle $\Theta_{i,j}$ $min\Theta$ because the motion is developed in a plane, i.e., $\Omega_{i,j} = 0$.

Based on the angles $\Theta_{i,j}$ and $\Omega_{i,j}$, and their correspond minimum angles $min\Theta$ or $min\Omega$, the contributions of the thesis are:

- Detecting Type II singularities planar or spatial non-redundant PRs analysing the loss of the contribution to the end-effector motion from a pair of actuators, i.e., $\Theta_{i,j} = \Omega_{i,j} = 0$.

- Using the $min\Theta$ or $min\Omega$ as an index for detecting the proximity to Type II singularities in planar or spatial PRs, respectively. The main advantages of these indices are physical meaning, sensitivity near a singularity, and identification of the robot kinematic chains producing the singular configuration. These features are analysed by an experimental benchmark between the index $min\Omega$ and the $\|J_D\|$ in a 4-DOF PR for knee rehabilitation. The knee rehabilitation PR is the 3U$\underline{\text{P}}$S+R$\underline{\text{P}}$U PR developed in the Universitat Politècnica de València.

- Developing an experimental procedure to define an effective limit of closeness to singularity to avoid singular configurations in general PRs. The protocol begins by combining essential movements of a PR to generate a set of trajectories that approach a Type II singularity from different non-singular configurations. The essential movements are defined by the application of the PR. A portion of the trajectories generated is executed in the actual PR while the pose of its end-effector is measured by an external sensor. Based on the experimental measurements, an average limit is set to the index for detection of the proximity to a Type II singularity under analysis, such as $min\Omega$. The trajectories non-executed during the setting of the limit of closeness to singularity are tested to verify the accuracy of the procedure. The proposed experimental procedure is not intended to consider the joint clearances model explicitly. However, this protocol can obtain limits of closeness to Type II singularities that are effective in avoiding singular configuration even under manufacturing errors in links and joints. The proposed procedure is employed to analyse the index $min\Omega$ and the $\|J_D\|$ in the 3U$\underline{\text{P}}$S+R$\underline{\text{P}}$U PR.

- An algorithm to release a PR by moving the pair of actuators identified by the $min\Theta$ or $min\Omega$ for planar and spatial cases. This algorithm is developed to verify that the $min\Theta$ or $min\Omega$ is a good option to escape from a singular configuration. The parameters of the releasing algorithm are defined by the control unit parameters and the working velocity of the PR under analysis. This algorithm is the basis for the avoidance algorithm presented below.

- An algorithm to avoid Type II singularities by modifying the trajectory of the pair of actuators involved in the singular configuration. The singularity avoidance algorithm works with one trajectory sample at a time.

In the vicinity of a Type II singularity, the avoidance algorithm calculates the deviation required in the two actuators responsible for the singularity approach. The actuators involved in the singular configuration are identified by the $min\Theta$ or $min\Omega$ for the planar or spatial case, respectively. Only the trajectory of the actuators identified by the index $min\Theta$ or $min\Omega$ are modified to avoid a Type II singularity, i.e., the reference trajectory requires a minimum modification. For this reason, the proposed algorithm is suitable for applications where major changes on the reference trajectory are risky, such as lower limb rehabilitation. The modification in the trajectory of the actuators is calculated using a straight-line equation, reducing the difficulty of setting the algorithm proposed. The straight line is defined by the sample time of the trajectory and the velocity of the PR. For an arbitrary sample of time, the proposed algorithm only needs the reference and the current location of the PR to avoid a singularity. The proposed algorithm is implemented in offline trajectory planning for a five-link mechanism and the 3UPS+RPU PR. For offline trajectory planning, the current location of the PR represents the previous reference trajectory sample. Moreover, the singularity avoidance algorithm is applied in online trajectory planning for the 3UPS+RPU PR. In this case, the current location of the PR could be measured by a 3D tracking sensor or by solving the Forward kinematics based on encoders in the actuators. The measurement of the computational cost and the analysis of the minimal requirements for implementation shows that the proposed algorithm is suitable for offline and real-time applications.

- A force/position controller improved with a real-time singularity avoidance algorithm for PRs. The complemented force/position controller ensures complete control over the end-effector during human-robot interaction without optimising the workspace or adding mechanical limits. The effectiveness of the complemented force/position controller in rehabilitation procedures is verified by executing patient-active exercises with the actual 4-DOF PR for knee rehabilitation. The patient-active exercises are performed with a mannequin limb and a human limb. The complemented force/position controller requires measuring the forces and moments exerted by the patient and the current location of the PR. The forces and moments are measured by a six-axis force/torque. The current location of the PR could be measured by solving the Forward kinematics based on encoders in the actuators. However, this method could be inaccurate since the solution is not unique near a Type II singularity (Morell et al., 2013). Therefore, the singularity avoidance algorithm is performed

using a 3D Tracking System (3DTS) to measure the actual pose of the 3UPS+RPU PR accurately.

1.4 Structure of the thesis

The present PhD. dissertation is structured as follows:

Chapter 2 describes the fundamentals of PRs including their main advantages and disadvantages with respect to the serial type. The features of the different types of singularities of a PR are reported with a special focus on Type II singularities. Subsequently, the analysis developed around the singularities, the metrics for the closeness to a Type II singularity, and the methods to deal with Type II singularities are presented. Finally, the possible improvements in the methods to measure the closeness of Type II singularities are discussed.

Chapter 3 describes the principle of motion decomposition by using OTSs. Based on the motion decomposition, a Type II singularity analysis is proposed by measuring the parallelism between the linear and angular components of two OTSs. The parallelism of the linear and angular components is measured by the angle $\Theta_{i,j}$, and the angle $\Omega_{i,j}$. Next, the proximity to a Type II singularity is measured based on the $min\Theta$ or $min\Omega$ depending on the type of parallel robot. Subsequently, a novel experimental procedure is introduced to set the limit for the proximity to a Type II singularity.

The capability of detecting Type II singularities based on the angle $\Theta_{i,j}$ and $\Omega_{i,j}$ is verified by theoretical and experimental analysis in a five bars planar mechanism and a 4-DOF PR. The proximity detection of singular configurations and the experimental procedure to set its proper closeness limit is applied in a 4-DOF PR for knee rehabilitation. The experimental results show the accuracy of the proposed experimental setting procedure. Moreover, novel non-singular configurations where the actual PR loses control over the mobile platform are identified by the angle $\Omega_{i,j}$.

Chapter 4 describes the development of an algorithm to release a non-redundant PR from a Type II singularity. The proposed release algorithm uses the angle $min\Theta$ and $min\Omega$ to detect the closeness to a singular configuration in planar and spatial cases, respectively. The Singularity Release Algorithm (SRA) is integrated into a vision-based two-level hybrid controller for a 4-DOF PR. Two versions of SRA are developed to verify that the index $min\Omega$ identifies the pair of actuators responsible for approaching a singular configuration. The first version of the SRA modifies the trajectory of the actuators on the limbs

identified by the angle $min\Omega$ to release the PR from a singularity, and the second version moves the opposite limbs. The two versions of SRA are evaluated by simulation and experimentation.

In the same chapter, the indices $min\Theta$ and $min\Omega$ are used to develop a Type II singularity avoidance algorithm. In the vicinity of a Type II singularity, the avoidance algorithm calculates the deviation required in the subset of actuators responsible for the singularity. In other words, only the trajectory of the actuators identified by the angles $min\Theta$ or $min\Omega$ is modified to avoid a Type II singularity. At each sample of the trajectory, only the trajectory of two actuators is modified according to a straight-line equation, i.e., optimisation procedures are unnecessary. Finally, the possible applications of the proposed algorithm are discussed.

Chapter 5 first introduces the fundamental control strategies employed for lower-limb rehabilitation, where admittance control is the most suitable for patient-active rehabilitation. Next, the drawbacks of conventional admittance control in the proximity to a Type II singularity are exposed. Subsequently, the conventional admittance controller is combined with the singularity avoidance algorithm proposed in the previous chapter to overcome the control issues in proximity to a Type II singularity. The complemented admittance controller is implemented in the 4-DOF PR for knee rehabilitation. The inability of conventional control to prevent Type II singularities is shown by experimentation over a mannequin leg. Then, the performance of the complemented admittance controller is evaluated by executing a patient-active knee rotation in the actual 4-DOF PR by using a mannequin and human lower limb.

Chapter 6 exposes the main conclusions of this thesis and the possible future works. Finally, the publications derived from this research are presented.

Chapter 2

Singularities in parallel robots

This chapter describes the fundamentals of Parallel Robots (PRs) including their main advantages and disadvantages with respect to the serial type. The features of the different types of singularities of a PR are reported with a special focus on Type II singularities. Subsequently, the analysis developed around the singularities, the metrics for the closeness to a Type II singularity, and the methods to deal with Type II singularities are presented. Finally, the possible improvements in the methods to measure the closeness of Type II singularities are discussed.

2.1 Parallel robots

Leinonen (1991) defines a Parallel Robot (PR) as a mechanism that controls the motion of the end-effector (mobile platform) by at least two open kinematics chains that link the end-effector to the base (fixed platform). Figure 2.1 shows a schematic representation of a general PR, also called parallel manipulator or Parallel Kinematic Machine (PKM). The mobile platform is a rigid body in the space that can perform three translations and three rotations. The translational motions are performed along the X_f, Y_f, and Z_f axes from the fixed reference frame $\{O_f - X_f Y_f Z_f\}$ in the base. The rotation motions could be represented with respect to the mobile reference frame $\{O_m - X_m Y_m Z_m\}$ attached to the end-effector or with respect to the previous fixed frame. The

position and orientation (pose) of the mobile platform of a PR $\vec{X}$ are known as degrees of freedom (DOFs).

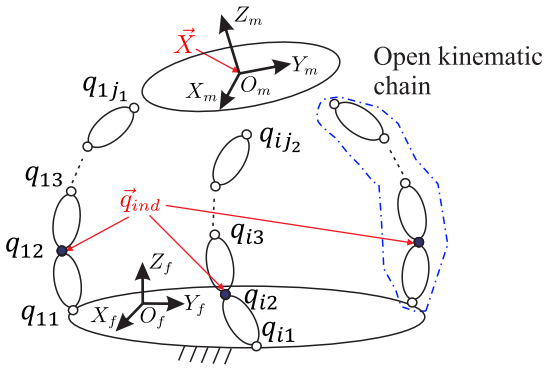

Figure 2.1: General scheme of a PR and its main elements.

The pose $\vec{X}$ is defined by the kinematic constraints imposed by the distribution of the limbs. In a limb consisting of several links connected by joints, the relative motion of a link with respect to another could be represented by generalised coordinates. A generalised coordinate represents a translation or a rotation at the time, with a non-unique definition. In Figure 2.1, the generalised coordinates q_{ij} represent the position or the orientation of a joint between two consequent links. Thus, a q_{ij} represents a revolute or a prismatic joint. The universal and spherical joints are presented as two or three orthogonal generalised coordinates q_{ij}, respectively. The independent generalised coordinates representing the active joints or actuators are collected in $\vec{q}_{ind}$, while the rest of the passive joints are represented by $\vec{q}_s$.

Based on the number of DOFs represented as F, the number of open chains or legs l, and the number of active joints or actuators a (Liu and Wang, 2014; Briot and Khalil, 2015), the PRs are classified as follows:

- Non-redundant PR or general case, $F = a = l$.
- Redundant PR:
  - Kinematic redundancy, $a \geq F$ and $l = F$
  - Actuation redundancy, $a \geq F$ and $l \geq F$

where $1 < F \leq 6$, $l > 1$, and $a \geq F$.

If $F \leq 3$ and the DOFs are limited to the plane, the robot is known as planar PR, otherwise it is a spatial PR ($F \geq 3$). In addition, a PR with $F < 6$ DOFs is also known as a limited-DOF robot and for $F = 6$ DOFs a robot is called fully PR.

Other types of PRs are:

- Hybrid: Serially connection of PRs, i.e., a serial robot or one open kinematic chain with PRs as links.
- Cable-driven: The rigid links are replaced by cables. The cables being used in tension only, i.e., for a PR with F DOF at least $F+1$ cables must be used.

In PRs, the external load is shared by the several legs or limbs increasing the stiffness and load capacity of a PR with respect to a serial robot (Taghirad, 2013; Staicu, 2019). Moreover, PRs have other advantages mainly due to the closed kinematic chain architecture, such as lower weight, higher working speed with high precision, and lower power consumption (Briot and Khalil, 2015). These advantages are key aspects that have increased the interest in using PRs in the academic, industrial, medical, and robotics service fields over the last three decades.

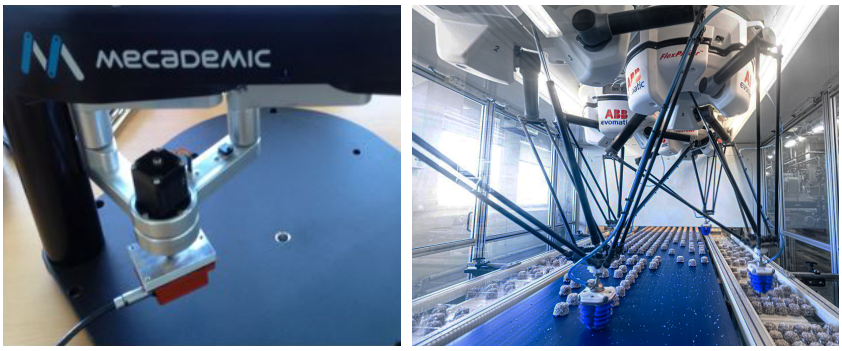

(a) **(b)**

Figure 2.2: (a) Five bars prototype developed by MECADEMIC (2022) (b) Delta robot built by ABB Group (2022).

In pick-and-place tasks, the five bars mechanism and the delta robot are the most representative PRs (Patel and George, 2012). Figure 2.2a shows a five bars mechanism that is a planar PR driven by two angular actuators developed

by MECADEMIC (2022) for academic purposes. The five bars mechanism is also known as 5R mechanism because its links are connected by revolute joints. Figure 2.2b presents a Delta PR built by ABB Group (2022). The Delta robot is a spatial PR with three translational DOFs for high-speed applications. (Clavel, 1988)

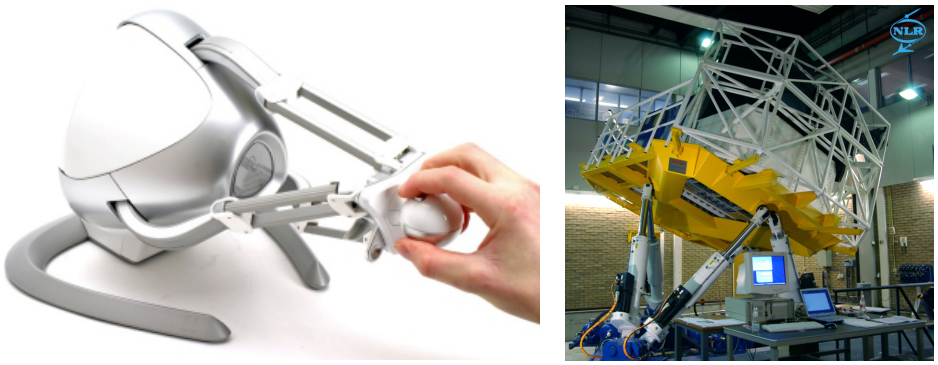

(a) **(b)**

Figure 2.3: (a) Haptic device based on a Delta robot (Block et al., 2013) (b) GRACE flight simulator (Heesbeen et al., 2006).

Figure 2.3 shows a haptic device and a flight simulation based on PRs. The haptic device is a Novint Falcon built for game application based on a Delta PR (Block et al., 2013). Figure 2.3b presents a flight simulator named GRACE based on a spatial PR built by the National Aerospace Laboratory in the Netherlands (Heesbeen et al., 2006).

Figure 2.4a shows a PR for robotic assisted minimally invasive surgery developed by Dalvand and Shirinzadeh (2012). This robot is composed of a 6-RR$\underline{P}$RR parallel micro-manipulator with a linear guide carrying an especially developed actuated 2-DOF laparoscopic instrument. A four bars mechanism connects the linear guide and the 6-RR$\underline{P}$RR micro-manipulator. The letters R and P represent revolute and prismatic joints, where "_" identifies the actuated joint. Figure 2.4b presents a Stewart platform for ankle telerehabilitation developed by Girone et al. (2001). The Stewart platform is a 6-DOF PR driven by six linear actuators with great versatility in application (Stewart, 1965).

However, the PR architecture reduces not only the size of the robot workspace but also its kinematic performance, owing to the possible presence of singularities within the workspace. The reduced workspace can be addressed by means

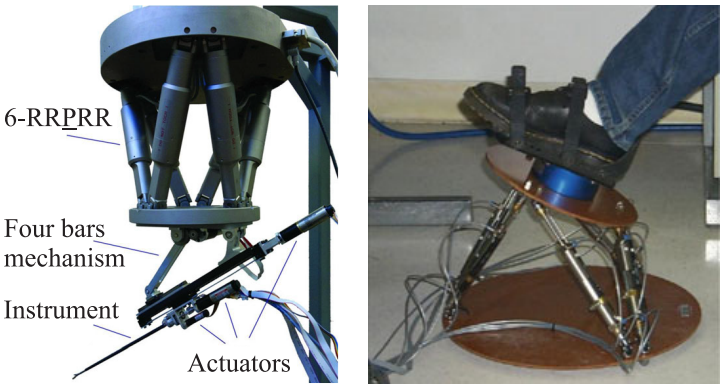

(a) (b)

Figure 2.4: (a) PR for robotic-assisted minimally invasive surgery (Dalvand and Shirinzadeh, 2012) (b) Stewart platform-based system for ankle rehabilitation (Girone et al., 2001).

of a proper mechanical design of the PR, while the singular configurations require further analysis.

2.2 Kinematic analysis

The kinematic analysis of a PR aims to define the position, velocity, and acceleration of the DOFs of the end-effector and the actuators. The pose of the PR and the equivalent location following each open kinematic chain define the vector closure equations $\vec{\Phi}_C$:

$$\vec{\Phi}_c(\vec{X}, \vec{q}_{ind}, \vec{q}_s) = \vec{0} \tag{2.1}$$

where $\vec{X}$ stands for the DOFs the end-effector or mobile platform, $\vec{q}_{ind}$ represents the subset of actuated joints or active generalized coordinates, and the $\vec{q}_s$ is the subset of passive joints or passive generalized coordinates.

In position kinematic analysis, two cases are distinguished:

- Forward Kinematic Problem (FKP): Determining the $\vec{X}$ for a given $\vec{q}_{ind}$.
- Inverse Kinematic Problem (IKP): Find the $\vec{q}_{ind}$ for a given $\vec{X}$.

Thus, the $\vec{\Phi}_C$ is often simplified to define the input-output constraint equations of the PR $\vec{\Phi}$ as follows:

$$\vec{\Phi}(\vec{X}, \vec{q}_{ind}) = \vec{0} \tag{2.2}$$

where $\vec{X}$ and $\vec{q}_{ind}$ becomes the input and output variables of the PR, respectively.

Due to the fact that the position model of a non-redundant PR involves different types of joints, $\vec{\Phi}$ contains F implicit non-linear equations with multiple solutions for the FKP and IKP. The different solutions for the FKP are called assembly modes because they are the possible $\vec{X}$ in which the PR can be assembled for a specific $\vec{q}_{ind}$ (Wenger and Chablat, 1998). Similarly, the multiple solutions for the IKP are called working modes. Figure 2.5a show two assembly modes of a five bars or 5R mechanism for a specific $\vec{q}_{ind}$. In Figure 2.5b two working modes of the 5R mechanism for a specific $\vec{X}$ are represented. The actuated joints $\vec{q}_{ind}$ are represented by two blue-filled circles.

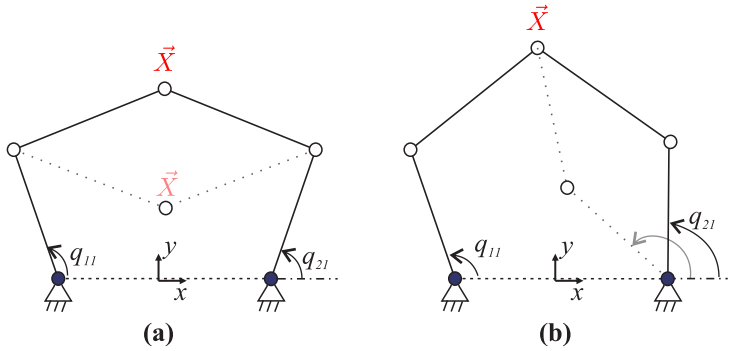

Figure 2.5: Example of (a) assembly modes (b) working modes for a 5R mechanism.

In the literature, the set of feasible $\vec{X}$ is known as the workspace of a PR, i.e, the set of poses that the PR can physically reach. The set of feasible $\vec{q}_{ind}$ is known as joint space. The representation of the workspace with respect to the joint space is named the configuration space. Usually the configuration space cannot be plotted because the dimensions are greater that a three-dimensional graph. For a non-redundant PR with two DOFs the configuration is a four-dimensional manifold. These concepts are used in the singularity analysis in the next section.

For the velocity and acceleration kinematic analysis the $\vec{\Phi}$ is derived with respect to the time. Then, the velocity and acceleration relationship are:

$$\frac{\partial \vec{\Phi}}{\partial \vec{q}_{ind}} \dot{\vec{q}}_{ind} + \frac{\partial \vec{\Phi}}{\partial \vec{X}} \dot{\vec{X}} = \vec{0} \tag{2.3}$$

$$\frac{\partial \vec{\Phi}}{\partial \vec{q}_{ind}} \ddot{\vec{q}}_{ind} + \frac{\partial \vec{\Phi}}{\partial \vec{X}} \ddot{\vec{X}} - \vec{b} = \vec{0} \tag{2.4}$$

where $\dot{\vec{X}}$ and $\ddot{\vec{X}}$ are the velocity and acceleration of the end-effector in the F DOFs, repectively. Analogously, $\dot{\vec{q}}_{ind}$ and $\ddot{\vec{q}}_{ind}$ are the velocity and acceleration of the active joints in generalised coordinates, and $\vec{b}$ represents the elements independent of the acceleration.

According to (2.3), the relationship between the velocities $\dot{\vec{X}}$ and $\dot{\vec{q}}_{ind}$ are always linear. In other words, there is one solution for the Forward and Inverse Kinematic Problem of velocities. This is the same for the acceleration relationship in (2.4). These facts are well-known in the literature.

2.3 Classification of singularities

Initially, Gosselin and Angeles (1990) established a classification of singular configurations by analysing the input-output kinematic velocity relationship calculated from $\vec{\Phi}$. Taking time derivatives of (2.2), the relationship between the outputs and inputs velocities in (2.3) is rewritten as follows:

$$J_I \dot{\vec{q}}_{ind} + J_D \dot{\vec{X}} = \vec{0} \tag{2.5}$$

with

$$J_I = \frac{\partial \vec{\Phi}}{\partial \vec{q}_{ind}},\ J_D = \frac{\partial \vec{\Phi}}{\partial \vec{X}} \tag{2.6}$$

where J_I and J_D represent the Inverse and Forward Jacobian matrices, respectively. Both matrices are square matrices ($F \times F$) for non-redundant PRs.

Based on (2.5), the degeneration of the J_I and J_D matrices defines three types of singularities:

Type I: The determinant of J_I matrix is zero ($\|J_I\| = 0$), i.e., J_I is rank deficient. In this case, the mobile platform cannot move ($\dot{\vec{X}} = \vec{0}$) despite having a set of non-zero velocities in the actuators ($\dot{\vec{q}}_{ind} = \vec{0}$). In other words, the mobile platform of the PR loses mobility in at least one direction. An example of this configuration is shown in Figure 2.6a for five bars mechanism or 5R PR, where R stands for revolute joint.

Type II: J_D matrix becomes rank deficient ($\|J_D\| = 0$). In this case, the mobile platform can perform some motion ($\dot{\vec{X}} \neq \vec{0}$) if an external action is applied to the mobile platform, despite any motion in the actuators ($\dot{\vec{q}}_{ind} = \vec{0}$). Under this condition, the mobile platform of the PR gains at least one uncontrollable motion despite all actuators being locked, see Figure 2.6b.

Type III: Both J_I and J_D become simultaneously singular. This configuration occurs only for the specific geometric parameters of the links. An example of this kind of singularity is shown in Figure 2.6c for a four bars mechanism or 4R PR.

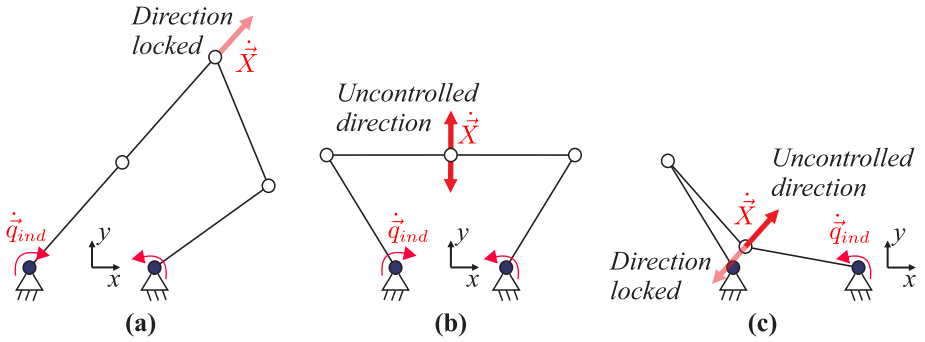

Figure 2.6: Input-output singularities: (a) 5R mechanism in a Type I singularity (b) 5R mechanism in a Type II singularity (c) 4R mechanism in a Type III singularity.

Park and Kim (1999) based on Riemannian and Jacobian matrix analysis, classified the singularities of a PR as actuator, end-effector, and configuration space singularities. The actuator and end-effector singularity are analogous to Type I and Type II singularity, respectively. The configuration space singularities are the self-intersections or the edges of the configuration space manifold, i.e., Type I singularities in the vertices of the workspace.

McAree and Daniel (1999) analysed the second-order degeneration of matrix J_D and defined the Type II singularity with second-order degeneration as cuspidal points. Considering that in a Type II singularity, at least two assembly modes match, a cuspidal point represents the matching of at least three assembly modes.

Type I, Type II singularities, and the configuration space singularities for a virtual two-DOF planar PRs are represented in Figure 2.7. This figure plots the workspace of one DOF on the axis x, with respect to the joint space of two active joints (axes q_{11} and q_{21}). The Type I singularities are in blue while the Type II singularities are in red. Moreover, in Figure 2.7 a cuspidal point and its projection on the joint space are represented.

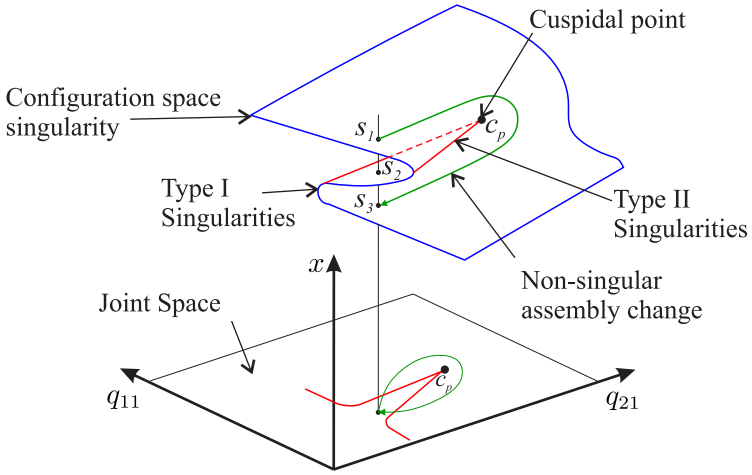

Figure 2.7: Representation of singularities in the reduced configuration space of a virtual two-DOF planar PR.

For PR with $F < 6$ DOFs, the other $6 - F$ DOFs are constrained by invariant mechanical restrictions or by the arrangement of the passive joints in the limbs. In the second case, if the constraint wrenches from the limbs disappear, the end-effector increases at least one DOF, this configuration is named constraint singularity (Zlatanov et al., 2002). The constraint singularities have an effect analogous to Type II singularities. However, constraint configurations are not detected by $\|J_D\|$ because they are defined by the passive joints. The constraint equations are analysed by Jacobian matrix defined by taking the partial derivatives of (2.1) respect to $\vec{q}_s$.

The input-output and constraint singularities were sub-classified according to physical causes of the singular configuration (di Gregorio and Parenti-Castelli, 1999; Liu et al., 2003; Conconi and Carricato, 2009). Based on the Screw theory, the analysis of motion/force transmission of a PR defined three types of singularities: input transmission, output transmission, and constraint singularities (Wu et al., 2011). The input and output transmission singularities are analogous to Type I and Type II singularities, respectively.

Type I singularities typically occur as the PR approaches the boundary of the workspace. In a Type I singularity the robot loses mobility in a certain direction without decreasing the stiffness of the PR. Therefore, Type I singularities are not serious practical limitations, as well as the singularities of serial robots. Type II singularities require special attention because they appear within the workspace. In these configurations, the mobile platform is unable to bear the external forces despite having all the actuators locked. Losing control of the motion of the end-effector represents a potential danger for the user or the PR itself. Another drawback of Type II singularities is that the solution of the Inverse Dynamic Problem (IDP) increases without bounds, i.e., the theoretical efforts of the actuators become infinite (Choudhury and Ghosal, 2000).

2.4 Analysis of Type II singularities

In the literature, Type II singularities are detected by analytical or geometrical methods. The calculation of $\|J_D\|$ presents a simple analytical method to detect a Type II singularity. By using Screw theory, Joshi and Tsai (2002) rewrite the input-output velocity relationship (2.5) to detect Type II singularities and constraint singularities with an overall Jacobian matrix J_O. This method was applied by Gallardo-Alvarado et al. (2018) to detect singularities on a Schönflies PR. However, combining rotational and translational joints produces a J_D or J_O matrix with not homogeneous units that make it difficult to interpret.

Another analytical method to detect Type II singularities is the error amplification factor between $\vec{q}_{ind}$ and $\vec{X}$ in FKP. This amplification factor is known as condition number κ (Merlet, 2006), that for a non-redundant PR is defined as:

$$\kappa = \|J^{-1}\|\|J\| \tag{2.7}$$

with

$$J = -J_D^{-1} J_I \tag{2.8}$$

where J is the Jacobian matrix for the FKP, defined solving $\dot{\vec{X}}$ from (2.5).

In the literature, the two-norm and the Euclidean norm are the most used matrix norm for calculating κ. A Type II singularity appears when $\kappa = 1$, thus, the inverse of the condition number is preferred for detecting singularities. Due to that κ is also difficult to interpret because it is defined based on a matrix with not homogeneous units. Kim and Ryu (2003) divided the columns of the J by the length of a link in a nominal position to normalise the units in the matrix. However, It still provides a non-intuitive interpretation of detecting singularities. Another disadvantage of $\|J_D\|$ and κ is the inability to identify the limbs involved in the Type II singularity.

Based on Grassmann line geometry, Merlet (1989) showed that a 6-DOF PR reaches a Type II singularity if, and only if, a subset of n lines, associated with the limbs of the robot, has a rank less than n. Monsarrat and Gosselin (2001) describes the different Grassmann geometric rules and the correspondence with Type I and Type II singularities. In this research, the Type II singularities were plotted in a constant-orientation workspace. Figure 2.8 shows an example of this geometrical procedure applied to 3-DOF and 6-DOF PRs.

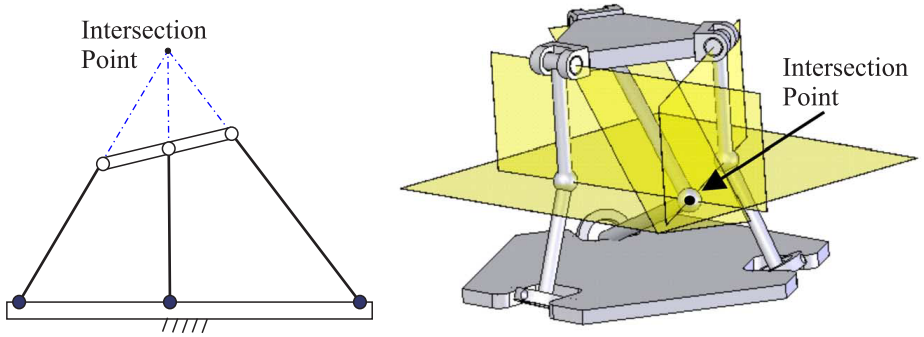

Figure 2.8: Detection of Type II singularity using Grassmann geometry applied to (a) planar PR with 3-DOF (Merlet, 1989) and (b) spatial PR named 3-USR with 6-DOF(Ben-Horin and Shoham, 2006).

Ben-Horin and Shoham (2006) combined Screw theory with Grassmann-Caley algebra to detect singularities in 6-DOF PRs with different architectures. In

this work, the join and meet operations detect a singularity by analysing the intersection of lines and planes from the limbs of the PR. Based on Screw Theory, Slavutin et al. (2019) proposed a graphical-analytical method to detect singular configuration in non-redundant spatial PRs. In this research, a spatial PR is divided into several 2-DOF PR, called minimal PRs. The possible Instantaneous Screw Axes (ISAs) of three minimal PRs define a cylindroid. A Type II singularity appears when an ISA crosses and is perpendicular to the centre axis of its cylindroid.

Liu et al. (2012) proposed a procedure based on motion/force transmissibility able to detect input transmission, output transmission, and constraint singularities. An output transmission singularity or Type II singularity is detected when the efforts of at least one actuator cannot contribute to the motion of the end-effector. This condition is represented by the work done by the actuator that is calculated as follows:

$$\$_{O_i} \circ \$_{T_i} = 0 \quad (i = 1, 2, \ldots, F) \tag{2.9}$$

where $\circ$ represents the reciprocal product, $\$_T$ stands for the Transmission Wrench Screw (TWS), $\$_O$ is the Output Twist Screw (OTS), and i identify the limb of the PR.

An TWS represents the force and moment transmitted by the actuator to the end-effector while a OTS is the instantaneous linear and angular motion of the moving platform considering all the actuators locked except the i-th one. The decomposition of the end-effector motion in F OTSs was proposed by Takeda and Funabashi (1995). Xie and Liu (2016) applied the reciprocal product of (2.9) to detect output transmission singularities in a Schönflies PR.

Bu (2016) analysed the characteristics angles between TWS submanifolds to detect Type II singularities. For a non-redundant PR, the characteristics angles between TWS submanifolds θ_i are defined as:

$$\theta_i = \arccos\left(\frac{\$_{n_i} \circ \$_{T_i}}{\|\$_{n_i}\|\|\$_{T_i}\|}\right) \quad (i = 1, 2, \ldots, F) \tag{2.10}$$

$\$_{n_i}$ stands for a screw that is normal to all TWSs except to the i-th one if all TWS are independent in the submanifold $F-1$. Thus, a singular configuration appears when $\theta_i = 90°$.

These methods are able to detect Type II singular configurations. However, a PR loses control in a singular configuration and its neighbourhood (Voglewede and Ebert-Uphoff, 2004; Liu et al., 2012). Hence, it is necessary to measure the closeness between a pose and a singular configuration.

2.5 Closeness measurement to Type II singularities

Accurate measurement of the closeness to a Type II singularity allows avoiding this configuration during the design and implementation phases of a PR. A singular configuration decreases the control of the PR over the pose of the end-effector; in other words, the dexterity of the robot is reduced. The $\|J_D\|$ and κ are local dexterity indices unable to measure the closeness to a Type II singularity. For serial robots, (Yoshikawa, 1985) proposed the manipulability index w to quantify the dexterity of the robot as:

$$w = \sqrt{\|JJ^T\|} \tag{2.11}$$

The index w quantifies the amplification in the workspace errors with respect to unitary circle join space errors. Thus, a robot has great dexterity for configurations with high values of w.

Gosselin (1988) proposed to evaluate the dexterity of a robot by averaging the inverse of κ for a given workspace W. Thus, the Global Condition Index GCI was defined as:

$$GCI = \frac{\int_W \left(\frac{1}{\kappa}\right)\, dW}{\int_W dW} \tag{2.12}$$

The GCI is suitable for the optimal design of PR where enlarging the workspace is an important parameter. However, w and GCI lack physical or geometrical meaning. Thus, they are unable to define a safe distance to a singular configuration. This is mainly because the Jacobian matrix involved in their calculus mixes translational and rotational units (Doty et al., 1995; Voglewede and Ebert-Uphoff, 2004; Merlet, 2006). Moreover, the accuracy of the GCI depends on the number of nodes taken during the discretisation of the workspace. Increasing the number of nodes for discretisation could be computationally intensive depending on the number of DOFs.

Voglewede and Ebert-Uphoff (2005) evaluated the closeness to a Type II singularity by two constrained optimisation problems. The first closeness index is the minimum velocity of the actuators constraining the power, the kinematic energy or the natural frequency of the PR. The second closeness index is the maximum feasible forces that the actuators transmit to the end-effector restricted to the input torque ranges, potential energy, the stiffness of the robot or the reciprocal of the natural frequency. Although this approach provides a physical interpretation, the optimisation problems require at least one constitutive quantity to combine the linear and rotational components together.

Hubert and Merlet (2009) measured the closeness to Type II singularities by computing a region of the workspace where the forces of the actuators are lower than a certain threshold. This approach defined the force workspace as the set of configurations of the PR where the forces of the actuators are feasible for an invariant payload.

Wang et al. (2010) defined the Input Transmission Index (ITI) and the Output Transmission Index (OTI) to evaluate the performance of non-redundant spatial PR. The ITI measures the power coefficient between the motion imposed by its actuator and the TWS at each limb. The OTI measures the power coefficient between the TWS at each limb and its instantaneous motion in the mobile platform.

For the limb i its ITI λ_i and its OTI η_i are obtained as:

$$\lambda_i = \frac{|\$_{T_i} \circ \$_{I_i}|}{|\$_{T_i} \circ \$_{I_i}|_{max}} \quad (i = 1, 2, \ldots, F) \tag{2.13}$$

$$\eta_i = \frac{|\$_{T_i} \circ \$_{O_i}|}{|\$_{T_i} \circ \$_{O_i}|_{max}} \quad (i = 1, 2, \ldots, F) \tag{2.14}$$

where $\$_{I_i}$ stands for the twist screw of the actuator in the limb i, and the subindex max is the maximum value for the reciprocal product in the denominator.

The performance of PR is better when its ITI and OTI are closer to 1. Thus, the performance evaluation of a PR is simplified by calculating the minimum value of all λ_i and η_i , i.e.:

$$\gamma = min\{\lambda_i, \eta_i\} \quad (i = 1, 2, \ldots, F) \tag{2.15}$$

with γ as the Local Transmission Index (LTI)

Wu et al. (2011) introduced the LTI as a uniform measurement of the closeness to a singularity (Type I and Type II). In this research, the motion/force evaluation was extended to the constraint singularities by defining a Local Constraint Index (LCoI). Subsequently, Liu et al. (2012) used the minimum value of λ_i (γ_I) to measure the closeness to a Type I singularity, and the minimum value of η_i (γ_O) to measure the proximity to a Type II singularity. The closeness to a constraint singularity is defined by the LCoI. Due to the fact that γ_I, γ_O and LCoI have a range from 0 to 1 for any non-redundant PR, these indices provide a uniform unitless measurement for closeness to a singularity.

Bu (2016) proposed the characteristics angles θ_i to measure the closeness to Type II singularities. In this case, this index has angular units where the proximity is defined around 90°.

2.6 Methods for addressing Type II singularities

The main methods developed to solve the problems related to Type II singularities are:

- Redundant mechanisms.
- Enlargement of the workspace.
- Trajectory planning.
- Control algorithms for singularity crossing or avoidance.

These methods are detailed below.

2.6.1 Redundant mechanisms

Adding redundant mechanisms to a PR is a method to avoid or remove the loss of control over the motions of the mobile platform. A redundant PR is achieved by:

- Actuation redundancy: Adding actuators in passive joints without modifying the mechanical structure. An example of a redundant 3-DOF PR is shown in Figure 2.9a. The actuation redundancy is analysed in (Wu et al., 2009b; Saafi et al., 2015; Wen et al., 2019).
- Redundant architectures: The number of open kinematics chains is increased as the number of actuators. Figure 2.9b shows an 2-DOF PR

controlled by 4 actuators. The kinematically redundant PRs are exposed in (Arakelian et al., 2008; Wu et al., 2013; Baron et al., 2020).

- Combination of the previous two options.

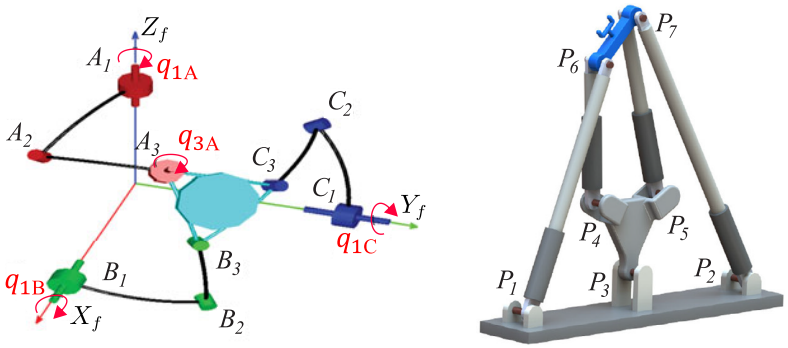

Figure 2.9: Redundant parallel robots (a) 3-RRR spherical (Saafi et al., 2015) PR for a haptic device, (b) 4-RPR planar PR (Baron et al., 2020).

The redundancy mechanism requires more electronic hardware to control the additional actuators and increases the complexity of the kinematic and dynamic model of the PR. Moreover, the motion planning and the control of the kinematically redundant PRs during singularity avoidance is a challenging problem (Baron et al., 2020; Nouri Rahmat Abadi and Carretero, 2022).

2.6.2 Enlargement of the workspace

An alternative way to deal with singularities is to design the PRs focusing on maximising the workspace by means of optimising procedures. The optimisation of the workspace requires special attention to performance evaluation. Hubert and Merlet (2009) define free-singularity zones by constraining the forces of the actuators to a feasible range. Davidson et al. (2004) introduced an optimisation procedure based on force/motion transmission efficiency. Wu et al. (2009a) limited the LTI to define a set of configurations where a PR has a good motion/force transmission and the robot is far away from singularities. This zone was named Good-Transmission Workspace (GTW) with the limit of LTI equal to 0.7. The GTW was analysed in different spatial PRs in (Wang et al., 2010).

Liu et al. (2006) maximised the workspace of a five bars mechanism based on GCI combined with velocity and stiffness indices. The optimisation of the workspace of a 5-DOF PR based on LTI was presented in (Xie et al., 2017). Araujo-Gómez et al. (2019) optimised the workspace of a non-redundant 4-DOF PR by maximising the manipulability index w. Valero et al. (2020) optimised the workspace of a re-configurable PR by minimising the actuators forces and the value of the $\|J_D\|$.

Araujo-Gómez et al. (2019) showed that even after optimising the workspace of a 4 DOF PR, a small percentage of singularities still remain inside the workspace of the robot. Innocenti and Parenti-Castelli (1998) showed that for PRs, there could be several assembly modes for a non-singular configuration. This introduced the possibility of switching from one assembly mode to another without passing through a Type II singularity, i.e., J_D does not pass through zero. Hernandez et al. (2009) defined the conditions to perform a non-singular assembly change by going around to a cuspidal point. Urízar (2012) developed a systematic procedure to enlarge the workspace of planar parallel manipulators by means of non-singular assembly modes transitions. Caro et al. (2012) analysed the non-singular assembly modes transitions in a 6-DOF PR.

2.6.3 Trajectory planning

Trajectory planning computes PR motions satisfying robot dynamics and actuator constraints, minimising energy consumption or execution time while avoiding collisions with obstacles such as Type II singularities (Shiller, 2015). The trajectory planning is performed by:

- Offline: Two desired PR poses are connected based on prior information about the PR workspace and the regions with Type II singularities (Gasparetto et al., 2015).
- Online: Two configurations of the PR are connected by means a partial view of the workspace (Shiller, 2015) or sensor feedback (Zhao and Ratchev, 2017).
- Combination of both previous methods.

Figure 2.10 shows a free-singularity trajectory generated between two desired poses of the PR after performing an offline or online trajectory technique. The singular regions plotted in Figure 2.10 contain Type II singularities.

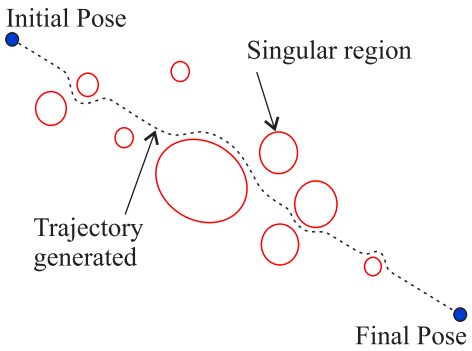

Figure 2.10: General view of a free-singularity trajectory generated by online or offline techniques.

Sen et al. (2003) proposed a path planning algorithm for PRs that constrains the potential energy of the PR to avoid singular configurations. Khoukhi et al. (2009) presented a multi-objective dynamic trajectory planning for PRs where a Type II singularity is avoided by maximising the manipulability w. A path planning method is proposed by generating singularity-free C-spaces defined in the vicinity of the two configurations to connect (Bohigas et al., 2013). Bourbonnais et al. (2015) proposed a stochastic cubic spline optimisation procedure for generating smooth trajectories for a five bars PR that avoids Type II singular regions simultaneously. Li et al. (2018) generated feasible trajectories for a 4-DOF PR using a quintic B-spline considering singular configurations as optimisation constraints. These offline methods for singularity-free trajectory planning are mathematically complex and require considerable effort to select the parameters of the optimisation problem.

The online trajectory planning methods for PRs are generally combined with discrete controllers. Hesselbach et al. (2005) based on integrated sensors, developed an online brake trajectory planning for a Hexa PR that is activated in the closeness to a Type II singularity. Hill et al. (2017) applied virtual constraints in a controller to online trajectory generation during a Type II singularity crossing. The next section presents the main controllers implemented in real-time applications for crossing or avoiding a Type II singularity.

2.6.4 Control algorithms for singularity crossing or avoidance

Briot and Arakelian (2008) define that a PR can cross a Type II singularity without perturbation of motion if the forces and moments applied on the end-effector are orthogonal to the direction of the uncontrollable DOFs. Based on this dynamic condition, Pagis et al. (2015) developed a muti-model Computed-Torque (CT) controller that switches from a complete dynamic model to a reduced dynamic model in the closeness to a Type II singularity. The change of the dynamic model avoids the degeneracy of the control actions calculation in the proximity to a Type II singularity. The control actions in CT controller represent the forces on the actuators, i.e., the solution of the IDP. Subsequently, Six et al. (2017) modifies the dynamic equations used in a CT controller to pass through a Type II singularity without degeneracy of the IDP.

The controller developed for Type II singularity crossing requires that the trajectory fulfils the kinodynamic conditions defined by Briot and Arakelian (2008). Moreover, the case of time-variant external efforts applied to the mobile platform was not considered. Thus, the online avoidance of Type II singularities emerges. Agarwal et al. (2016) proposed a task-priority controller where a potential function allows online singularity avoidance that requires reducing one DOF of a non-redundant PR. Nouri Rahmat Abadi and Carretero (2022) combined real-time trajectory planning with a feedback linearisation controller to avoid singularities for a planar redundant PR. These methods require setting the control law to track location and avoid singularities simultaneously.

2.7 Discussion and Conclusions

The literature review reveals that Type II singularities, due to the loss of control over the mobile platform, are an important problem to solve in non-redundant PR. The Type II singularities are generally analysed without considering not deterministic errors such as joint clearances and manufacturing errors, i.e., the analysis of Type II singularities requires an experimental perspective. The limit of closeness to a singular configuration lacks an experimental procedure for setting this threshold according to the application of the non-redundant PRs. In addition, the measurement of proximity to a Type II singularity is not able to identify the kinematic chains involved in the singularity configuration.

Despite optimising the workspace of PR, a percentage of Type II singularities still remains. The techniques used for Type II singularities crossing constrain the external efforts applied to the mobile platform. In lower limb rehabilitation

the patient applied non-controller forces and moments to the PR. Thus, the Type II singularities crossing techniques are not suitable for robotic rehabilitation of the human lower limb.

The offline avoidance of Type II singularities requires optimisation procedures that involve complex mathematical modelling. Moreover, the online avoidance algorithms for Type II singularity are not used in tasks with human interaction, such as the force/position control of a PR for human rehabilitation.

Therefore, the objectives of this thesis are:

- Developing a new index to measure the closeness to a Type II singularity with physical meaning and even to identify the kinematics chains involved in the singular configuration. The new index is developed based on the angle between the components of two OTSs in Chapter 3.
- Developing an experimental procedure to define an effective limit of closeness to singularity to avoid Type II singularities in general PRs even the presence of joint clearances, see Chapter 3.
- Developing a deterministic algorithm to release or avoid a singularity by using the new index based on the angle between the components of two OTSs, see Chapter 4. The novel avoidance algorithm is applied to offline and online trajectory planning to evaluate its computational cost and the modification of the original trajectory.
- Developing a force/position controller improved with the proposed singularity avoidance algorithm for PRs. The complemented force/position controller ensures complete control over the end-effector during human-robot interaction without optimising the workspace or adding mechanical limits. The effectiveness of the complemented force/position controller in rehabilitation procedures is verified by executing patient-active exercises with the actual 4-DOF PR for knee rehabilitation in Chapter 5.

Chapter 3

Analysis of Type II singularities

This chapter describes the principle of motion decomposition by using Output Twist Screws (OTSs). Based on the motion decomposition, a Type II singularity analysis is proposed by measuring the parallelism between the linear and angular components of two OTSs. The parallelism of the linear and angular components is measured by the angle $\Theta_{i,j}$, and the angle $\Omega_{i,j}$, respectively where i, j represent the OTSs under analysis. Next, the proximity to a Type II singularity is measured based on the minimum angle $\Theta_{i,j}$ or $\Omega_{i,j}$ depending on the type of Parallel Robot (PR). Subsequently, a novel experimental procedure is introduced to set the limit for the proximity to a Type II singularity.

The capability of detecting Type II singularities based on the angle $\Theta_{i,j}$ and $\Omega_{i,j}$ is verified by theoretical and experimental analysis in a five bars planar mechanism and a spatial PR with four degrees of freedom (DOFs). The proximity detection of singular configurations and the experimental procedure to set its proper closeness limit is applied in a 4-DOF PR for knee rehabilitation. The experimental results show the accuracy of the proposed experimental setting procedure. Moreover, novel non-singular configurations where the actual PR loses control over the mobile platform are identified by the angle $\Omega_{i,j}$.

3.1 Motion decomposition in a non-redundant parallel robot

In a non-redundant PR, the motion of the mobile platform is produced by the combined action of F actuators. The motion of the mobile platform can be represented by the twist screw $\$_m$ as follows:

$$\$_m = \left(\begin{array}{ccc} \vec{\omega}_m{}^T & ; & \vec{\nu}_m{}^T \end{array} \right) \tag{3.1}$$

where $\vec{\omega}_m$ stands for the angular velocity of the mobile platform and $\vec{\nu}_m$ represents the linear velocity in an arbitrary point of the end-effector.

The actions transmitted by each actuator i to a specific point of the mobile platform are represented by the Transmission Wrench Screw (TWS) $\$_{T_i}$:

$$\$_{T_i} = \left(\begin{array}{ccc} \vec{F}_{ind_i}{}^T & ; & \vec{T}_{ind_i}{}^T \end{array} \right) \quad (i = 1, 2, \ldots, F) \tag{3.2}$$

with $\vec{F}_{ind_i}$ and $\vec{T}_{ind_i}$ representing the forces and moments coming from by the active joint i, respectively.

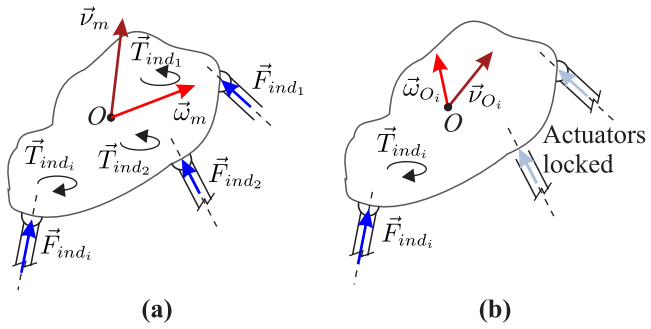

Figure 3.1: (a) Motion of the mobile platform generated by the combined actions of the actuators and (b) Instantaneous motion of the mobile platform considering all actuators locked except one.

Due to the fact that several actuators work in parallel to generate a unique motion, the individual contribution of each actuator is challenging to identify, see Figure 3.1a. According to Takeda and Funabashi (1995), if all actuators are locked except one, the instantaneous motion of the mobile platform is represented by an OTS (Figure 3.1b). Therefore, the $\$_m$ is a linear combination of F OTSs:

$$\$_m = \$_{O_1} + \$_{O_2} + \ldots + \$_{O_F} \tag{3.3}$$

The OTS $\$_{O_i}$ generated by the limb $i = 1, 2, \ldots, F$, is defined as follows:

$$\$_{O_i} = \left(\begin{array}{ccc} \vec{\omega}_{O_i}{}^T & ; & \vec{\nu}_{O_i}{}^T \end{array} \right) \tag{3.4}$$

where $\vec{\omega}_{O_i}$ and $\vec{\nu}_{O_i}$ stand for the angular and linear components of $\$_{O_i}$, respectively.

If fixing all actuators except the one in the i-th limb, only the TWS $\$_{T_i}$ contributes to the motion $\$_{O_i}$ while all other TWSs apply no power to the moving platform. Thus, the F $\$_{O_i}$ can be obtained using the expression:

$$\$_{O_i} \circ \$_{T_j} = \vec{\omega}_{O_i} \cdot \vec{T}_{ind_j} + \vec{F}_{ind_j} \cdot \vec{\nu}_{O_i} = 0 \quad (i, j = 1, 2, \ldots, F,\ i \neq j) \tag{3.5}$$

where $\circ$ stands for the reciprocal product.

3.2 Detection of Type II singularities based on Output Twist Screws

The definition of the $\$_{O_i}$ in (3.4) can be rewritten as:

$$\$_{O_i} = k_i \hat{\$}_{O_i} \tag{3.6}$$

where k_i stands for the module or the intensity of the $\$_{O_i}$, and $\hat{\$}_{O_i}$ represent an unit or normalised screw defined as:

$$\hat{\$}_{O_i} = \left(\begin{array}{ccc} \vec{\mu}_{w_{O_i}}{}^T & ; & \vec{\mu}^*_{v_{O_i}}{}^T \end{array} \right) \tag{3.7}$$

with the unit vectors $\vec{\mu}_{w_{O_i}}$ and $\vec{\mu}^*_{v_{O_i}}$ as the Instantaneous Screw Axis (ISA) and the direction of the linear part of the $\$_{O_i}$, respectively.

In the same way, the $\$_{T_i}$ in (3.2) can be rewritten as:

$$\$_{T_i} = c_i \hat{\$}_{T_i} \tag{3.8}$$

with

$$\hat{\$}_{T_i} = \left(\begin{array}{ccc} \vec{\mu}_{F_{ind_i}}{}^T & ; & \vec{\mu}^*_{T_{ind_i}}{}^T \end{array} \right) \tag{3.9}$$

where c_i stands for the module of the $\$_{T_i}$. $\vec{\mu}_{T_{ind_i}}$ and $\vec{\mu}^*_{T_{ind_i}}$ represent the direction of the forces and moments transmitted to the end-effector by the actuator in limb i, respectively.

Substituting (3.6) and (3.8) into (3.5) gives:

$$k_i c_j \, \hat{\$}_{O_i} \circ \hat{\$}_{T_j} = 0 \quad (i, j = 1, 2, \ldots, F, \; i \neq j) \tag{3.10}$$

The k_i is defined by the desired motion on the mobile platform, and c_j is only determined by the external loads on each limb. In contrast, the $\hat{\$}_{T_j}$ is constant at a certain position and orientation (pose) of the PR. Thus, simplifying (3.10), the direction in which an actuator can contribute to the motion of the end effector $\hat{\$}_{O_i}$ $(i = 1, 2, \ldots, F)$ is given by:

$$\hat{\$}_{O_i} \circ \hat{\$}_{T_j} = 0 \quad (j = 1, 2, \ldots, F, \; i \neq j) \tag{3.11}$$

The reciprocal product in (3.11) was used for detecting Type II singularities, see Section 2.4. However, the linear dependency of the unit OTSs has not been used for detecting Type II singularities. Wang et al. (2010), proved that for a non-singular configuration the F $\hat{\$}_{O_i}$ are linearly independent. Hereby, the condition to assert the presence of a Type II singularity is given by the linear dependence of at least two $\hat{\$}_{O_i}$, i.e.:

$$\hat{\$}_{O_i} = k_d \hat{\$}_{O_j} \quad (i \neq j) \tag{3.12}$$

where k_d defines the linear dependence between the i and j unit OTSs. The value of k_d can be 1 or -1 because the $\vec{\mu}_{w_{O_j}}$ in $\hat{\$}_{O_j}$ is a unit vector.

From a geometrical point of view, in a Type II singularity the linear and angular components of the $\hat{\$}_{O_i}$ and $\hat{\$}_{O_j}$ are parallel. Based on this property, this research proposes to analyse Type II singularities considering the parallelism between the elements of two normalised OTSs. The parallelism between the linear and angular components is measured by the angles $\Theta_{i,j}$ and $\Omega_{i,j}$, respectively.

Considering F $\hat{\$}_{O_i}$ grouped in pairs, there are $\binom{F}{2}$ angles $\Theta_{i,j}$ defined as:

$$\Theta_{i,j} = \arccos\left(\frac{\vec{\mu}^*_{v_{O_i}} \cdot \vec{\mu}^*_{v_{O_j}}}{|\vec{\mu}^*_{v_{O_i}} \cdot \vec{\mu}^*_{v_{O_j}}|}\right) \quad (i,j = 1,2,\ldots,F, i \neq j) \tag{3.13}$$

where i, j identify the limbs under analysis.

Analogously, the angles $\Omega_{i,j}$ are:

$$\Omega_{i,j} = \arccos\left(\frac{\vec{\mu}_{w_{O_i}} \cdot \vec{\mu}_{w_{O_j}}}{|\vec{\mu}_{w_{O_i}} \cdot \vec{\mu}_{w_{O_j}}|}\right) \quad (i,j = 1,2,\ldots,F, i \neq j) \tag{3.14}$$

From a theoretical perspective, a PR undergoes a Type II singularity, if and only if $\Theta_{i,j}$ and $\Omega_{i,j}$ are equal to zero. The detection of singularities based on the indices $\Theta_{i,j}$ and $\Omega_{i,j}$ provides a physical meaning because both of them are angular measures. Moreover, regardless of the type of joints in the limbs, the angles $\Theta_{i,j}$ and $\Omega_{i,j}$ measure the proximity to a singularity in angular units. The detection of Type II singularities based on the angles $\Theta_{i,j}$ and $\Omega_{i,j}$ are applied to a planar PR in Section 3.5.2 and to a spatial case in Section 3.6.3.

3.3 Closeness to Type II singularities based on Output Twist Screws

The closeness to a Type II singularity is measured by decreasing $\Theta_{i,j}$ and $\Omega_{i,j}$. However, (3.13) and (3.14) defined $\binom{F}{2}$ angles for each one. The minimum condition to reach a singular configuration is that at least two $\hat{\$}_{O_i}$ become parallel. Therefore, the closeness to a singular configuration is measured by the set of minimum angles $\Theta_{i,j}$ and $\Omega_{i,j}$ named as $min\Theta$ and $min\Omega$, respectively.

For a planar non-redundant PR with $F = 2$, the closeness to a Type II singularity is measured by decreasing $min\Theta$. It is because the $\vec{\mu}_{w_{O_i}}$ and $\vec{\mu}_{w_{O_j}}$ are perpendicular to the plane maintaining $min\Omega = 0$.

For a spatial non-redundant PR ($F > 2$), the proximity to a Type II singularity is defined by the angles $min\Theta$ and $min\Omega$. However, in (3.7), the $\vec{\mu}^*_{v_{O_i}}$ can be rewritten with respect to the $\vec{\mu}_{w_{O_i}}$ as follows:

$$\vec{\mu}^*_{v_{O_i}} = h\vec{\mu}_{w_{O_i}} + \vec{r}_{OP} \times \vec{\mu}_{w_{O_i}} \tag{3.15}$$

where h is the screw's pitch and $\vec{r}_{OP}$ is the minimal distance between the selected point of the mobile platform O and $\vec{\mu}_{w_{O_i}}$, see Figure 3.2.

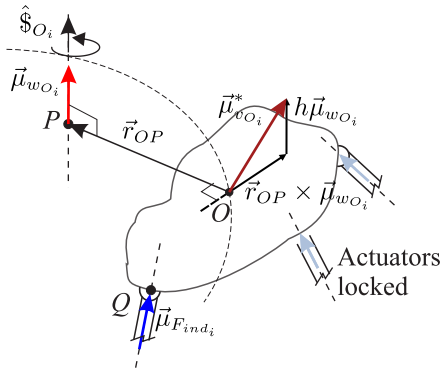

Figure 3.2: Components of a normalised OTS.

Rewriting the cross product with matrix multiplication, (3.15) becomes:

$$\vec{\mu}^*_{v_{O_i}} = (H + \tilde{R})\vec{\mu}_{w_{O_i}} \tag{3.16}$$

with the matrix H and the skew-symmetric matrix $\tilde{R}$ defined as:

$$H = \begin{bmatrix} h & 0 & 0 \\ 0 & h & 0 \\ 0 & 0 & h \end{bmatrix} \quad \tilde{R} = \begin{bmatrix} 0 & -r_{OP_z} & r_{OP_y} \\ r_{OP_z} & 0 & -r_{OP_x} \\ -r_{OP_y} & r_{OP_x} & 0 \end{bmatrix} \tag{3.17}$$

According to (3.16), if H and $\tilde{R}$ are null matrices, $\vec{\mu}^*_{v_{O_i}} = \vec{0}$ even though $\vec{\mu}_{w_{O_i}} \neq \vec{0}$, i.e., the limb i contributes with pure angular motion. Then, there are arbitrary non-singular configurations with $\Theta_{i,j} = 0$ and $\Omega_{i,j} \neq 0$ because the $\vec{\mu}^*_{v_{O_i}}$ or $\vec{\mu}^*_{v_{O_j}}$ could disappear, or become parallel. In contrast, the angle $\Omega_{i,j} = 0$ if and only if the $\vec{\mu}_{w_{O_i}}$ and $\vec{\mu}_{w_{O_j}}$ become parallel. Therefore, in a spatial PR, the closeness to a Type II singularity depends mainly on decreasing the $min\Omega$. The effectiveness of the $min\Omega$ as a Type II singularity proximity detector is proved by an experimental benchmark for a 4-DOF PR for knee rehabilitation and diagnosis in Section 3.6.

The indices $min\Theta$ and $min\Omega$ are used to develop a novel Type II singularity avoidance algorithm for a planar and spatial non-redundant PR in Chapter 4.

The applications of the proposed avoidance algorithm are presented in Chapter 5.

3.4 Experimental procedure to set the limit of proximity to Type II singularities

This thesis proposes to establish the limit of closeness to Type II singularities by an experimental procedure to ensure proper detection and avoidance of a singularity in an actual non-redundant PR. The proposed experimental procedure for setting the singularity closeness limit is shown in Figure 3.3.

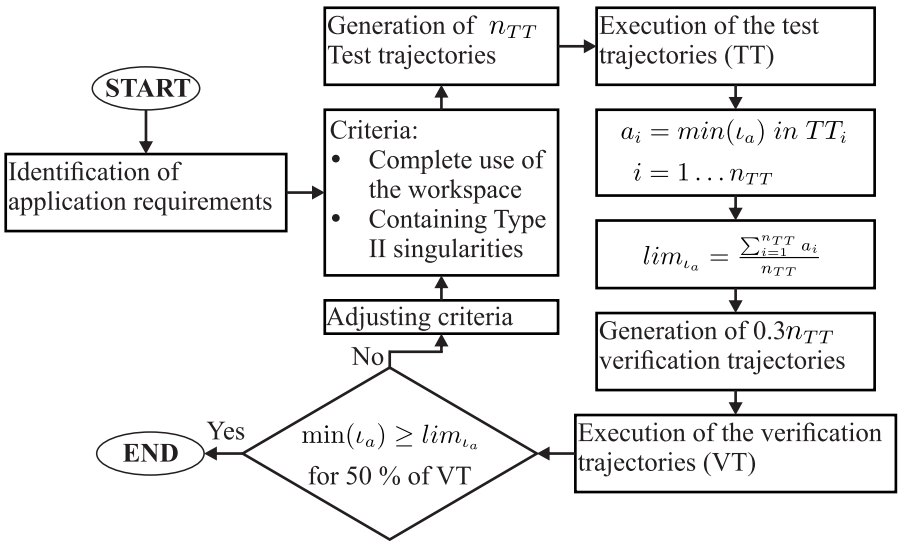

Figure 3.3: Flowchart of the experimental procedure to set the limit of proximity to Type II singularities.

First, fundamental trajectories of the PR under study are selected based on their application. Subsequently, from the fundamental trajectories, a set of trajectories is generated according to the criteria of containing Type II singularities and using the entire workspace. These trajectories are named test trajectories and the number of them n_{TT} is defined according to the application. Then, each test trajectory is executed on the actual PR to measure the minimum values reached for the index under analysis ι_a, for example, $\iota_a = \|J_D\|$. In a singular trajectory, the minimum value of ι_a is calculated for the last pose before losing control over the mobile platform. The experimental

limit lim_{ι_a} for the index ι_a is calculated as the average of the minimum values reached in the test trajectories.

From the fundamental trajectories, a new set of trajectories is developed to verify that the experimental limit can detect the proximity to a singular configuration. These trajectories are named verification trajectories and they must be at least 30 % of the n_{TT}. The 50 % of the verification trajectories have the final pose next to the closeness limit ($\min(\iota_a) \geq lim_{\iota_a}$). The rest of the trajectories have a final configuration within the closeness threshold, $min(\iota_a) < lim_{\iota_a}$.

If the execution of the verification trajectories with the final configuration next to the closeness limit ($\min(\iota_a) \geq lim_{\iota_a}$) does not cause control problems, the process is finished. Otherwise, it is necessary to modify the criteria to generate the test trajectories, according to the PR application.

The proposed experimental procedure for setting the closeness limit aims to guarantee that the actual PR does not reach a singularity avoiding the need to model the error produced by clearances in the PR joints. However, this research was not intended to establish a direct relation between Type II singularities and manufacturing errors such as joint clearances.

3.5 Case Study: five bars mechanism

The five bars mechanism or 5R mechanism is a planar PR with 2-DOF used for positioning a point P on a defined plane (see Figure 3.4). Point P is connected to the base by two limbs each of which consists of two links. The mechanism is named 5R because the links are connected by revolute joints (letter R) where the two joints connected to the base are actuated.

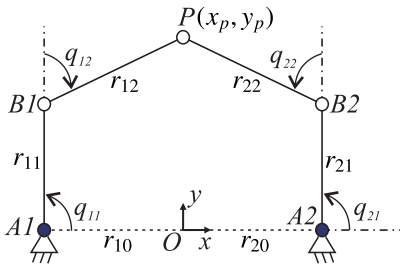

Figure 3.4: Simplified representation of the 5R mechanism.

The kinematic model of the 5R mechanism is shown in Figure 3.4 where r_{11}, r_{12}, r_{21} and r_{22} are the length of the links. r_{10} and r_{20} are the horizontal

distance to the connecting points $A1$ and $A2$ measured from O in the fixed frame $\{O{-}xyz\}$, respectively. The active joints are defined as q_{11}, q_{21}, while the passive joints are q_{12}, q_{22}. In this research, the 5R mechanism has a symmetrical architecture where the inverse kinematic model considers the working mode $-+$ Liu et al. (2006). The geometrical parameters of the 5R mechanism are shown in Table 3.1.

Table 3.1: Geometrical parameters of the 5R mechanism in meters

$r_{10},\ r_{20}$ (m)	$r_{11},\ r_{21}$ (m)	$r_{12},\ r_{22}$ (m)
0.04	0.06	0.05

3.5.1 Analysis of Type II singularities using Output Twist Screws

The movement of the 5R mechanism is divided into $\hat{\$}_{O_1}$ and $\hat{\$}_{O_2}$, which by using (3.13) and (3.14) define the indices $\Theta_{1,2}$ and $\Omega_{1,2}$, respectively. In the 5R mechanism, $\Omega_{1,2} = 0$ because the movement takes place in the plane xy remaining the Instantaneous Screw Axis in the z axis.

At point P, the $\hat{\$}_{O_1}$ represents the contribution of limb 1 to the motion of the point P, i.e.:

$$\hat{\$}_{O_1} = \begin{pmatrix} 0 & 0 & 1 & ; & v_{O_x} & v_{O_y} & 0 \end{pmatrix} \tag{3.18}$$

Considering the reciprocal product property and the unitary norm of the linear motion, the components v_{O_x}, v_{O_y} are calculated by solving the non-linear system:

$$\begin{aligned} \hat{\$}_{O_1} \circ \hat{\$}_{T_2} &= 0 \\ {v_{O_x}}^2 + {v_{O_y}}^2 &= 1 \end{aligned} \tag{3.19}$$

Due to the rotational actuator on limb 2 (q_{21}) transmitting pure force to point P, the $\hat{\$}_{T_2}$ is:

$$\hat{\$}_{T_2} = \begin{pmatrix} {\vec{\mu}_{F_2}}^T & ; & 0 & 0 & 0 \end{pmatrix} \tag{3.20}$$

$\vec{\mu}_{F_2}$ stands for the unitary force vector in the direction of the link $B2P$ represented on the fixed frame $\{O-xyz\}$. Considering two moving frames attached to the links $A2B2$ and $B2P$, the $\vec{\mu}_{F_2}$ is calculated as follow:

$$\vec{\mu}_{F_2} = \boldsymbol{R}_1 {}^1\boldsymbol{R}_2 \begin{bmatrix} 1 & 0 & 0 \end{bmatrix}^T \tag{3.21}$$

where the rotation matrix $\boldsymbol{R}_1$ and ${}^1\boldsymbol{R}_2$ are defined as:

$$\boldsymbol{R}_1 = \begin{bmatrix} \cos q_{21} & -\sin q_{21} & 0 \\ \sin q_{21} & \cos q_{21} & 0 \\ 0 & 0 & 1 \end{bmatrix} \quad {}^1\boldsymbol{R}_2 = \begin{bmatrix} \cos q_{22} & -\sin q_{22} & 0 \\ \sin q_{22} & \cos q_{22} & 0 \\ 0 & 0 & 1 \end{bmatrix} \tag{3.22}$$

Developing (3.21) with (3.22), $\vec{\mu}_{F_2}$ is:

$$\vec{\mu}_{F_2} = \begin{bmatrix} \cos q_{21} \cos q_{22} - \sin q_{21} \sin q_{22} \\ \sin q_{21} \cos q_{22} + \cos q_{21} \sin q_{22} \\ 0 \end{bmatrix} \tag{3.23}$$

The $\hat{\$}_{O_2}$ is calculated solving (3.19) replacing $\hat{\$}_{T_2}$ with the pure force screw $\hat{\$}_{T_1}$ as:

$$\hat{\$}_{T_1} = \begin{pmatrix} \vec{\mu}_{F_1}{}^T & ; & 0 & 0 & 0 \end{pmatrix} \tag{3.24}$$

with the force $\vec{\mu}_{F_1}$ in the direction of the link $B1P$ defined as follow:

$$\vec{\mu}_{F_1} = \begin{bmatrix} \cos q_{11} \cos q_{12} - \sin q_{11} \sin q_{12} \\ \sin q_{11} \cos q_{12} + \cos q_{11} \sin q_{12} \\ 0 \end{bmatrix} \tag{3.25}$$

3.5.2 Detection of Type II singularities based on Output Twist Screw

The 5R mechanism is a planar PR used for pick and place tasks. The fundamental movement is a translation between two configurations in the workspace. Thus, this Section defines a set of four test trajectories (TT1-TT4) to verify the capability of the angle $\Theta_{i,j}$ in detecting Type II singularities. All test trajectories start at a non-singular configuration and stop at a singular (TT1-

TT2) or non-singular pose (TT3-TT4). The description of the test trajectories is shown in Table 3.2.

Table 3.2: Description of test trajectories for 5R mechanism.

	Description
TT1	Linear motions between $x_p = 0.0m$, $y_p = 0.09m$ and $x_p = -0.030m$, $y_p = 0.050m$
TT2	Linear motions between $x_p = 0.01m$, $y_p = 0.09m$ and $x_p = 0.029m$, $y_p = 0.050m$
TT3	Linear motions between $x_p = 0.0m$, $y_p = 0.09m$ and $x_p = 0.002m$, $y_p = 0.101m$
TT4	Linear motions between $x_p = 0.002m$, $y_p = 0.101m$ and $x_p = 0.05m$, $y_p = 0.08m$

The detection of Type II singularities based on $\Theta_{i,j}$ is compared with respect to the $\|J_D\|$. The $\|J_D\|$ is calculated using (2.6) with $\vec{X} = [x_p \quad y_p]^T$ and $\vec{q}_{ind} = [q_{11} \quad q_{21}]^T$, the detailed expression of $\|J_D\|$ is shown in Sosa-Lopez et al. (2017). The $\Theta_{1,2}$ and $\|J_D\|$ calculated for each test trajectory are shown in Figure 3.5 and Figure 3.6, respectively. The time between two different configurations is 0.1 s for all the trajectories in this study. Figure 3.5 shows that the $\Theta_{1,2}$ becomes zero only in TT1 and TT2, these results are equal for the values of $\|J_D\|$ shown in Figure 3.6. Therefore, the capability of $\Theta_{i,j}$ detecting Type II singularities is verified.

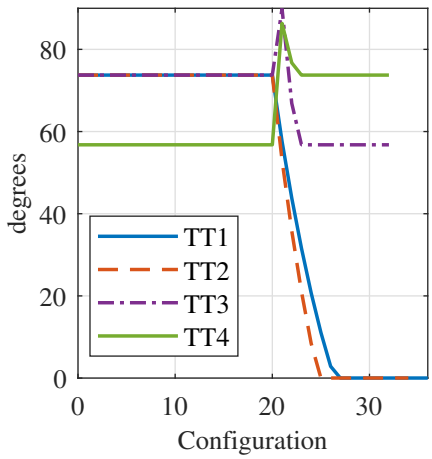

Figure 3.5: $\Theta_{1,2}$ for TT1-TT4 during simulation in the 5R PR.

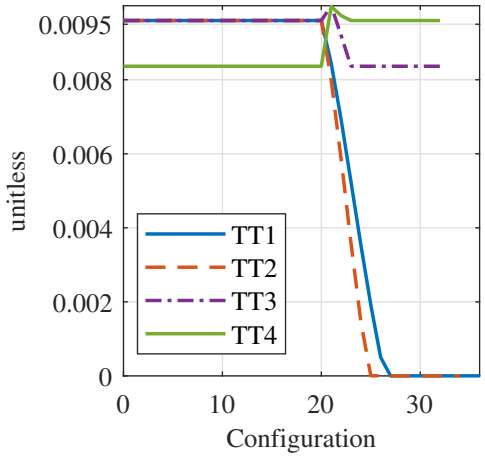

Figure 3.6: $\|J_D\|$ for TT1-TT4 during simulation in the 5R PR.

By using a prototype of the 5R mechanism under study the previous test trajectories are executed. The prototype of the 5R PR is controlled by an Arduino Uno board at a rate of 200 Hz where the test trajectories are sent from Matlab. Figure 3.7 shows the results of $\Theta_{1,2}$ after executing the test trajectories in the actual 5R mechanism.

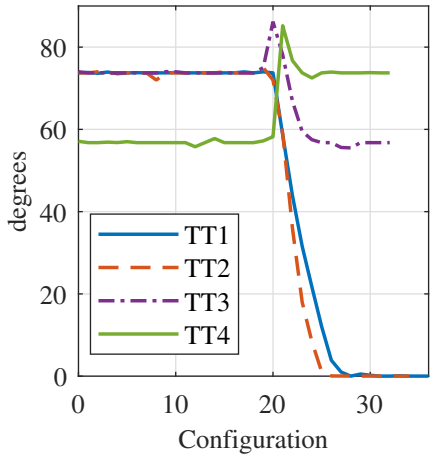

Figure 3.7: $\Theta_{1,2}$ for TT1-TT4 measured in the actual prototype of the 5R PR.

An external force is applied at the end of the execution of the test trajectories. The five bars mechanism loses control only in the trajectories TT1 and TT2,

i.e., these two trajectories reached a Type II singularity. Figure 3.8 shows a frame sequence of the external force applied at the end of the TT1 where the control over point P is lost. These results verify that the angle $\Theta_{1,2}$ is suitable for detecting Type II singularities of non-redundant planar PRs.

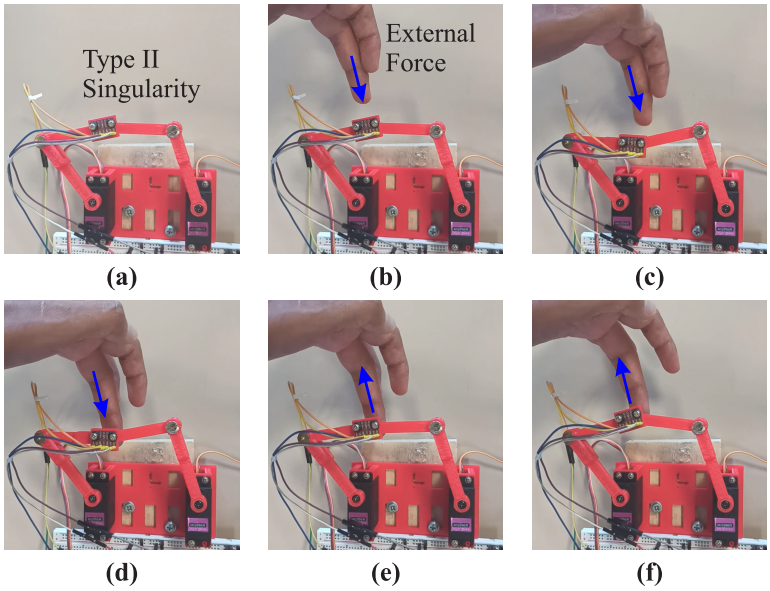

Figure 3.8: External force applied on a Type II singularity in the trajectory TT1 for the actual 5R PR at different consecutive instants of time. The frame sequence starts at (a) and ends at (f).

3.6 Case Study: Parallel robot for knee rehabilitation

The 3UPS+RPU PR is a 4-DOF mechanism for knee rehabilitation and diagnosis purposes. Figure 3.9 shows the actual prototype and its kinematic model. The designation 3UPS+RPU refers to the three external limbs with UPS configuration and the central one with RPU configuration (Figure 3.9b). The letters R, U, S and P represent revolute, universal, spherical and prismatic joints, respectively, and "_" identifies the actuated joint. The 3UPS+RPU robot was designed and built at Universitat Politècnica de València.

The 4-DOF of the PR are two translational movements in the tibiofemoral plane (x_m, z_m), one rotation around the coronal plane (ψ) and one rotation around the tibiofemoral plane (θ). These four DOFs are controlled by four

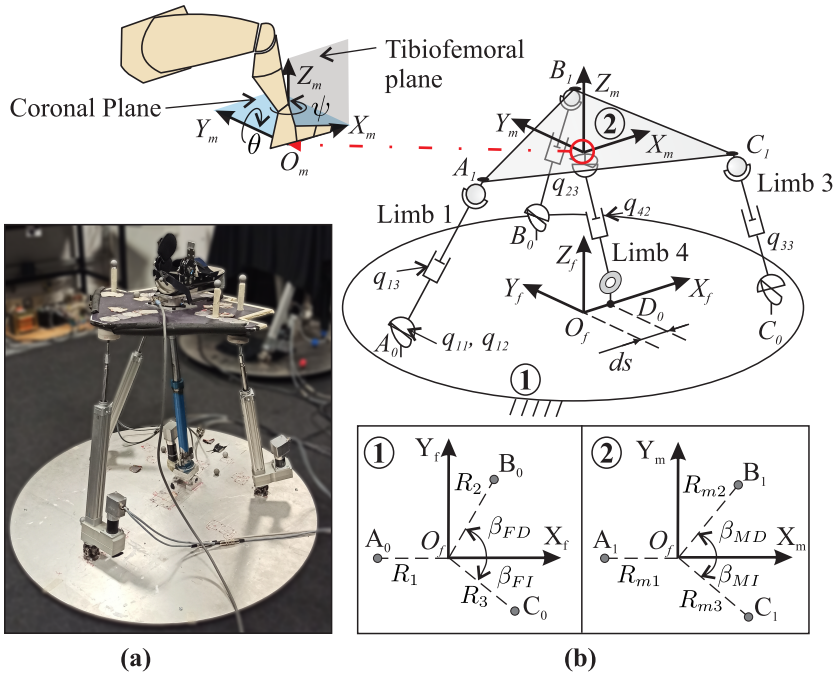

Figure 3.9: 3UPS+RPU PR: (a) actual prototype (b) simplified representation.

linear actuators. The length of the actuators is represented by the generalised coordinates q_{13}, q_{23}, q_{33} and q_{42}, see Figure 3.9b. The translation on the Y_f axis is constrained by the R and U joint of the central limb. In addition, the U joint linking the central limb with the mobile platform constrains the rotations around the X_m axis. The kinematic model of this PR was developed in (Araujo-Gómez et al., 2017; Vallés et al., 2018) and its optimisation was presented in (Araujo-Gómez et al., 2019; Valero et al., 2020).

The four points that connect the limbs with the fixed platform $(A_0, \ldots, D_0)$ are located by the geometric variables R_1, R_2, R_3, β_{FD}, β_{FI} and ds. The four points that connect the limbs with the mobile platform (A_1, B_1, C_1, O_m) are located by the geometric variables R_{m1}, R_{m2}, R_{m3}, β_{MD} and β_{MI}. The geometric parameters on the fixed platform are measured with respect to the fixed frame $\{O_f - X_f Y_f Z_f\}$ while the parameters on the mobile platform with respect to the moving frame $\{O_m - X_m Y_m Z_m\}$. The geometrical parameters of the PR under analysis are shown in Table 3.3.

Table 3.3: Geometrical parameters of the 3UPS+RPU PR

$R_1,\ R_2,\ R_3$ (m)	β_{FD} (°)	β_{FI} (°)	ds (m)
0.4	90	45	0.15
$R_{m1},\ R_{m2},\ R_{m3}$ (m)	β_{MD} (°)	β_{MI} (°)	-
0.3	50	90	-

3.6.1 Analysis of Type II singularities using Output Twist Screws

The movement of the 3UPS+RPU PR is divided into $\hat{\$}_{O_1}$, $\hat{\$}_{O_2}$, $\hat{\$}_{O_3}$ and $\hat{\$}_{O_4}$ that using (3.14) define the six indices $\Omega_{1,2}$ $\Omega_{1,3}$, $\Omega_{1,4}$, $\Omega_{2,3}$, $\Omega_{2,4}$ and $\Omega_{3,4}$. Analogously, (3.13) generates six indices $\Theta_{1,2}, \ldots, \Theta_{3,4}$. The contribution to the motion of the limb 1 $\hat{\$}_{O_1}$ in point O_m with respect to the fixed frame is:

$$\hat{\$}_{O_1} = \begin{pmatrix} w_{O_x} & w_{O_y} & w_{O_z} & ; & v_{O_x} & 0 & v_{O_z} \end{pmatrix} \tag{3.26}$$

For an arbitrary point on the mobile platform of the 3UPS+RPU PR, w_{O_x} is related to w_{O_z} as follows:

$$w_{O_x} = w_{O_z} \tan\theta \tag{3.27}$$

The expression in (3.27) is determined by taking the time derivatives of the rotation matrix between the moving and fixed frame ${}^f\boldsymbol{R}_m$. Considering the Euler Y-Z' angle convention ${}^f\boldsymbol{R}_m$ is:

$${}^f\boldsymbol{R}_m = \begin{bmatrix} \cos\theta\cos\psi & -\cos\theta\sin\psi & \sin\theta \\ sin\psi & \cos\psi & 0 \\ -\sin\theta\cos\psi & \sin\theta\sin\psi & \cos\theta \end{bmatrix} \tag{3.28}$$

Based on the reciprocal product (3.11), the relationship (3.27) and the unitary norm of the ISA. The variables w_{O_x}, w_{O_y}, w_{O_z}, v_{O_x} and v_{O_z} are calculated by solving the non-linear system:

$$\begin{gathered}\hat{\$}_{O_1} \circ \hat{\$}_{T_2} = 0 \\ \hat{\$}_{O_1} \circ \hat{\$}_{T_3} = 0 \\ \hat{\$}_{O_1} \circ \hat{\$}_{T_4} = 0 \\ w_{O_x} - w_{O_z} \tan\theta = 0 \\ {w_{O_x}}^2 + {w_{O_y}}^2 + {w_{O_z}}^2 = 1\end{gathered} \tag{3.29}$$

In this case, the actuators transmit force and moment to the mobile platform because the external limbs are not connected directly to the point O_m. Thus the transmission wrench $\hat{\$}_{T_1}$, $\hat{\$}_{T_2}$ and $\hat{\$}_{T_3}$ are defined as:

$$\hat{\$}_{T_1} = \left(\ {\vec{\mu}_{F_1}}^T \quad ; \quad (\vec{r}_{O_m A_1} \times \vec{\mu}_{F_1})^T \ \right) \tag{3.30}$$

$$\hat{\$}_{T_2} = \left(\ {\vec{\mu}_{F_2}}^T \quad ; \quad (\vec{r}_{O_m B_1} \times \vec{\mu}_{F_2})^T \ \right) \tag{3.31}$$

$$\hat{\$}_{T_3} = \left(\ {\vec{\mu}_{F_3}}^T \quad ; \quad (\vec{r}_{O_m C_1} \times \vec{\mu}_{F_3})^T \ \right) \tag{3.32}$$

where $\vec{r}_{O_m A_1}$, $\vec{r}_{O_m B_1}$ and $\vec{r}_{O_m C_1}$ stand for the location vector between the point O_m and the vertices A_1, B_1 and C_1, respectively.

The central limb is connected to the point O_m, so the $\hat{\$}_{T_4}$ is:

$$\hat{\$}_{T_4} = \left(\ {\vec{\mu}_{F_4}}^T \quad ; \quad 0 \quad 0 \quad 0 \ \right) \tag{3.33}$$

$\vec{\mu}_F$ is the unit vector of the force applied by each actuator with respect to the fixed frame. The direction of the $\vec{\mu}_{F_1}$, $\vec{\mu}_{F_2}$ and $\vec{\mu}_{F_3}$ depends on the universal joint that connects the external limbs with the fixed platform, see Figure 3.9b. The direction of the $\vec{\mu}_{F_4}$ depends on the revolute joint that connects the central limb with the fixed frame.

The universal joint in limb 1 is represented by two orthogonal rotations q_{11} and q_{12} (Figure 3.9b). Thus, the $\vec{\mu}_{F_1}$ is defined as follows:

$$\vec{\mu}_{F_1} = \boldsymbol{R}_1 {}^1\boldsymbol{R}_2 \begin{bmatrix} 0 & 0 & 1 \end{bmatrix}^T \tag{3.34}$$

with the rotation matrix $\boldsymbol{R}_1$ and ${}^1\boldsymbol{R}_2$ as:

$$\boldsymbol{R}_1 = \begin{bmatrix} \cos q_{11} & 0 & -\sin q_{11} \\ 0 & 1 & 0 \\ \sin q_{11} & 0 & \cos q_{11} \end{bmatrix} \quad {}^1\boldsymbol{R}_2 = \begin{bmatrix} \cos q_{12} & 0 & \sin q_{12} \\ \sin q_{12} & 0 & -\cos q_{12} \\ 0 & 1 & 0 \end{bmatrix} \tag{3.35}$$

Developing (3.34) with (3.35), $\vec{\mu}_{F_1}$ is:

$$\vec{\mu}_{F_1} = \begin{bmatrix} \cos q_{11} \sin q_{12} & -\cos q_{12} & \sin q_{11} \sin q_{12} \end{bmatrix}^T \tag{3.36}$$

The $\vec{\mu}_{F_2}$ is equal to the (3.36) with q_{21} and q_{22} instead of q_{11} and q_{12}, respectively. The same replacement is performed to $\vec{\mu}_{F_3}$, considering q_{31} and q_{32}.

In the central limb, the $\vec{\mu}_{F_4}$ is defined by the orientation of the revolute joint (q_{41}) as follows:

$$\vec{\mu}_{F_4} = \begin{bmatrix} -\sin q_{41} & 0 & \cos q_{41} \end{bmatrix}^T \tag{3.37}$$

The $\hat{\$}_{O_2}$ is calculated based on (3.29) by modifying the reciprocal product as follows:

$$\begin{gathered} \hat{\$}_{O_2} \circ \hat{\$}_{T_1} = 0 \\ \hat{\$}_{O_2} \circ \hat{\$}_{T_3} = 0 \\ \hat{\$}_{O_2} \circ \hat{\$}_{T_4} = 0 \\ w_{O_x} - w_{O_z} \tan\theta = 0 \\ {w_{O_x}}^2 + {w_{O_y}}^2 + {w_{O_z}}^2 = 1 \end{gathered} \tag{3.38}$$

The $\hat{\$}_{O_3}$ and $\hat{\$}_{O_4}$ are calculated with the analogous process of removing the reciprocal product related to $\hat{\$}_{T_3}$ and $\hat{\$}_{T_4}$, respectively.

Section 3.3 mentioned that for a spatial PR, the angle $\min\Theta = 0$ in some non-singular configurations. Figure 3.10a shows the angles $\Theta_{1,3}$ and $\Theta_{3,4}$ during a trajectory that goes from a non-singular configuration to a Type II singularity in the 4-DOF PR. Figure 3.10b shows the angles $\Omega_{1,3}$ and $\Omega_{3,4}$ for the same trajectory to a Type II singularity. This figure shows that the angle $\min\Theta$, $\Theta_{1,3}$ in this case, disappears for non-singular configurations. Only the minimum angle $\Omega_{i,j}$ ($\Omega_{3,4}$) has a continuous decrement in the proximity to singularity. Therefore, the closeness to a Type II singularity is measured by the minimum angle $\Omega_{i,j}$. The constraint singularities are not analysed because the 3U<u>P</u>S+R<u>P</u>U PR has invariant mechanical constraints, see Section 3.6. Hereby, the constraint wrench screws are always linearly independent.

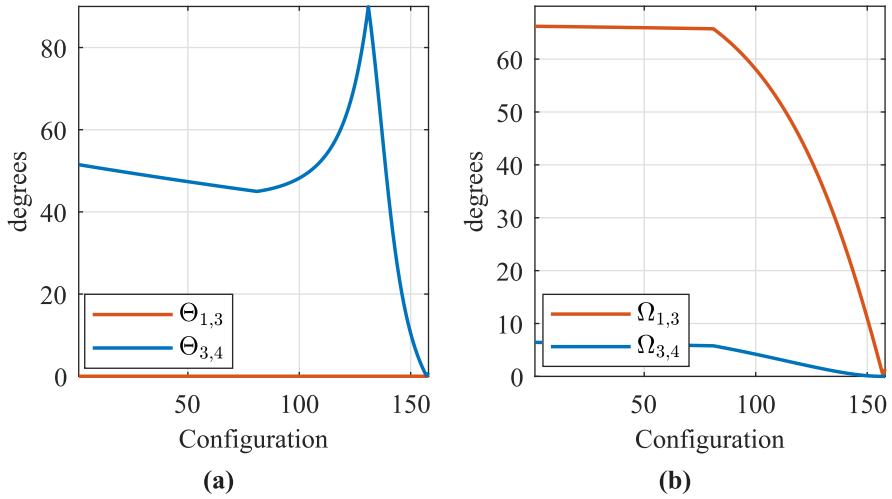

Figure 3.10: Angles (a) $\Theta_{i,j}$ (b) $\Omega_{i,j}$ during a trajectory approaching a Type II singularity.

3.6.2 Experimental setup

In this case, the proposed experimental procedure to set a proper closeness limit is developed for the $\min\Omega$ and $\|J_D\|$. The index $\|J_D\|$ is analysed for verifying the features of the angle $\min\Omega$. The calculation of $\|J_D\|$ is detailed in (Araujo-Gómez et al., 2017) considering $\vec{X} = [x_m \quad z_m \quad \theta \quad \psi]^T$ and $\vec{q}_{ind} = [q_{13} \quad q_{23} \quad q_{33} \quad q_{42}]^T$. The experiments conducted in the prototype of the 3UPS+RPU PR are controlled by an industrial PC and a 3D Tracking System (3DTS) measures its actual pose, see Figure 3.11.

The experimental procedure for setting the limit of proximity to Type II singularities is developed by using the diagram shown in Figure 3.12. At each execution, $\vec{X}_r$ stands for an element of the test or verification trajectory under analysis. The reference $\vec{X}_r$ is in cartesian coordinates. Thus. the reference in generalised active coordinates $\vec{q}_{ind_r}$ is defined by solving the IKP. The $\vec{q}_{ind_r}$ is used as a reference for the robot control unit that works at 100 Hz. This control unit is embedded in a high-performance industrial PC with a processor Core i7 3.4 GHz. It is equipped with data acquisition cards for reading the encoders' signal $\vec{q}_{ind_c}$ and supplying the control actions $\vec{u}$ for the four actuators of the PR. The $\vec{u}$ are proportional to the mechanical forces applied by the linear actuators $\vec{\tau}$. The control law implemented is a linear algebra-based (LAB) controller. During the execution of a trajectory, the position and orientation of

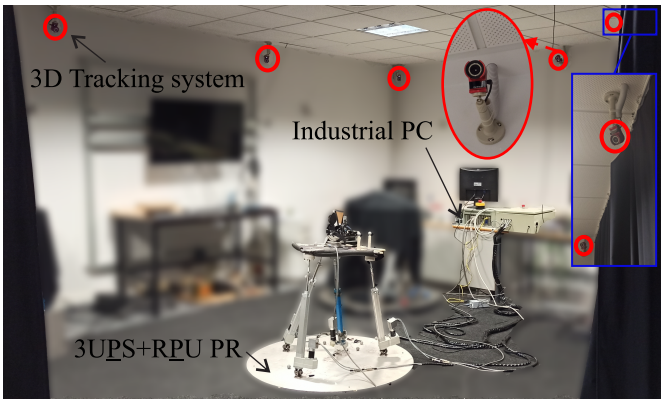

Figure 3.11: Equipment used for experiments with the 3UPS+RPU PR.

the mobile platform are measured by a redundant 3D Tracking System running at 120 Hz. The measured pose $\vec{X}_c$ is stored at each time instant.

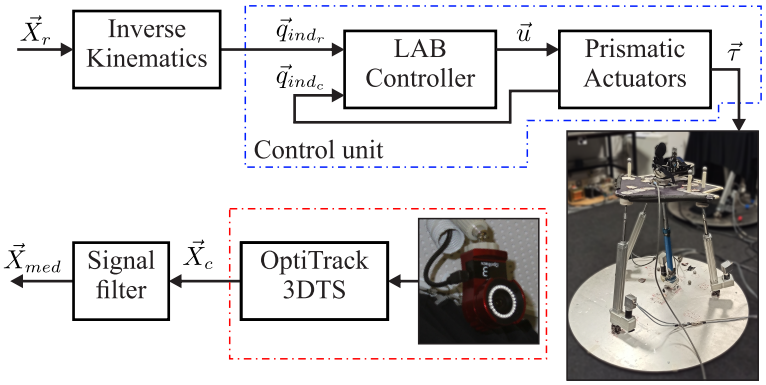

Figure 3.12: Experimentation diagram for Type II singularity analysis in the 3UPS+RPU PR.

After performing a trajectory, the pose measured of the PR $\vec{X}_c$ is filtered ($\vec{X}_{med}$) before being analysed. The filtering of $\vec{X}_c$ is performed in order to: (i) reduce the noise on the measurements and; (ii) adjust the sampling time from 8.3 ms to 0.1 s. The signal smoothing uses the Loess algorithm by Cleveland and Loader (1996). Based on the reference $\vec{X}_r$ and the measurement $\vec{X}_{med}$, the $\|J_D\|$ and $\Omega_{i,j}$ are calculated. The experimental analysis is focused on $\Omega_{i,j}$ while the $\|J_D\|$ is an index to compare.

A critical element in the experimental study is the precise measurement of $\vec{X}_c$. For this purpose, the 3D Tracking System is an OptiTrack ® photogrammetry system consisting of 10 infrared cameras with an accuracy of 0.5 mm. The architecture and specifications of the 3D Tracking System are detailed at Section 5.2.2.

Table 3.4: Description of test trajectories for 3UPS+RPU PR

	Lower limb	4-DOF PR
TT1	Complete internal-external knee rotation	Rotation of ψ for the interval $\begin{bmatrix}0 & 60\end{bmatrix}^\circ$, with $X_f = -0.15\ m$
TT2	Flexion-extension of knee combined with hip flexion, ankle, and knee rotations	Simultaneous motion of 0.2 m on the X_f axis, 0.1 m on Z_f, while θ rotates 15 ° and ψ rotates 60 °
TT3	Flexion-extension of knee combined with hip flexion, ankle, and knee rotations	Elliptical motion on the Z_f axis as a function of 0.2 m displacement on the X_f axis, simultaneously turns 4 ° in θ and 4 ° for ψ
TT4	Flexion-extension of knee combined with hip flexion, ankle, and knee rotations	Elliptical motion on Z_f axis as a function of 0.2 m displacement on the X_f axis, simultaneously rotates 5 ° in θ and 10 ° for ψ
TT5	Partial internal-external knee rotation	Rotation around the Z_m axis for the interval $\begin{bmatrix}0 & 20\end{bmatrix}^\circ$, with $X_f = 0.012\ m$
TT6	Flexion-extension of knee combined with ankle and knee rotations	Displacement of 0.1 m on the X_f axis, while θ rotates 20 ° and ψ rotates 10 °
TT7	Flexion-extension of knee combined with hip flexion	Elliptical motion on Z_f axis as a function of the 0.1 m displacement on the X_f axis
TT8	Flexion-extension of knee combined with ankle and knee rotations	Displacement of 0.16 m on X_f axis, while θ rotates 20 ° and ψ rotates 20 °
TT9	Flexion-extension of knee combined with ankle and knee rotations	Displacement of 0.2 m on X_f axis, while θ rotates 20 ° and ψ rotates 20 °

3.6.3 Test trajectories

The 3UPS+RPU PR was designed to perform human knee rehabilitation and diagnosis. These tasks require three fundamental movements: (i) flexion of hip, (ii) flexion-extension of knee, and (iii) internal-external rotation knee (Neumann, 2016).

The combination of these three knee movements and ankle rotation generates nine test trajectories (TT1-TT9). The nine trajectories were designed to make complete use of the workspace of the PR under study. Table 3.4 describes the movement performed by each trajectory in the lower limb and their corresponding motions in the PR under study.

During the simulation of the test trajectories, the $min\Omega$ and $\|J_D\|$ calculated for each test trajectory are shown in Figure 3.13 and Figure 3.14, respectively. The time between two different configurations is 0.1 s for all the trajectories in this Section. For every test performed in the 3UPS+RPU PR, the $\Omega_{3,4}$ is the closest to zero, i.e., $min\Omega = \Omega_{3,4}$.

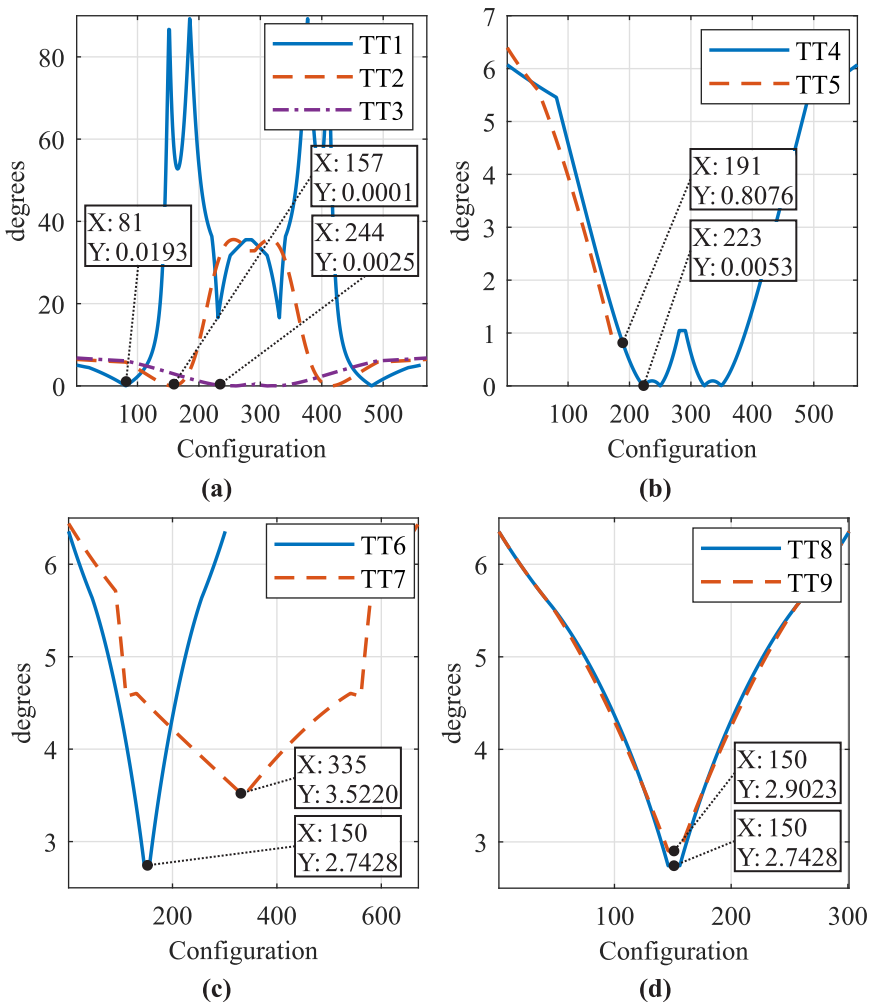

Figure 3.13: $min\Omega$ for (a) TT1-TT3, (b) TT4-TT5, (c) TT6-TT7, (d) TT8-TT9 during simulation in the 4-DOF PR.

The simulation of TT1 shows that $\|J_D\|$ does not reach zero. In this trajectory the minimum value of the $min\Omega$ index (0.0193 °) is reached in configuration 81 (see Figure 3.13a), where the $\|J_D\|$ has a value of 0.0143 (Figure 3.14a). The execution of TT1 shows that the PR loses control of its mobile platform, see Section 3.6.4.

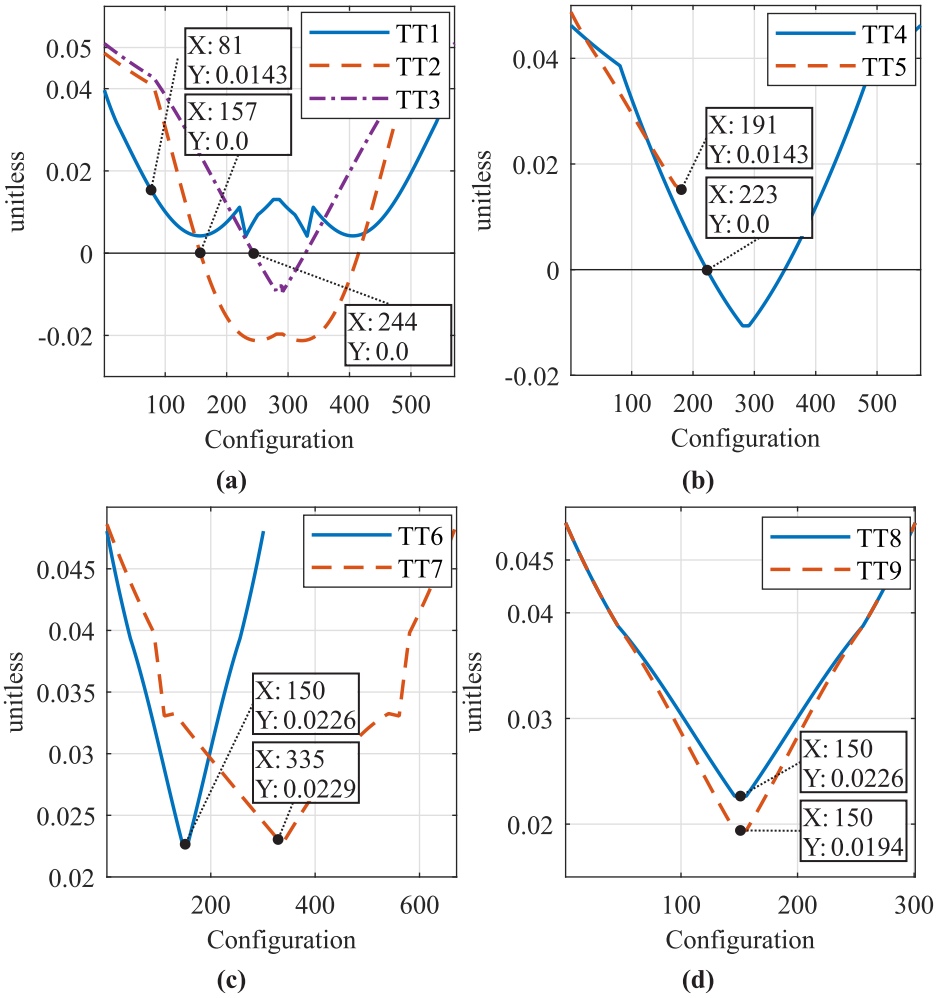

Figure 3.14: $\|J_D\|$ for (a) TT1-TT3, (b) TT4-TT5, (c) TT6-TT7, (d) TT8-TT9 during simulation in the 4-DOF PR.

In trajectories TT2-TT4 when the PR undergoes a configuration with $\|J_D\| = 0$ (see Figure 3.14a, Figure 3.14b), the $min\Omega$ index is zero (see Figure 3.13a, Figure 3.13b). These configurations in TT2, TT3, TT4 are 157, 244 and 233, respectively. Subsequently, in the simulations of TT5-TT9 the minimum $\|J_D\|$ (see Figure 3.14b-Figure 3.14d) is different from zero, as is the $min\Omega$ index (see Figure 3.13b-Figure 3.13d). For TT5-TT9 the configurations mentioned are 191, 150, 335, 150 and 150, respectively.

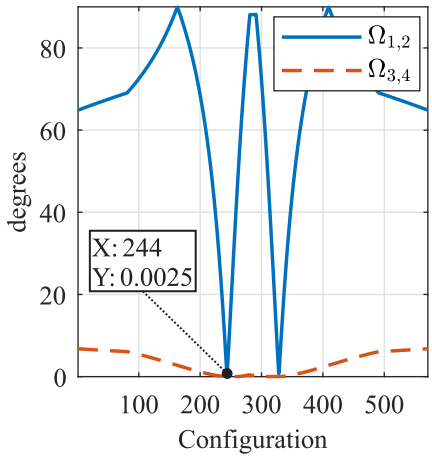

Figure 3.15: Two indices $\Omega_{i,j}$ during simulation of TT3 in the 4-DOF PR.

At every singular configuration detected by $min\Omega = 0$, it is verified that $min\Theta = 0$. All $\Omega_{i,j}$ presented in Section 3.6.1 are calculated. Nevertheless, only $\Omega_{3,4}$ is presented in Figure 3.13, as it corresponds to the angle closer to the singularity $min\Omega$. Thus, in the test trajectories the index $\Omega_{3,4}$ is the first to detect the Type II singularities. For TT3, Figure 3.15 shows that both $\Omega_{1,2}$ and $\Omega_{3,4}$ decrease until they become zero in a Type II singular configuration with $\Omega_{3,4}$ as the closer to zero. In configuration 244 the $\|J_D\| = \Omega_{1,2} = \Omega_{3,4} = \Theta_{1,2} = \Theta_{3,4} = 0$. According to these simulation results, we can establish that the $min\Omega$ is suitable for detecting the proximity to Type II singularities. Moreover, the simulation results verify that a theoretical Type II singularity is detected when $\Omega_{i,j} = \Theta_{i,j} = 0$.

3.6.4 Limit for the proximity to a singularity

When executing the trajectories of Table 3.4 on the actual PR, the trajectory TT1 was stopped in configuration 89 because of the loss of control of the mobile platform. Trajectory TT1 is theoretically non-singular. In configuration 89, where control of the PR is lost, $min\Omega = 0$ but $\|J_D\| = 0.0148$ not zero, see Figure 3.16a and Figure 3.17a.

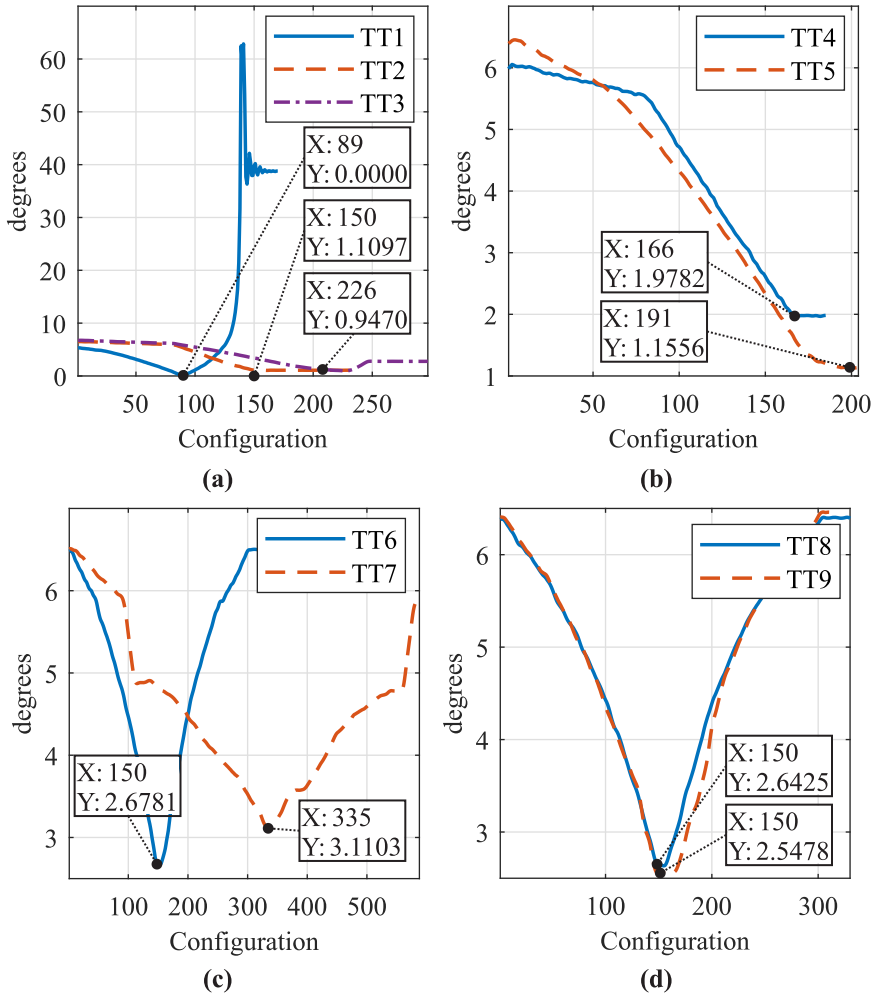

Figure 3.16: $min\Omega$ for (a) TT1-TT3, (b) TT4-TT5, (c) TT6-TT7, (d) TT8-TT9 measured in the actual 4-DOF PR.

In TT2, TT3, TT4 and TT5 control of the PR is lost in configurations 150, 226, 166, and 191, respectively. In those configurations, the value of the $min\Omega$ is greater than zero (Figure 3.16a and Figure 3.16b). The same results are shown for the $\|J_D\|$ in Figure 3.17a and Figure 3.17b. Therefore, these results verify experimentally that the control of the end-effector is lost in the vicinity of a theoretical Type II singularity $min\Omega = 0$. The results presented in Figure 3.16 and Figure 3.17 were calculated based on the measurements from the 3DTS.

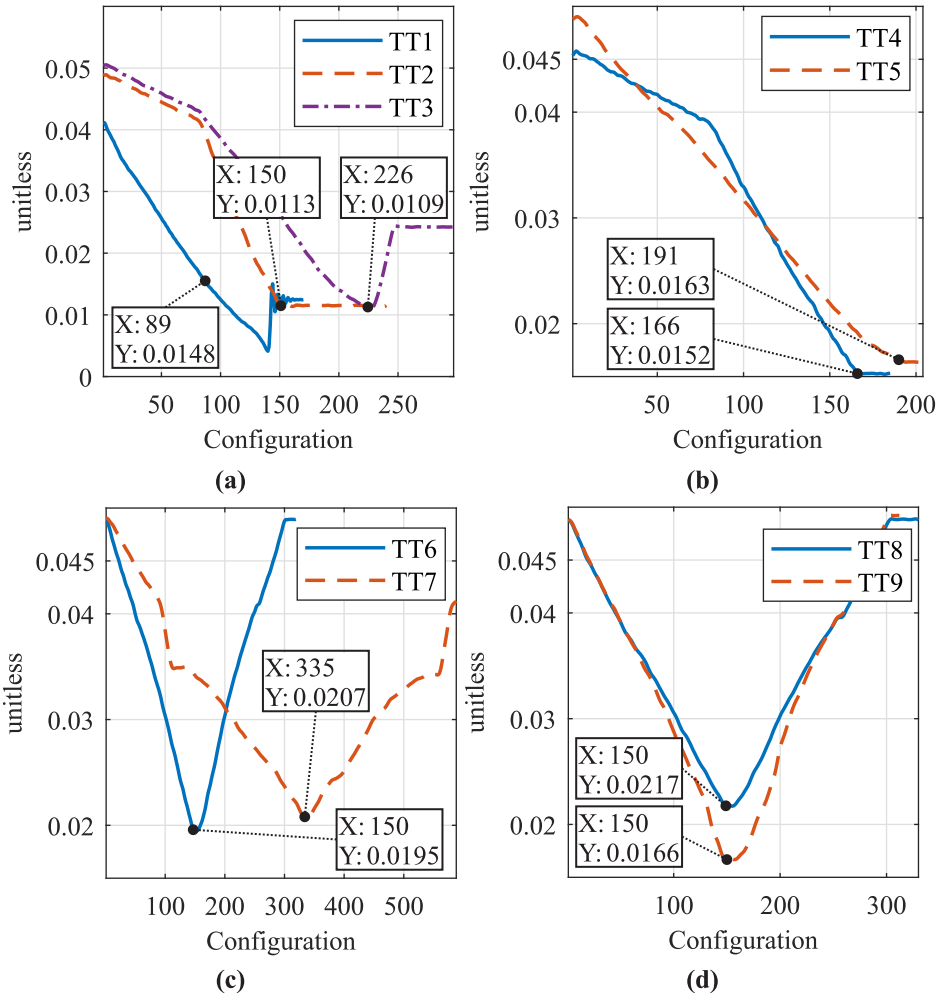

Figure 3.17: $\|J_D\|$ for (a) TT1-TT3, (b) TT4-TT5, (c) TT6-TT7, (d) TT8-TT9 measured in the actual 4-DOF PR.

In the case of TT6-TT9, the trajectories are performed easily. The values reached by the actual PR for the $min\Omega$ in each configuration are presented in Figure 3.16b to Figure 3.16d. The behaviour of the $\|J_D\|$ index in each configuration is presented in Figure 3.17b to Figure 3.17d. The Figure 3.16 provides a physical measurement of the proximity to a Type II singularity based on the $min\Omega$. On the other hand, the results for the $\|J_D\|$ show the difficulty of knowing how far the actual PR is from the Type II singularity due

to its dimensionless nature. Moreover, if $min\Omega = \Omega_{3,4}$ the approaching a Type II singularity is produced by the actuators on limbs three and four.

Table 3.5: Setting of the limit for proximity to a Type II singularity for 3UPS+RPU PR

Min.	$\|J_D\|$ (unitless)		$min\Omega$ (°)		Execution
	Theoretical	Measured	Theoretical	Measured	
TT1	0.0041	0.0041	0.0193	0.0000	It stops at sample 89
TT2	-0.0213	0.0113	0.0000	1.0508	It stops at sample 150
TT3	-0.0094	0.0109	0.0011	0.9470	It stops at sample 226
TT4	-0.0106	0.0152	0.0000	1.9782	It stops at sample 166
TT5	0.0143	0.0163	0.8077	1.1556	It stops at sample 191
TT6	0.0227	0.0195	2.7428	2.6781	Complete
TT7	0.0229	0.0207	3.5220	3.1103	Complete
TT8	0.0227	0.0217	2.7428	2.6425	Complete
TT9	0.0194	0.0166	2.9023	2.5478	Complete
Average		**0.0151**		**1.7900**	

The minimum values of $min\Omega$ and $\|J_D\|$ measured during the execution of the test trajectories are shown in Table 3.5. The theoretical minimum values are included in this table to contrast them with the measurements on the actual PR. Based on the proposed procedure in Section 3.4, the experimental limits for $min\Omega$ or $\|J_D\|$ are obtained by averaging the minimum values in Table 3.5. The closeness limit for $min\Omega$ (lim_Ω) is 1.80° on average. However, $min\Omega$ is a physical magnitude with a range between [0 180], hereby, the lim_Ω is set to 2°. For the case of the limit for the $\|J_D\|$ (lim_{J_D}) results in 0.015, this value is approximated to thousandths of a unit, as the $\|J_D\|$ has dimensionless values between [0 1].

3.6.5 Verification trajectories

In Section 3.6.3, nine test trajectories were generated ($n_{TT} = 9$) based on the fundamental movements for knee rehabilitation. Thus, three verification trajectories (VT1-VT3) were required in this experimental procedure to set the limit of closeness to a singular configuration. The verification trajectories start from a non-singular configuration ($min\Omega >> 0$) and progressively go to a singular configuration, i.e., $min\Omega$ decreases up to the final pose. The description of the movements of the three trajectories is shown in Table 3.6. Based on the lim_Ω set previously, the final configuration of VT1 is a singular configuration while the final pose for VT2 and VT3 are non-singular configurations.

Table 3.6: Description of verification trajectories for 3UPS+RPU PR

	Description
VT1	Independent linear motions to reach $X_f = 0.217\ m$, $Z_f = 0.705\ m$, $\theta = 27.74\ ^\circ$ and $\psi = 14\ ^\circ$
VT2	Independent linear motions to reach $X_f = 0.087\ m$, $Z_f = 0.705\ m$, $\theta = -3.93\ ^\circ$ and $\psi = 3.38\ ^\circ$
VT3	Independent linear motions to reach $X_f = 0.088\ m$, $Z_f = 0.724\ m$, $\theta = 6.39\ ^\circ$ and $\psi = 15.66\ ^\circ$

Figure 3.18 and Figure 3.19 show the values of the $min\Omega = \Omega_{3,4}$ and $\|J_D\|$ for the execution of the verification trajectories. After performing the trajectory VT1, the mobile platform does not lose control of its motions throughout the test. In VT1 the minimum value of the $min\Omega$ and the $\|J_D\|$ are higher than the limits established in Section 3.6.4. In the final configuration of trajectory VT2 the values of the angle $min\Omega$ and $\|J_D\|$ are below the established limits (see Figure 3.18 and Figure 3.19, respectively). In this configuration of VT2 an external force is applied, hereby the parallel robot cannot maintain its pose, i.e., the configuration is a Type II singularity. VT1 and VT2 confirm that the experimental limits lim_Ω and lim_{J_D} were correctly established.

Finally, trajectory VT3 is performed easily, where the final configuration has the $\|J_D\|$ greater than the experimental limit. However, for the same configuration the angle $min\Omega < lim_\Omega$. These particular configurations will be explained in detail in Section 3.7.

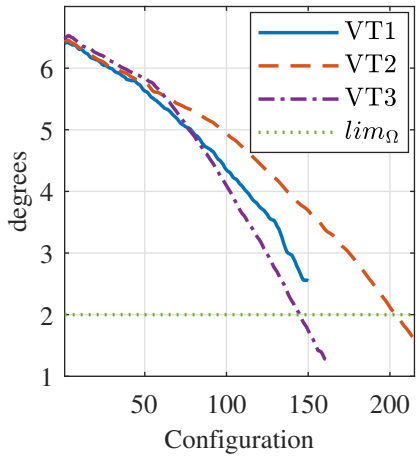

Figure 3.18: $min\Omega$ for VT1-VT3 measured in the actual 4-DOF PR.

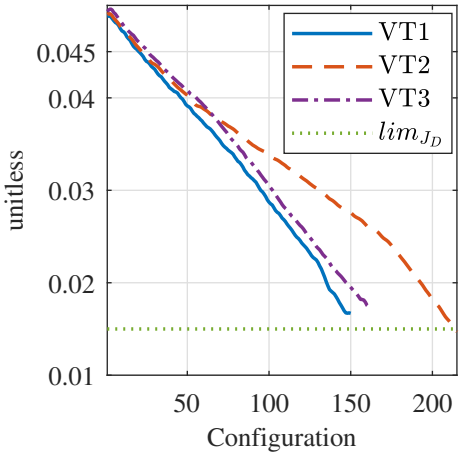

Figure 3.19: $\|J_D\|$ for VT1-VT3 measured in the actual 4-DOF PR.

3.7 Trajectories with assembly change points

In the previous section, the final configuration of trajectory VT3, the actual PR is not able to keep its position while an external force is applied to the mobile platform. In this configuration, the $\|J_D\|$ calculated is greater than the lim_{J_D} but the $min\Omega < lim_\Omega$ and $min\Theta >> 0$. Under these conditions, this configuration cannot be considered a Type II singularity or a cusp point.

However, due to that two actuators are contributing to the angular motion of the PR in the same direction, the control over the platform is lost.

These configurations with these characteristics are referred to herein as assembly change points (ACPs) because the loss of control over the end-effector experimentally allows an assembly mode change.

Based on the condition $min\Omega < lim_{\Omega}$ and $\|J_D\| > lim_{J_D}$, three trajectories with start in a non-singular pose and stop in an ACP are defined and named as ACT1-ACT3. Table 3.7 provides a brief description of the movements performed in each trajectory.

Table 3.7: Description of assembly change trajectories for 3U$\underline{P}$S+R$\underline{P}$U PR

	Description
ACT1	Independent linear motions to reach $X_f = 0.016\ m$, $Z_f = 0.707\ m$, $\theta = -14.67\ ^\circ$ and $\psi = -20\ ^\circ$
ACT2	Independent linear motions to reach $X_f = -0.1\ m$, $Z_f = 0.75\ m$, $\theta = -15\ ^\circ$ and $\psi = 0\ ^\circ$
ACT3	Independent linear motions to reach $X_f = -0.144\ m$, $Z_f = 0.704\ m$, $\theta = 7.78\ ^\circ$ and $\psi = 16.8\ ^\circ$

The execution of the three assembly change trajectories on the actual PR verifies the loss of control at the ACP. According to FKP, there are three feasible assembly modes for the final pose reached in ACT1.

Figure 3.20 shows the assembly mode change performed by the actual 3U$\underline{P}$S+R$\underline{P}$U PR. The figure shows the values of the indices $min\Omega$ and $\|J_D\|$ during the assembly change mode.

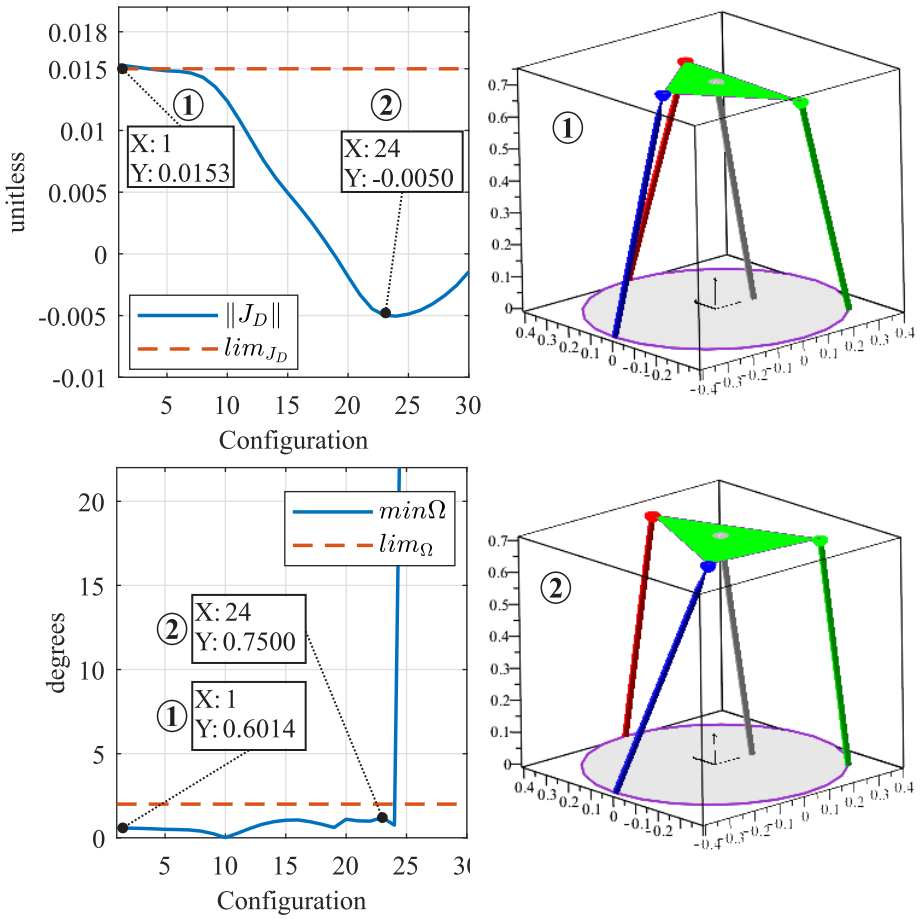

Figure 3.20: Representation of the assembly modes change in the final pose of the ATC1, with its indices $min\Omega$ and $\|J_D\|$.

Finally, for the ACP at the end of ATC3, four real assembly modes can be achieved, two of which are feasible. Figure 3.21 shows the non-singular assembly change performed by applying an external force to the mobile platform.

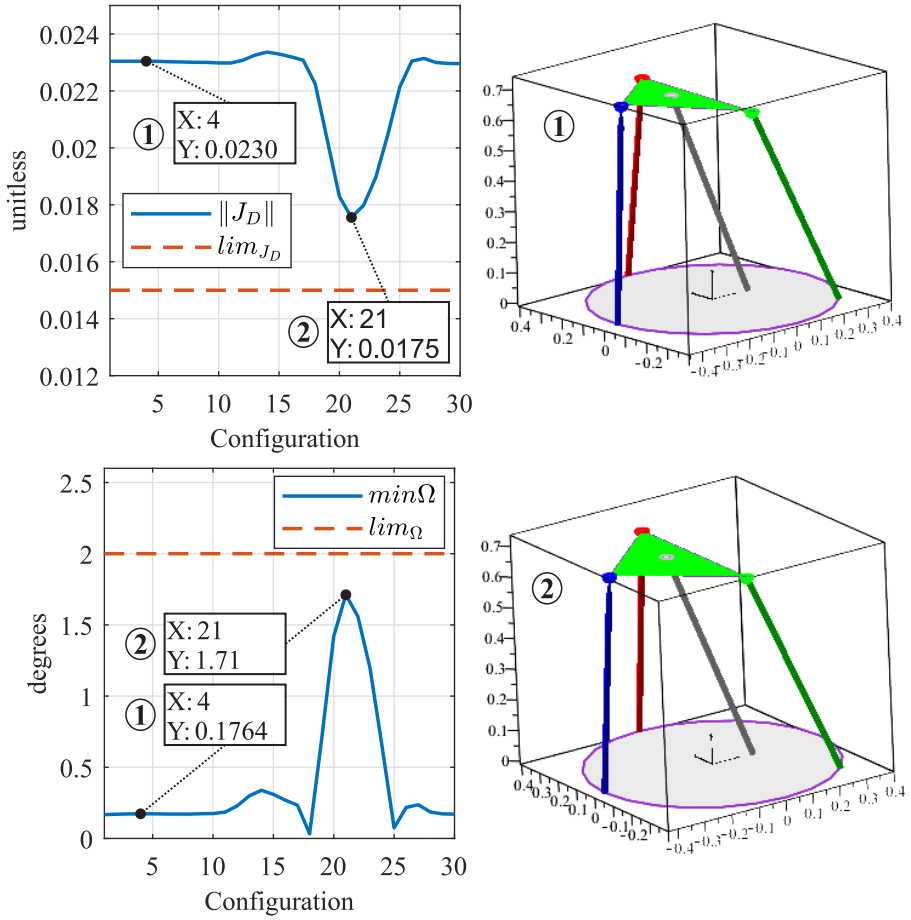

Figure 3.21: Representation of the assembly modes change in the final pose of the ATC3, with its indices $min\Omega$ and $\|J_D\|$.

The previous experimental observation allows us to state that, in fact, when a partial degeneration in a pair of unit OTS occurs, the actual robot loses the control capacity of at least one DOF. It is necessary to highlight the capability of the $min\Omega$ index to detect this type of configurations, both analytically and experimentally, something that cannot be done by $\|J_D\|$. Therefore, the ACPs are a contribution of this thesis because only the angle $min\Omega$ could identify these novel non-singular configurations.

3.8 Discussion and Conclusions

The detection of Type II singularities based on the angles $\Omega_{i,j}$ and $\Theta_{i,j}$ provides a novel index with physical meaning for a general non-redundant PR. The closeness to a Type II singularity is measured by the minimum angle $\Theta_{i,j}$ ($min\Theta$) in planar robots. In spatial case, the proximity to a singular configuration is measured by the minimum angle $\Omega_{i,j}$ ($min\Omega$) because the linear component could vanish in non-singular configurations.

The angle $min\Theta$ or $min\Omega$ identifies the pair of limbs that contributes to the motion of the end-effector in a similar direction. In other words, the limbs identified by these angles cause the loss of control over the mobile platform in the vicinity of a Type II singularity. Therefore, taking actions on the actuators in the limbs identified by the $min\Theta$ or $min\Omega$ could prevent a PR to reach a singular configuration. The next Chapter presents a novel Type II singularity avoidance algorithm for general purposes based on the $min\Theta$ and $min\Omega$.

The proposed experimental setting procedure, see Figure 3.3, is applied to the actual 3U$\underline{P}$S+R$\underline{P}$U PR to set a proper limit of the proximity to a Type II singularity. The experimental procedure verified that the loss of control over the movements of a PR appears in the vicinity of Type II singularities due to that non-modelled errors. In the 3U$\underline{P}$S+R$\underline{P}$U PR the non-modelled errors come from the clearances in the spherical joints. Note that the spherical joints were fabricated by the authors, using a steel sphere and a semi-spherical Teflon case.

The procedure to set a proper limit of proximity to a singularity cannot establish a direct relation between joint clearances and Type II singularities. However, the experimental measurements implicitly consider manufacturing errors such as joint clearances. In the 4-DOF PR, the joint clearances were quantified by measuring the pose of the end-effector while an external force is applied to a non-singular configuration. The 3DTS measured a maximum displacement of 2 mm and a maximum rotation of 2.5 ° from the origin of the mobile platform with the actuators locked.

The proposed procedure to set the limit of proximity to a singularity can be applied to another PR by modifying the set of trajectories based on the requirements of the new PR application. The set of test trajectories must be carefully selected because they directly affect the experimental limit of $\Omega_{i,j}$. For the 3U$\underline{P}$S+R$\underline{P}$U PR by using only nine singular and non-singular trajectories ensures enough accuracy for the specific knee rehabilitation application.

The angle $min\Omega$ identifies non-singular configurations where the angular contribution of motion of two limbs disappears. Despite being non-singular configurations the behaviour for practical purposes is equivalent, due to the loss of control of the mobile platform. The loss of control was verified by experimentation. This research named this configuration as assembly change point ACP due to a PR changes from one assembly mode to another.

Chapter 4

Algorithms to release and avoid Type II singularities

This chapter starts developing an algorithm to release a non-redundant Parallel Robot (PR) from a Type II singularity. The proposed release algorithm uses the minimum angle $\Theta_{i,j}$ and $\Omega_{i,j}$ to detect the closeness to a singular configuration in planar and spatial cases, respectively. The Singularity Release Algorithm (SRA) is integrated into a vision-based two-level hybrid controller for a 4-DOF PR. Two versions of SRA are developed to verify that the minimum angle $\Omega_{i,j}$ identifies the pair of actuators responsible for approaching a singular configuration. The first version of the SRA modifies the trajectory of the actuators on the limbs identified by the minimum angle $\Omega_{i,j}$ to release the PR from a singularity, and the second version moves the opposite limbs. The two versions of SRA are evaluated by simulation and experimentation.

Subsequently, the minimum angle $\Theta_{i,j}$ and $\Omega_{i,j}$ are used to develop a Type II singularity avoidance algorithm. In the vicinity of a Type II singularity, the avoidance algorithm calculates the deviation required in the subset of actuators responsible for the singularity. In other words, only the trajectory of the actuators identified by the minimum $\Theta_{i,j}$ or $\Omega_{i,j}$ is modified to avoid a Type II singularity. At each sample of the trajectory, only the trajectory of two actuators is modified according to a straight-line equation, i.e., optimisation procedures are unnecessary. Finally, the possible applications of the proposed algorithm are discussed.

4.1 Algorithm to release a parallel robot from Type II singularities

If a non-redundant PR reaches a Type II singularity, a strategy to escape or release the PR from this configuration is moving the actuators. However, the controller of the robot could move F actuators. Hence a method to identify the best set of actuators to be moved is needed. In addition, the movement of the actuators to release the PR from the singularity must maintain a minimum deviation from the original configuration. The previous chapter stated that the minimum angle $\Theta_{i,j}$ ($min\Theta$) or the minimum $\Omega_{i,j}$ ($min\Omega$) identifies the pair of limbs that contribute to the motion in the same direction. Thus, a trajectory change on the correspondent pair of actuators could prevent the PR to reach a singularity. However, this statement has not been verified yet. For this reason, a novel algorithm to release a PR from a Type II singularity is developed based on the $min\Theta$ and $min\Omega$ for the planar and spatial case, respectively.

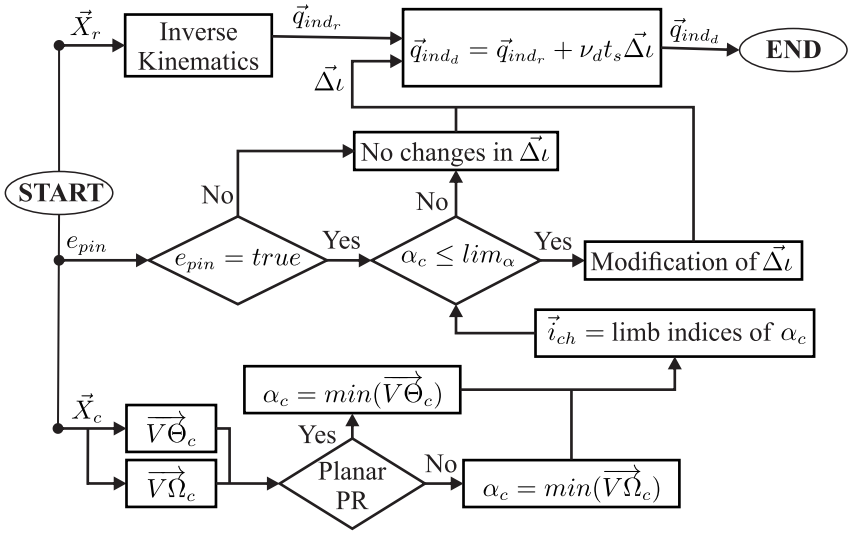

Figure 4.1: Block diagram for the algorithm to release a parallel robot from a Type II singularity.

The algorithm to release a PR from a Type II singularity is represented in a block diagram in Figure 4.1. For a discretised time instant, the proposed algorithm requires the reference pose $\vec{X}_r$ and the actual pose of the PR $\vec{X}_c$ simultaneously. In the closeness to a Type II singularity, the measurement of the $\vec{X}_c$ requires an external sensor because the pose of the PR calculated by the

Forward Kinematic Problem (FKP) has no unique solutions. The activation of the proposed Singularity Release Algorithm (SRA) is controlled by the Boolean variable e_{pin}.

The SRA first takes $\vec{X}_c$ to determine the F normalised Output Twist Screw (OTS), and calculates the arrays $\overrightarrow{V\Theta}_c$ and $\overrightarrow{V\Omega}_c$ that store all possible angles $\Theta_{i,j}$ and $\Omega_{i,j}$, respectively. Next, α_c calculates the minimum element in $\overrightarrow{V\Theta}_c$ for planar PRs or in $\overrightarrow{V\Omega}_c$ for a spatial case. $\vec{i}_{ch}$ stores the two limbs identified by α_c. The α_c defines if the algorithm uses the $min\Theta$ or $min\Omega$ to release the non-redundant PR from a Type II singularity. The SRA calculates a non-singular desired reference for the actuators $\vec{q}_{ind_d}$ as follows:

$$\vec{q}_{ind_d} = \vec{q}_{ind_r} + \nu_d t_s \vec{\Delta\iota} \tag{4.1}$$

where $\vec{q}_{ind_r}$ stands for the reference location in joint space calculated by solving the Inverse Kinematic Problem (IKP) of the PR with $\vec{X}_r$. ν_d is a constant velocity to escape from a Type II singularity in joint space, t_s the sample time for the trajectory discretisation, i.e., the controller sample time. $\vec{\Delta\iota}$ represents an integer vector ($F \times 1$) that counts the deviation required in the actuators during the releasing period.

The proposed algorithm is initialised with $\vec{\Delta\iota} = \vec{0}$, then $\vec{q}_{ind_d} = \vec{q}_{ind_r}$. If $e_{pin} = true$ and α_c is below a predefined threshold (lim_α), the $\vec{\Delta\iota}$ is modified to release the PR from a Type II singularity. Two rows of $\vec{\Delta\iota}$ are modified by one at each discretised instant time until the $\vec{q}_{ind_d}$ drives the PR to a non-singular configuration $\vec{X}_c$, i.e., $\alpha_c > lim_\alpha$. lim_α is determined according to the experimental procedure introduced in Section 3.4.

The $\vec{\Delta\iota}$ is modified by one only in the two rows corresponding to the elements in $\vec{i}_{ch}$, see Figure 4.2. Each row, identified by $\vec{i}_{ch}$, could hold, increase or decrease, generating eight possible modifications of $\vec{\Delta\iota}$. Considering that an actuator could stop (0), go forwards (1) or go backwards (-1), the eight possible modifications are grouped as columns of the matrix M_{av} as follows:

$$M_{av} = \begin{bmatrix} 1 & -1 & 1 & -1 & 1 & -1 & 0 & 0 \\ 1 & -1 & -1 & 1 & 0 & 0 & 1 & -1 \end{bmatrix} \tag{4.2}$$

For each k possible modification of $\vec{\Delta\iota}$, the $\vec{q}_{ind_d}$ and α_d are calculated. The index α_d is the element in $\overrightarrow{V\Theta}_d$ or in $\overrightarrow{V\Omega}_d$ for the limbs $\vec{i}_{ch}$. The $\overrightarrow{V\Theta}_d$ and

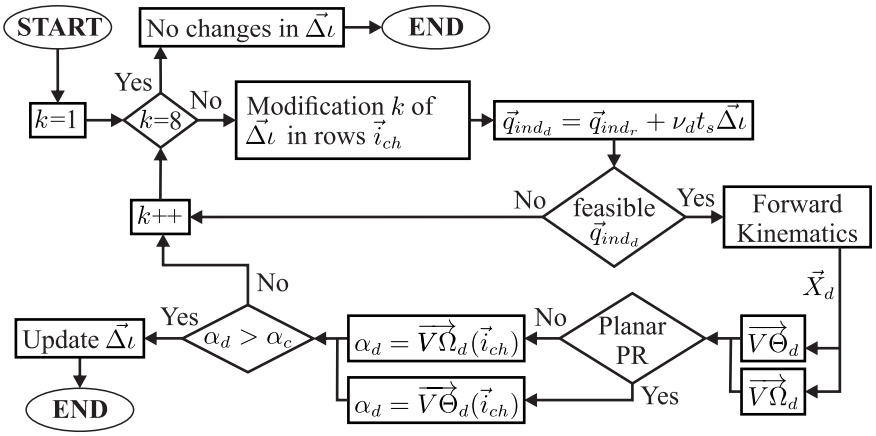

Figure 4.2: Block diagram for modifying $\vec{\Delta\iota}$ in the singularity release algorithm.

$\overrightarrow{V\Omega}_d$ allocate all possible angles $\Theta_{i,j}$ and $\Omega_{i,j}$ for the location $\vec{X}_d$. The best modification of $\vec{\Delta\iota}$ is selected to generate a feasible $\vec{q}_{ind_d}$ that steps the PR away from the singularity, i.e., $\alpha_d > \alpha_c$.

The effectiveness of the SRA is verified by implementing a vision-based hybrid controller to release the 3UPS+RPU PR from a Type II singularity. The prototype of the 3UPS+RPU PR, its control unit and a part of the 3D Tracking System (3DTS) are shown in Figure 4.3.

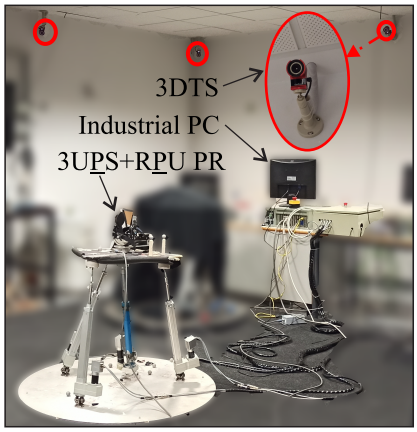

Figure 4.3: Equipment for implementing the algorithms to release and avoid Type II singularities in the 3UPS+RPU PR.

The hybrid controller combines two-level closed loops, the SRA works in the outer loop and a Linear Algebra-Based (LAB) algorithm is executed in the inner loop, see Figure 4.4. In this case, the $\vec{X}_c$ is measured by a OptiTrack® 3DTS detailed in Section 5.2.2.

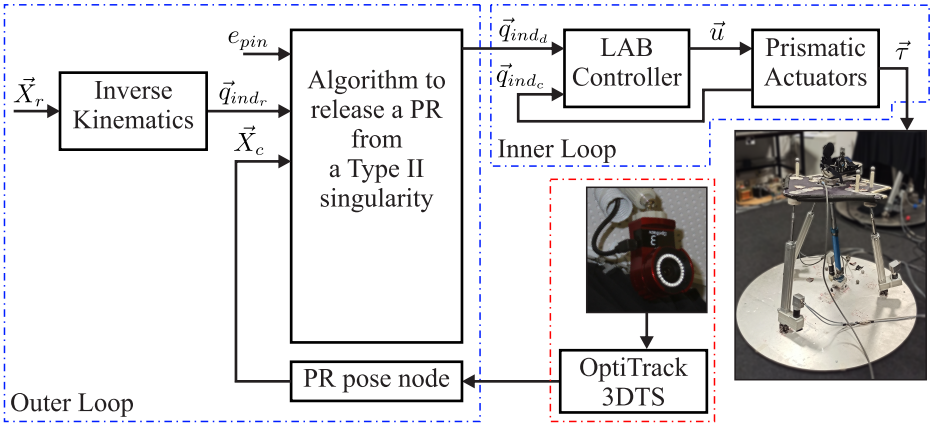

Figure 4.4: Architecture of the vision-based hybrid controller to release the 3UPS+RPU from a Type II singularity.

In the inner loop, the control signals $\vec{u}$ to track the desired trajectory $\vec{q}_{ind_d}$ are calculated by an LAB algorithm based on the measured location of the actuators $\vec{q}_{ind_c}$. The $\vec{u}$ is proportional to the effort from the actuators $\vec{\tau}$. In the outer loop, the SRA defines the desired trajectory $\vec{q}_{ind_d}$ based on the diagram of Figure 4.1 for a spatial case ($\alpha = min\Omega$).

Two versions of the SRA have been proposed to contrast the results when (i) moving the actuators that cause the singularity (SRA-V1) and (ii) moving the actuators that are unrelated to the Type II singularity (SRA-V2). The first version SRA-V1, releases a PR from a Type II singularity by moving the limbs identified by α_c. The SRA-V2 modifies the rows of $\vec{\Delta\iota}$ that are non-identified by α_c ($\vec{i}_{nc}$) to release the PR from the Type II singularity. The $\vec{i}_{nc}$ allocates the rows that are not in $\vec{i}_{ch}$. The SRA-V2 is designed to verify that moving the actuators identified by α_c is the best way to release the 3UPS+RPU PR from a Type II singularity.

In the next subsections, the vision-based hybrid controller with the SRA-V1 and SRA-V2 is evaluated through computer simulation, and the best version of both is implemented in the actual prototype of the 3UPS+RPU PR. The main objective of the simulation is verifying that only moving the limbs identified

by $min\Omega$ the PR under study is released from a Type II singularity. Thus, the capability of the angle $min\Omega$ to identify the pair of limbs involved in a singular configuration is also verified.

4.1.1 Simulation proofs

The simulations of the vision-based trajectory controller are performed with a kinematic and dynamic model of the 3UPS+RPU PR designed in MATLAB/Simulink. In both simulation and experimentation, the PR is moved from an initial non-singular pose to a singular configuration without activating the SRA. Then, it remains in the singular configuration for 15 s, after which the SRA (SRA-V1 or SRA-V2) in the outer loop is activated via e_{pin}. After launching the SRA, it has a lapse of 15 s to move the PR under study to a non-singular configuration.

Since the 3UPS+RPU PR is able to execute three fundamental knee movements, see Section 3.6.3. Combining these three fundamental movements, five knee rehabilitation trajectories ending in a Type II singularity (ST) have been generated, see Table 4.1. All knee trajectories are designed with a constant velocity of 0.02 m/s for the translational DOFs of the mobile platform and 0.03 rad/s for the rotational ones. The PR under study is controlled at a rate of 100 Hz with a maximum velocity of 0.01 m/s in the actuators. Thus, the parameters of the SRA are $\nu_d = 0.01\ m/s$ and $t_s = 10\ ms$.

Table 4.1: Description of trajectories with a Type II singularity at the end for 3UPS+RPU PR

	Lower limb	Type II singularity			
		x_m (m)	z_m (m)	θ (degrees)	ψ (degrees)
ST1	Hip flexion	0.01	0.70	8.60	17.76
ST2	Partial internal–external knee rotation	0.01	0.70	-1.15	8.02
ST3	Flexion–extension of the knee combined with ankle and knee rotations	0.05	0.72	-0.57	8.60
ST4	Flexion–extension of the knee combined with hip flexion	0.12	0.77	-3.44	6.30
ST5	Complete internal–external knee rotation	-0.05	0.73	5.73	18.91

The singular configurations of these five trajectories have $\Omega_{i,j}$ lower than the lim_{Ω} but different from zero, avoiding several forward kinematic solutions in the simulation. Thus, for simulation in MATLAB, $\vec{X}_c$ is calculated directly by solving the FKP avoiding the model of the 3DTS shown in Figure 4.4. The value of lim_{Ω} was taken from Section 3.6.4

The simulation of the five knee rehabilitation trajectories verifies that SRA-V1 and SRA-V2 release the 3UPS+RPU PR from a singular configuration. In trajectories ST1-ST4 $\alpha = \Omega_{3,4}$, and $\alpha = \Omega_{2,3}$ for ST5. Figure 4.5 presents the values of the Type II singularity index α during the simulation of the trajectories ST1 and ST4. The reference of the index α is represented as α_r. The α_c reached by the virtual PR are labelled according to the version of the SRA, i.e., SRA-V1 and SRA-V2. Figure 4.5 shows how the index α_c increases when e_{pin} is activated until the lim_{Ω} is crossed. The results of the index α for the rest of the trajectories are not plotted because they have an analogous behaviour.

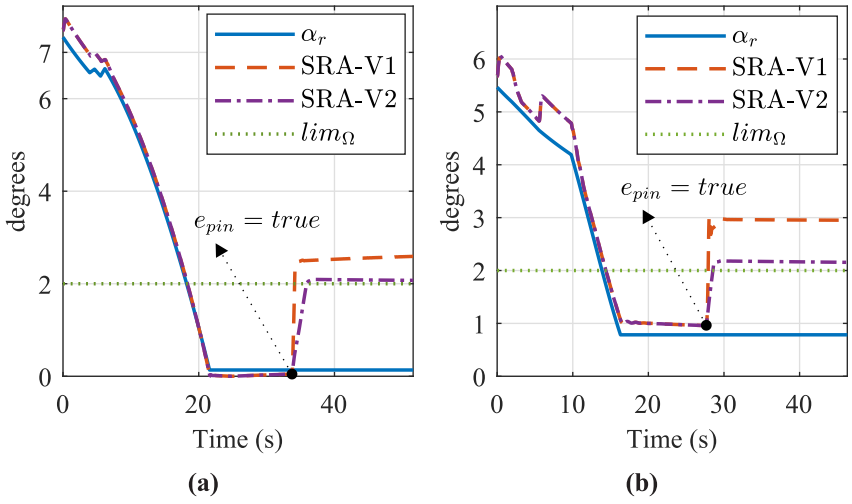

Figure 4.5: α for (a) ST1 and (b) ST4 during simulation in the 4-DOF PR.

The performance of the SRA-V1 and SRA-V2 is evaluated by quantifying the deviation on the reference $\vec{q}_{ind_r}$. This deviation is defined by the Mean Absolute Error (MAE) in tracking $\vec{q}_{ind_r}$ as follows:

$$MAE = \frac{1}{F}\sum_{i=1}^{F}\left(\frac{1}{n_s}\sum_{j=1}^{n_s}\left|q_{ind_r}(i,j) - q_{ind_c}(i,j)\right|\right) \tag{4.3}$$

where n_s is the number of samples taken after the activation of e_{pin}, i stands for the actuator under analysis, and j represents an arbitrary sample.

The deviation on the reference $\vec{q}_{ind_r}$ is represented in percentage by the Mean Absolute Percentage Error (MAPE):

$$MAPE = \frac{100}{F} \sum_{i=1}^{F} \left(\frac{1}{n_s} \sum_{j=1}^{n_s} \left| \frac{q_{ind_r}(i,j) - q_{ind_c}(i,j)}{q_{ind_r}(i,j)} \right| \right) \tag{4.4}$$

Table 4.2 shows the MAE and MAPE results for the simulation of the vision-based hybrid controller using SRA-V1 and SRA-V2. In this table, the MAE and the MAPE show that SRA-V1 has less error in position tracking than that of SRA-V2 during release from the Type II singularity. It means that SRA-V1 needs fewer movements of the actuators than SRA-V2 to release the PR from a singular configuration. These results show that moving the pair of actuators identified by the index $\alpha_c = \Omega_{3,4}$ is the best option to release a PR from a Type II singularity.

Table 4.2: Performance of the SRA-V1 and SRA-V2 in simulation for 3UPS+RPU PR

	MAE (mm)		MAPE (%)	
	SRA-V1	SRA-V2	SRA-V1	SRA-V2
ST1	3.87	10.74	0.53	1.40
ST2	1.09	2.04	0.14	0.28
ST3	1.77	6.15	0.24	0.82
ST4	3.00	10.24	0.38	1.25
ST5	10.74	10.44	1.43	1.37
Average	**4.09**	**7.92**	**0.54**	**1.02**

4.1.2 Experimental proofs

After testing the novel SRA in simulation, the next step is implementing the vision-based controller with SRA-V1 on the real robot according to the diagram shown in Figure 4.4. Although both the simulation and experimentation have the same procedure, the experimentation presents three notable differences:

- $\vec{X}_c$ is provided by processing the data stream from the 3DTS in real time, see Section 5.2.2.

- During the 15 s before the SRA is activated, an external perturbation is applied to the PR. The external perturbation is a force that the researcher applies to the PR by hand to check whether the mobile platform experiences uncontrolled motion. This is because, in a Type II singularity, the PR can vary its pose despite the actuators being blocked.
- After the SRA is activated, the same external perturbation is applied to the PR. In this case, the 3UPS+RPU PR will regain its stiffness and the researchers can move the robot.

Regarding the actual PR, the external limbs are driven by Festo DNCE 32-BS10 prismatic actuators, and the central limb is driven by a NIASA M100-F16 prismatic actuator. All the actuators are attached to Maxon 148867 150 W DC motors commanded by ESCON 50/5 servo controllers. The ESCON 50/5 controls the force of the linear actuators $\vec{\tau}$ by limiting the current consumed by the DC motors. The current is proportional to the control signals $\vec{u}$, and the DC motors are equipped with incremental encoders with a resolution of 500 counts per turn. The incremental encoders are read from an industrial computer using a PCI 1784 Advantech card. The PCI 1784 Advantech has four 32-bit quadruple AB phase encoder counters. The $\vec{u}$ are generated by the same computer by means of a 12-bit, 4-channel PCI 1720 Advantech card.

The proposed vision-based hybrid controller runs on the Robot Operating System 2 (ROS2) (Maruyama et al., 2016). The two levels of the proposed controller are implemented in a modular way using the C++ programming languages. The processing of the data stream from the 3DTS is carried out by a C++ handler named ***PR pose node*** based on libraries provided by OptiTrack, see Section 5.2.2.

For the experimental evaluation, the proposed trajectory controller is executed at 100 Hz with a maximum velocity of 0.01 m/s in joint space, hereby the SRA is set with $\nu_d = 0.01\ m/s$ and $t_s = 10\ ms$. For the actual PR, a third performance index is added to evaluate the smoothness of the movements performed by the controller. It is measured with the absolute variation rate (AVR) of the forces exerted by the actuators $\vec{\tau}$:

$$AVR = \frac{1}{F}\sum_{i=1}^{F}\left(\sum_{j=2}^{n_s}\left|\tau\left(i,j\right)-\tau\left(i,j-1\right)\right|\right) \tag{4.5}$$

Table 4.3 shows the results of performance tracking of $\vec{q}_{ind_r}$ of the vision-based hybrid controller implemented on the 3UPS+RPU PR. The MAE and MAPE

for experimentation are similar to the simulation results (see Table 4.2), with a low AVR ensuring smooth movements of the mobile platform.

Table 4.3: Performance of the SRA-V1 in the actual 3UPS+RPU PR

	MAE (mm)	MAPE (%)	AVR (N)
ST1	3.26	0.45	0.22
ST2	3.02	0.41	0.52
ST3	2.05	0.27	0.17
ST4	2.14	0.27	0.46
ST5	10.66	1.42	1.44
Average	**4.22**	**0.56**	**0.56**

Figure 4.6 shows the index α when the actual PR is released from a singular configuration in the trajectory ST1 and ST4 with $\alpha = \Omega_{3,4}$. This figure shows that the reference of the $\Omega_{3,4}$ (signal α_r) is followed by the actual PR (α_c) until the SRA is activated. The variation of α_c before SRA activation is due to the external force applied to the actual PR. It is important to mention that the actual PR recovers its stiffness at the end of all experiments. To the best of the author's knowledge, this is the first time that an actual PR has been driven to a Type II singularity and successfully released from it by using the index $min\Omega$.

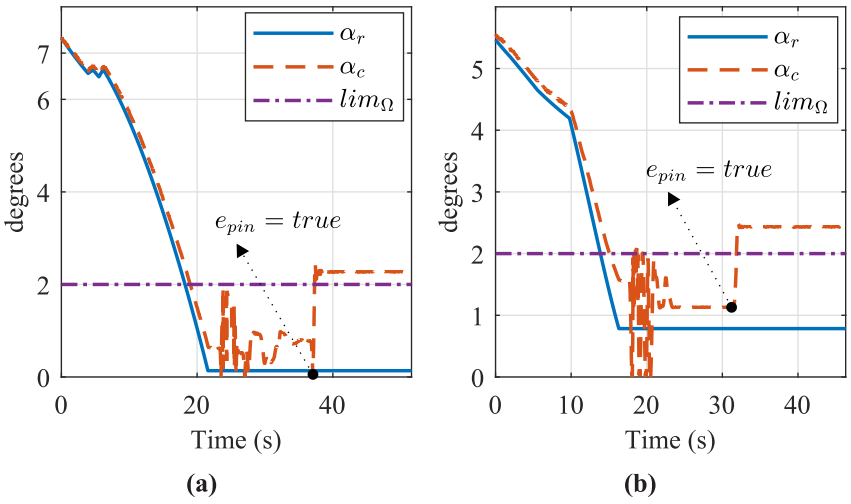

Figure 4.6: α measured for (a) ST1 and (b) ST4 in the actual 4-DOF PR.

The recording of the experimental evaluation of the hybrid controller for trajectories ST1 and ST5 are available in *https://imbio3r.ai2.upv.es/videos/TypeII_singularities*.

Due to that $\alpha_c = \Omega_{3,4}$, limbs 3 and 4 are involved in the Type II singularity. Figure 4.7 shows the location for the actuator on limb 3 ($* = q_{33}$) and limb 4 ($* = q_{42}$) with respect to the time during ST1. In this figure, the measured position ($*_c$) accurately tracks the desired position ($*_d$), which differs from the reference ($*_r$) only after SRA activation. Furthermore, this figure clearly shows that the desired position is modified by a few millimetres (see Figure 4.7b) from the reference to release the actual PR from the Type II singularity.

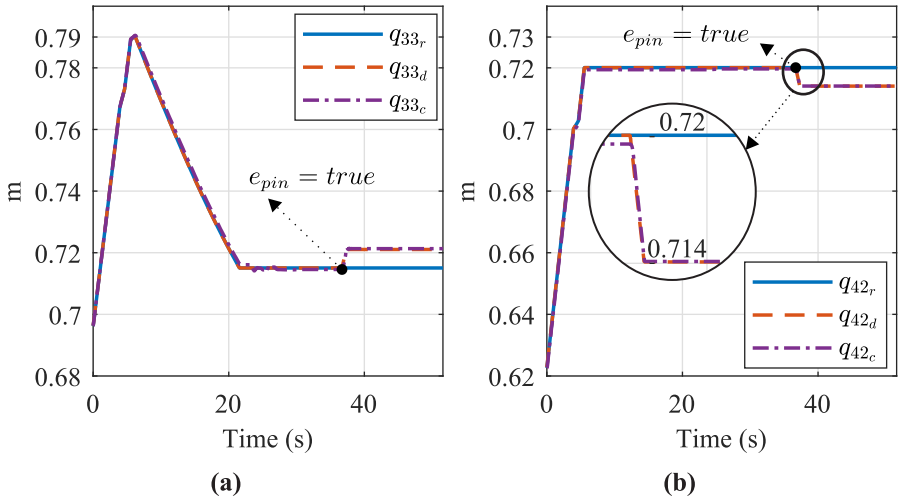

Figure 4.7: Location tracking for the actuators in limb (a) 3 and (b) 4 during the execution of ST1 in the actual 4-DOF PR.

Figure 4.8 shows the smooth forces exerted by the actuators on limbs 3 and 4 during the trajectory ST1 on the actual PR. These forces are proportional to control actions calculated by the hybrid controller implemented.

Figure 4.9 shows the measures of the 3DTS for x_m and θ, that represents two DOFs of the actual 3UPS+RPU PR. The reference trajectory ($*_r$) for x_m and θ is plotted in contrast to they measure ($*_c$) from the 3DTS. This figure also shows the estimation ($*_{\hat{c}}$) of x_m and θ by solving FKP based on the encoder's feedback. Despite both estimated and experimental measures being calculated online, only the experimental measure detects the movement produced by the external force applied to the PR.

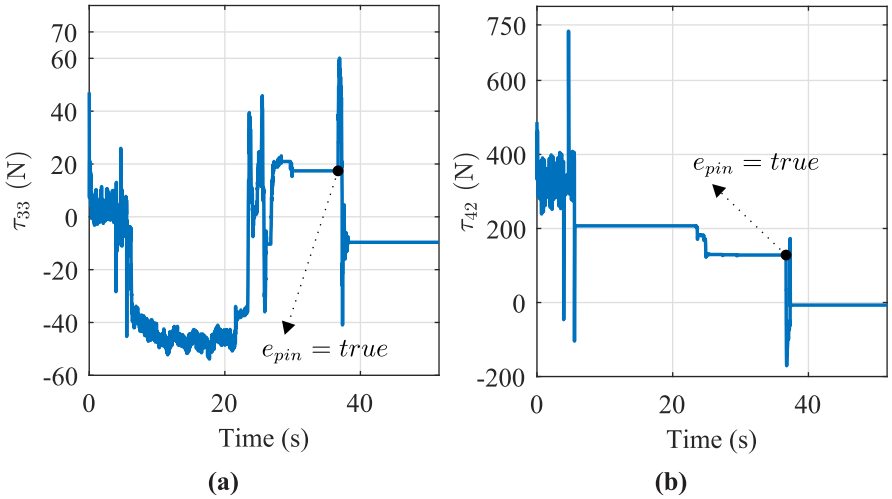

Figure 4.8: Forces exerted by the actuators in limb (a) 3 and (b) 4 during the execution of ST1 in the actual 4-DOF PR.

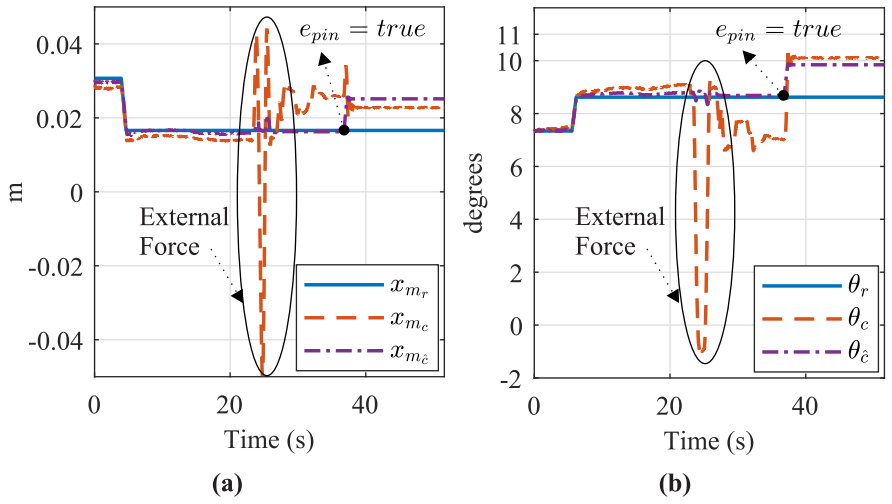

Figure 4.9: Measures of the DOFs (a) x_m and (b) θ during execution of ST1 in the actual 4-DOF PR.

The period of time when the external force is applied is circled in Figure 4.9. This verifies that when the 3UPS+RPU PR is in a Type II singularity, the actual pose cannot be determined by solving the FKP.

The experimental results conclude that the vision-based hybrid controller with SRA-V1 releases an actual PR from a Type II singularity with minimum deviation from the original reference. Therefore, the $min\Theta$ or $min\Omega$ are able to identify the pair of limbs that contributes to reaching a Type II singularity.

4.2 Type II singularity avoidance algorithm

In contrast to the singularity release algorithm, the Type II singularity avoidance algorithm has to modify the trajectory of a non-redundant PR before being close to the singular configuration. Moreover, after avoiding the singular configuration the modification introduced in the original trajectory must vanish.

For a discretised instant time, the reference pose of the mobile platform $\vec{X}_r$ and the actual pose reached by the PR $\vec{X}_c$ are the inputs required by the avoidance algorithm. Each discretised instant time, the inputs $\vec{X}_r$ and $\vec{X}_c$ are taken simultaneously. Solving IKP defines the correspondent reference location in joint space $\vec{q}_{ind_r}$. Figure 4.10 shows an overview of the algorithm proposed.

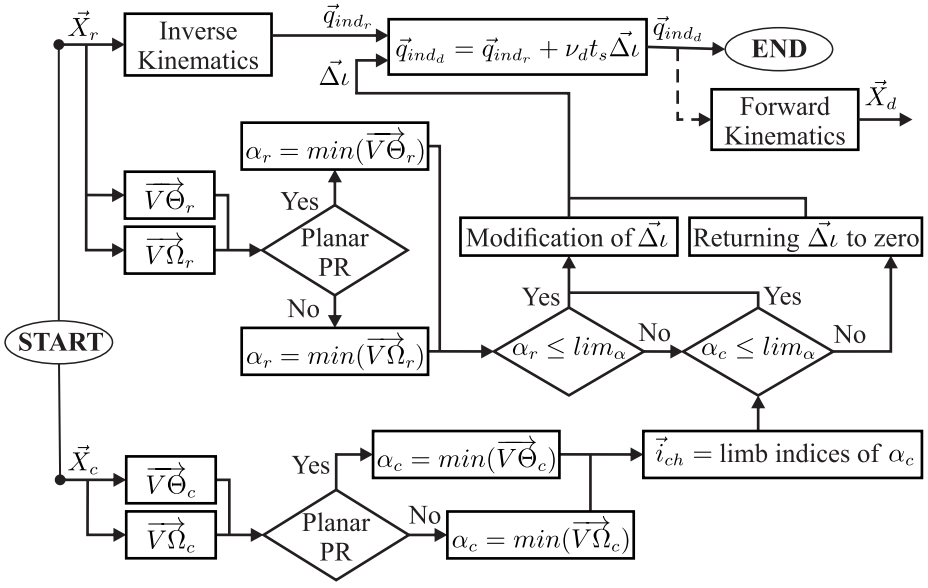

Figure 4.10: Block diagram for Type II singularity avoidance algorithm.

The avoidance algorithm first takes $\vec{X}_r$ to calculate all $\hat{\$}_{O_i}$ $(i = 1 \dots F)$, and calculates the arrays $\overrightarrow{V\Theta}_r$ and $\overrightarrow{V\Omega}_r$ that store all possible angles $\Theta_{i,j}$ and $\Omega_{i,j}$ $(i, j = 1 \dots F, i \neq j)$, respectively. Next, α_r calculates the minimum element in $\overrightarrow{V\Theta}_r$ for planar PRs or in $\overrightarrow{V\Omega}_r$ for a spatial case. Analogously, the $\overrightarrow{V\Theta}_c$, $\overrightarrow{V\Omega}_c$, α_c are calculated for the measured $\vec{X}_c$, and $\vec{i}_{ch}$ stores the two limbs identified by α_c.

The proposed algorithm calculates a non-singular desired location $\vec{q}_{ind_d}$ by using (4.1). In this case, the ν_d and t_s are the constant velocity for singularity avoidance and the sample time for the trajectory discretisation, respectively. The non-singular desired reference in configuration space $\vec{X}_d$ could be calculated by solving the FKP for $\vec{q}_{ind_d}$.

The proposed algorithm starts with $\vec{q}_{ind_d} = \vec{q}_{ind_r}$, i.e., $\vec{\Delta\iota} = \vec{0}$. If α_r is below a predefined threshold (lim_α), the $\vec{\Delta\iota}$ is modified because the reference $\vec{X}_r$ is proximal to a Type II singularity. Two rows of $\vec{\Delta\iota}$ are modified by one at each discretised instant time until the $\vec{q}_{ind_d}$ drives the PR to a non-singular configuration $\vec{X}_c$, i.e., $\alpha_c > lim_\alpha$. With $\alpha_c > lim_\alpha$, if the reference $\vec{X}_r$ becomes non-singular ($\alpha_r > lim_\alpha$), $\vec{\Delta\iota}$ must return progressively to zero because a Type II singularity has been avoided. The process of modifying $\vec{\Delta\iota}$ is identical to the one used in the singularity release algorithm, see Figure 4.2. In contrast, Figure 4.11 explains how $\vec{\Delta\iota}$ returns to zero after Type II singularity avoidance.

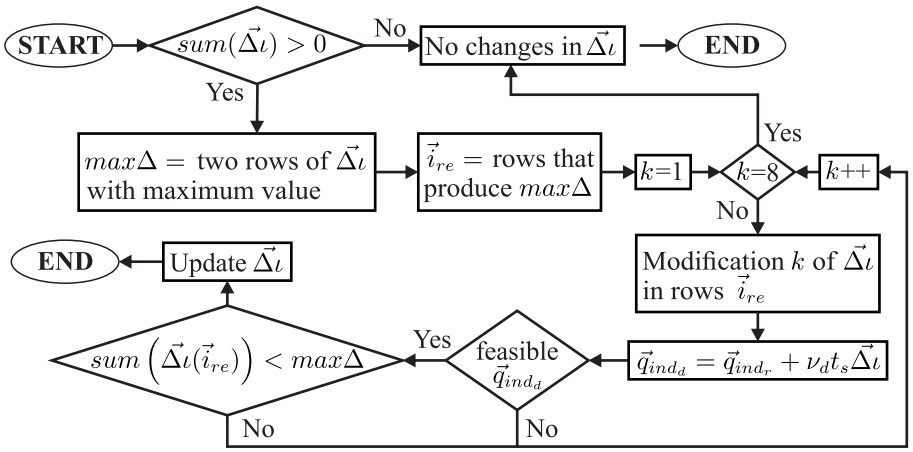

Figure 4.11: Block diagram for returning $\vec{\Delta\iota}$ to zero in the singularity avoidance algorithm.

In Figure 4.11, the two rows of $\vec{\Delta\iota}$ with the maximum value ($max\Delta$) are identified and saved in $\vec{i}_{re}$. The $\vec{\Delta\iota}$ is modified in the rows $\vec{i}_{re}$ according to the columns of M_{av}, (4.2), generating eight new possible $\vec{\Delta\iota}$. The proper $\vec{\Delta\iota}$ is selected to ensure a feasible $\vec{q}_{ind_d}$ and to decrease the absolute value of $\vec{\Delta\iota}$. The returning procedure continues until $\vec{\Delta\iota} = \vec{0}$. The value of lim_α is calculated previously to implement the Type II singularity avoidance algorithm by the experimental setting procedure presented in Section 3.4.

The proposed avoidance algorithm is designed to modify the trajectory of two actuators because, in the closeness of a Type II singularity, at least two normalised OTSs are parallel. The case of three $\hat{\$}_{O_i}$ aligned appears when the PR already reaches the singular configuration, see Figure 3.10. However, if three $\hat{\$}_{O_i}$ become parallel in closeness to a singular configuration, the algorithm modifies the trajectory of the actuators by pairs. For example, consider a spatial PR at an arbitrary instant time. If the $\Omega_{1,2}$ and $\Omega_{1,3}$ are the minimum elements in α_c the avoidance algorithm modifies the trajectory for actuators 1 and 2. Assuming that the $\Omega_{1,2}$ has increased for the next discretised instant time, the proposed algorithm modifies the trajectory on actuators 1 and 3.

It is important to emphasise that the proposed avoidance algorithm is limited to Type II singularities. It is because the angles $min\Omega$ and $min\Theta$ measure when two actuators transmit motion to the end-effector in the same direction, i.e., they detect the loss of controlled DOFs. The proposed avoidance algorithm is unsuitable for Type I singularities because, in that configuration, the PR retains control over all DOFs.

Figure 4.10 shows that the proposed algorithm does not require complex optimisation problems, making it suitable for offline trajectory planning and combining with controllers for online Type II singularity avoidance.

In offline trajectory planning, the avoidance algorithm is applied at each sample of a discrete reference trajectory of n_T samples ($n_T > 1$). The reference trajectory could have different shapes, including a linear interpolation between two different desired points. The avoidance parameter t_s is set to the sample time of the reference trajectory while ν_d is the average of the velocity reference trajectory. In offline case, the $\vec{X}_c$ is initialised with $\vec{X}_r$, and for the consequent iterations, $\vec{X}_d$ is used as a feedback signal, i.e., $\vec{X}_c = \vec{X}_d$.

For online applications, the algorithm is implemented by setting t_s as the controller sample time and ν_d as the average feasible velocity for the PR under analysis. In the online case, $\vec{X}_c$ could be measured by a 3DTS or by estimation

based on embedded encoders. It is possible because the proposed Type II singularity avoidance algorithm ensures non-singular configuration of the PR at every time, i.e., the FKP is solved with accuracy.

Therefore, The Type II singularity avoidance algorithm presents the following advantages:

- At each discretised instant time, only two actuators require modifications for singularity avoidance.
- The avoidance parameters ν_d and t_s are set directly by the PR application.
- Low computational cost due to the absence of optimisation functions.

The proposed algorithm is applied to the planar and spatial case to verify the advantages presented above. The novel Type II singularity avoidance algorithm is applied to offline trajectory planning using a five bars mechanism in Section 4.2.1, and Section 4.2.2 applies the proposed avoidance algorithm for offline and online trajectory planning in a 4-DOF PR for knee rehabilitation.

4.2.1 Planar case: five bars mechanism

The offline trajectory planning starts with generating a constant velocity trajectory on the plane xy with a Type II singularity in the middle. The description of the trajectory in configuration space is shown in Table 4.4. Next, the singularity avoidance algorithm is applied to the original trajectory to obtain the non-singular version of the trajectory. The 5R mechanism is driven by an Arduino Uno board at a rate of 200 Hz with a maximum working velocity of 29 $^\circ/s$. Therefore, the singularity avoidance algorithm is set to $t_s = 20\ ms$ and $\nu_d = 0.5\ rad/s$.

Table 4.4: Description of the trajectory for offline planning in the 5R mechanism.

Location	x_p (m)	y_p (m)	time (s)
Start	0	0.09	0
Singularity	-0.03	0.05	2
End	0	0.09	4

Due to that the 5R mechanism is a planar PR, the closeness to a Type II singularity is measured by $\Theta_{1,2}$, see Section 3.5. For offline trajectory planning, $\alpha = \Theta_{1,2}$ and the threshold for avoidance is set to 6 $^\circ$ ($lim_\alpha = lim_\Theta = 0.1047\ rad$). Based on simulation results, lim_Θ is defined based on the experimental pro-

cedure to set the limit of proximity to a singular configuration described in Section 3.4.

Figure 4.12a shows that the non-singular trajectory holds α_d greater than lim_α while the original trajectory reaches a singularity at 2 s ($\alpha_r = 0$). The Type II singularity avoidance is verified by analysing the $\|J_D\|$ of the original ($\|J_D\|_r$) and the non-singular trajectory ($\|J_D\|_d$). Figure 4.12b shows that $\|J_D\|_d$ always differs from zero while $\|J_D\|_r$ reaches a Type II singularity at 2 s. In this research, the $\|J_D\|$ is not deeply analysed. However, Sosa-Lopez et al. (2017) shows the expression of $\|J_D\|$ considering $\vec{X} = [x_p \quad y_p]^T$ and $\vec{q}_{ind} = [q_{11} \quad q_{21}]^T$.

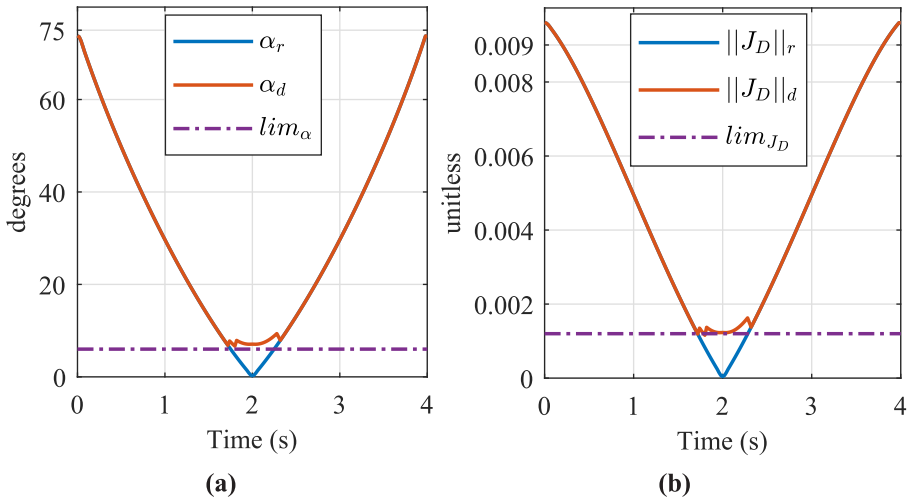

Figure 4.12: Type II singularity proximity indices (a) α (b) $\|J_D\|$ for the 5R mechanism in offline trajectory planning.

Figure 4.13 shows the original ($*_r$) and the non-singular trajectory ($*_d$) generated for the actuator on limbs 1 ($* = q_{11}$) and 2 ($* = q_{21}$). This figure shows that the proposed algorithm requires a maximum deviation of 1.2 ° in the joint trajectories to avoid a Type II singularity.

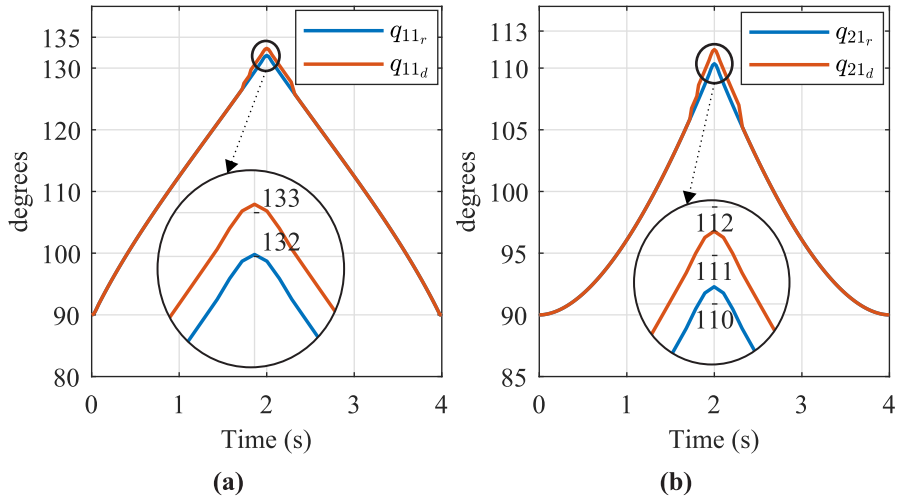

Figure 4.13: Non-singular trajectory generated for (a) q_{11} (b) q_{21} in the 5R mechanism.

The offline trajectory planning was performed in MATLAB on a desktop PC with 32 GB of RAM. Table 4.5 compares the proposed algorithm with a Constrained Multi-Objective (CMO) algorithm and roadmap (C-space) algorithm. In Table 4.5, t_I represents the average elapsed time in each iteration, and t_T is the total trajectory time. The results for the CMO algorithm were taken from Khoukhi et al. (2009) for offline trajectory planning in a planar PR. The results for the C-space algorithm were calculated based on the information reported in Bohigas et al. (2013) for offline path planning in 3-RRR mechanism.

According to Table 4.5, the proposed avoidance algorithm is the fastest during offline trajectory planning, with an average elapsed time of 0.5 ms. Thus, the Type II singularity avoidance algorithm is suitable for offline trajectory planning with a minimum modification of the original trajectory and low computational cost.

Table 4.5: Comparative results of avoidance algorithm for offline trajectory planning in planar PRs.

Algorithm	t_I (s)	t_T (s)	Processor
Proposed	0.0005	4	Intel Core i7 3.7 GHz
CMO (Khoukhi et al., 2009)	1.2620	9.5	unspecified
C-space (Bohigas et al., 2013)	0.0756	1	Intel Core i7 2.66 GHz

4.2.2 Spatial case: 3UPS+RPU parallel robot

For offline trajectory planning, the original trajectory represents a knee rehabilitation exercise, specifically a hip flexion, where a singular configuration arises halfway. The description of the trajectory for hip flexion in configuration space is shown in Table 4.6. Then, the proposed Type II singularity avoidance algorithm is applied to generate a new non-singular trajectory. The control unit works at a rate of 100 Hz and the maximum working velocity is 0.01 m/s because the actual PR works in knee rehabilitation. For these reasons, the singularity avoidance algorithm is adjusted to $t_s = 10\ ms$ and $\nu_d = 0.01\ m/s$.

Table 4.6: Description of the trajectory for offline planning in the 3UPS+RPU PR.

Location	x_m (m)	z_m (m)	θ (degrees)	ψ (degrees)	time (s)
Start	0.038	0.640	1.14	3.64	0
Singularity	0.016	0.707	8.619	18.15	12.76
End	0.038	0.640	1.14	3.64	40.53

The 3UPS+RPU PR is an spatial case, hereby $\alpha = min(\overrightarrow{V\Omega})$ with $\overrightarrow{V\Omega} = [\Omega_{1,2} \quad \Omega_{1,3} \quad \Omega_{1,4} \quad \Omega_{2,3} \quad \Omega_{2,4} \quad \Omega_{3,4}]$. According to the Section 3.6.4, the threshold for avoidance is set to 2 ° ($lim_\alpha = lim_\Omega = 0.0349\ rad$).

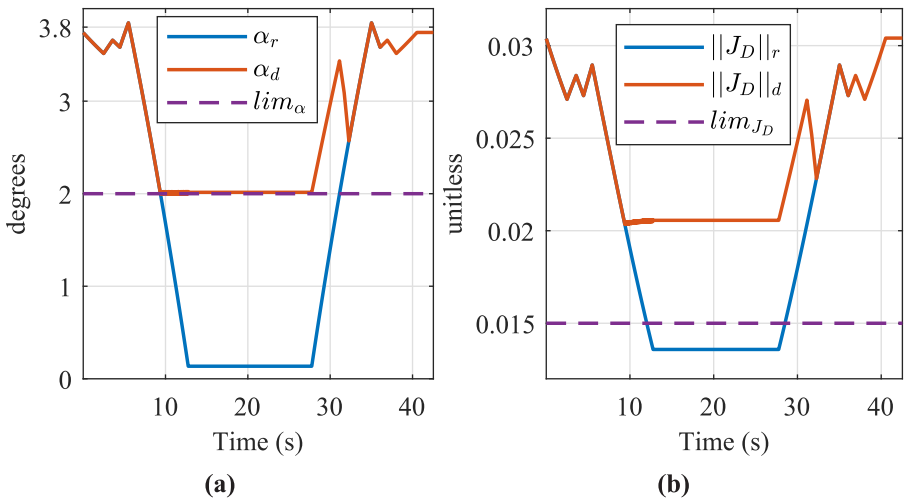

Figure 4.14: Indices (a) α (b) $\|J_D\|$ for the 3UPS+RPU PR in offline trajectory planning.

Figure 4.14a verifies that the non-singularity trajectory holds $\alpha_d > lim_\alpha$ and the original trajectory decreases α_r under lim_α, for the trajectory under anal-

ysis $\alpha = \Omega_{3,4}$. Figure 4.14b shows that $\|J_D\|$ for the non-singular trajectory ($\|J_D\|_d$) is farther from zero than the original trajectory ($\|J_D\|_r$). These results verify the effectiveness of the Type II singularity avoidance algorithm. The detailed procedure to calculate $\|J_D\|$ could be found in (Araujo-Gómez et al., 2017) with $\vec{X} = [x_m \quad z_m \quad \theta \quad \psi]^T$ and $\vec{q}_{ind} = [q_{13} \quad q_{23} \quad q_{33} \quad q_{42}]^T$.

The avoidance algorithm deviates the original trajectory of the linear actuators q_{33} and q_{42} to generate a non-singular trajectory because $\alpha = \Omega_{3,4}$. Figure 4.15a presents the original trajectory for actuators 3 (q_{33_r}) and the non-singular trajectory q_{33_d} generated by the proposed algorithm. Figure 4.15b presents the original (q_{42_r}) and non-singular (q_{42_d}) trajectory for actuator 4. In this case, the maximum $\vec{\Delta}\iota$ was $[0 \; 0 \; 56 \; -57]^T$. This figure verifies that the proposed algorithm introduces a smooth deviation in actuators 3 and 4 to avoid a Type II singularity with a maximum modification of 6 mm.

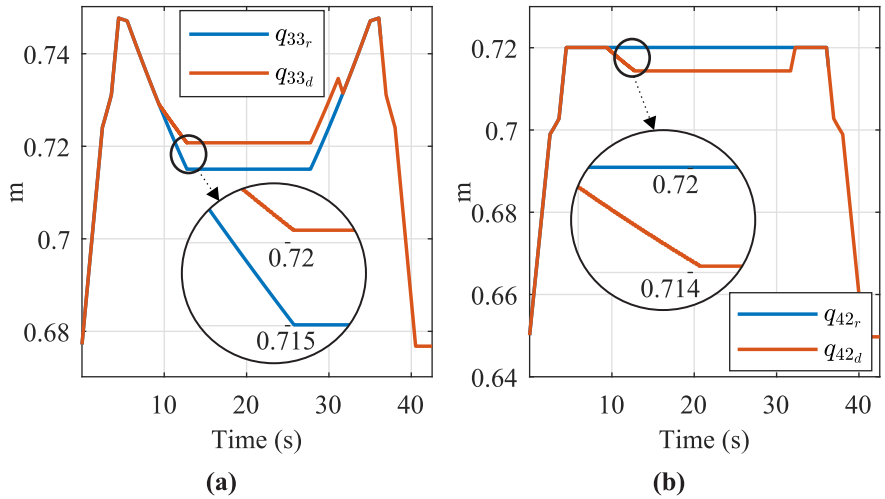

Figure 4.15: Results of the offline trajectory planning for the actuator in limb (a) 3 (b) 4.

In this case, the original and the non-singular trajectory are executed in the actual 3UPS+RPU PR. The actual PR is driven by the inner control loop shown in Figure 4.4, where the LAB control law is replaced by a PID algorithm. During the execution of the trajectories, the pose of the mobile platform is measured by the 3DTS shown in Section 5.2.2.

The measurements of z_m and θ provided by the 3DTS are plotted in Figure 4.16 for both trajectories. The z_m and θ represent the height and the orientation around the tibiofemoral plane for the actual 3UPS+RPU PR, respectively. An

external perturbation occurs at instant $t = 18\ s$ where in the original trajectory $(*_r)$ the PR yields to the force and moves unexpectedly. In contrast, in the trajectory modified by the proposed algorithm $(*_d)$ the PR remains stiff.

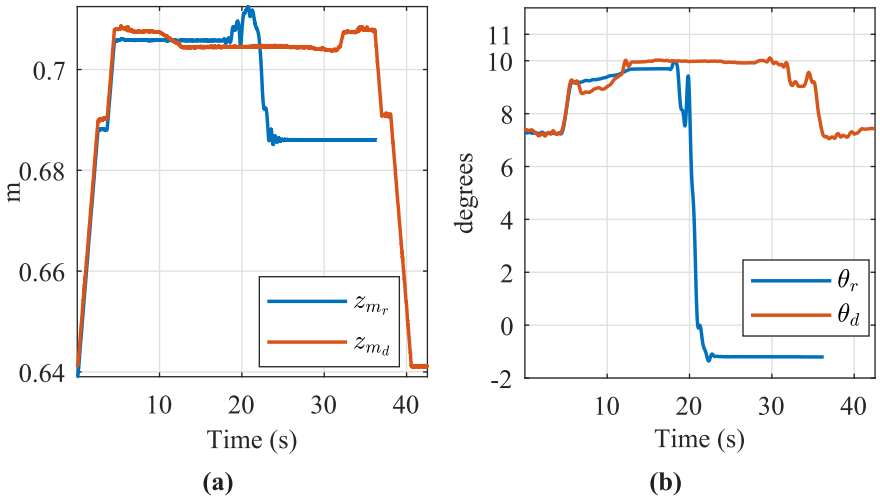

Figure 4.16: Pose tracking: (a) location on z_m (b) rotation around θ for the 4-DOF PR in offline trajectory planning.

During the offline trajectory planning, the proposed Type II singularity avoidance algorithm has modified only the trajectory of two actuators with a maximum modification of 6 mm. The offline trajectory planning is implemented in MATLAB on a desktop PC with a processor Core i7 3.7 GHz. In this case, the avoidance algorithm takes on average 1 ms in each iteration. Note that although the proposed algorithm is applied in a spatial case, the execution time is lower than in other algorithms for the planar case, see Table 4.5. Therefore, these results verify that the Type II singularity avoidance algorithm requires minimum deviation from the original trajectory with low computational cost.

For online trajectory planning, the original trajectory is a hip flexion movement used previously in offline trajectory planning with a different starting location, see Table 4.7. In this case, the block diagram in Figure 4.4 is modified to implement the proposed Type II singularity avoidance algorithm in the outer loop. The outer loop receives the original trajectory and generates a non-singular trajectory for the inner loop that runs a PID algorithm. The feedback signal for the singularity avoidance algorithm is provided by the 3DTS according to the Section 5.2.2. As in the offline trajectory planning, the singularity avoidance algorithm is set to $t_s = 10\ ms$ and $\nu_d = 0.01\ m/s$.

Table 4.7: Description of the trajectory for online planning in the 3UPS+RPU PR.

Location	x_m (m)	z_m (m)	θ (degrees)	ψ (degrees)	time (s)
Start	0.170	0.668	12.560	8.70	0
Singularity	0.016	0.707	8.619	18.15	16.35
End	0.170	0.668	12.560	8.70	47.69

Figure 4.17 presents the original ($*_r$) and non-singular ($*_d$) trajectory calculated online for the actuators in limbs 3 ($* = q_{33}$) and 4 ($* = q_{42}$). This figure verifies that the proposed algorithm introduces a maximum modification of 7 mm in actuators 3 and 4 during an online Type II singularity avoidance.

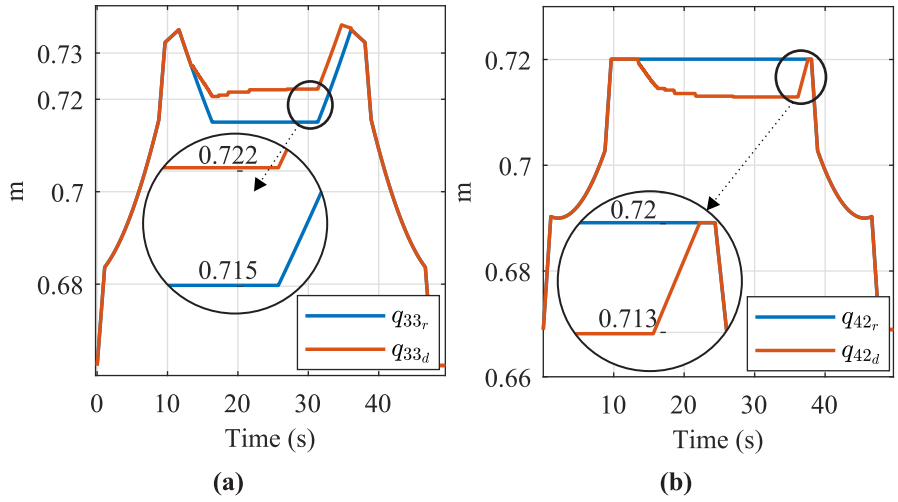

Figure 4.17: Results of the online trajectory planning for the actuator in limb (a) 3 (b) 4.

The original and the actual trajectory in the cartesian coordinates z_m and θ are presented in Figure 4.18. The original trajectory with a Type II singularity is represented by the subindices $_r$ while the non-singular trajectory generated by the proposed algorithm is labelled as $_d$. Figure 4.18 shows that the original trajectory on the configuration space is modified maximum 7 mm and 1.5 °.

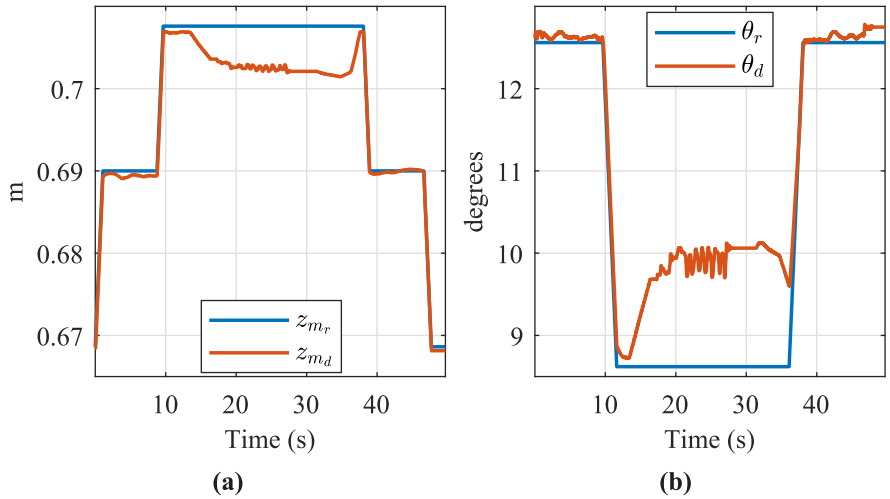

Figure 4.18: Pose tracking: (a) location on z_m (b) rotation around θ for the 4-DOF PR in online trajectory planning.

The Type II singularity avoidance algorithm with the PID algorithm for online trajectory planning is implemented in an industrial PC with a processor Core i7 3.4 GHz. The proposed avoidance algorithm requires on average 3.86 ms at each iteration during the online trajectory planning, and the PID controller is executed in 2 ms. If the controller is executed every 10 ms, the avoidance algorithm employs 38.6 % of the control period and the PID controller 20 %, i.e., 41.4 % of the control period is free. Thus, these results verify that the Type II singularity avoidance algorithm is suitable for online trajectory planning. The Type II singularity avoidance algorithm running in real-time control for the actual 3UPS+RPU PR is shown in `http://roboprop.ai2.upv.es/wp-content/uploads/2023/03/video_con_sin_evasor_vf.mp4`.

4.3 Discussion and Conclusions

A strategy to release a non-redundant spatial PR from a Type II singularity based on the minimum angle $\Omega_{i,j}$ ($min\Omega$)is introduced. The same strategy could be applied to a planar case by using the minimum angle $\Theta_{i,j}$ ($min\Theta$) instead of $min\Omega$. The singularity release algorithm (SRA) aims to verify that the limbs identified by $min\Omega$ or $min\Theta$ are responsible for being close to a Type II singularity. Thus, two versions of the SRA are implemented in a vision-based hybrid controller for a 3UPS+RPU PR. The first version SRA-V1 moves the

limbs identified by $min\Omega$ to release the PR from a singularity and the second one SRA-V2, moves the opposite limbs.

The simulation of the vision-based hybrid controller with SRA-V1 shows a better performance with respect to SRA-V2. The SRA-V1 release the 3U$\underline{P}$S+R$\underline{P}$U PR with an average deviation of 0.54 % (4.09 mm) in the actuator's trajectory. The implementation of the vision-based hybrid controller with SRA-V1 verifies the minimum deviation 0.56 % (4.22 mm) to release the PR from a Type II singularity. Therefore, the capability of $min\Omega$ to identify the pair of actuators responsible for approaching a Type II singularity is verified. The vision-based hybrid controller with SRA-V1 is not implemented in a planar case because with $F = 2$ all actuators modify the trajectory. In addition, the experimental evaluation state that releasing a PR from a Type II singularity requires an external measure of the actual pose of the mobile platform. It is because the solution of FKP is inaccurate in the proximity to a singular configuration.

Subsequently, a novel Type II singularity avoidance algorithm for general purposes based on the $min\Theta$ and $min\Omega$ is proposed. The avoidance algorithm uses $min\Theta$ to detect the proximity to a singularity in the planar PR and $min\Omega$ for the spatial case. In the planar case, the Type II avoidance algorithm has been successfully applied in offline trajectory planning for a symmetrical 5R mechanism. In the spatial case, the proposed singularity avoidance is implemented for offline and online trajectory planning for a 3U$\underline{P}$S+R$\underline{P}$U PR.

Table 4.8 summarises the results of the Type II avoidance algorithm during offline and online trajectory planning. In this table, t_I represents the execution time in each iteration, Δ_q stands for the maximum modification in the trajectory of actuators, and $\Delta_{\dot{q}}$ is the average deviation in the velocity reference in joint space.

Table 4.8: Results for the proposed Type II singularity avoidance algorithm for planar and spatial PRs.

Planning type	PR	t_I (ms)	Δ_q	$\Delta_{\dot{q}}$
Offline	5R	0.5	1.2 °	0.58 °/s
Offline	3U$\underline{P}$S+R$\underline{P}$U	1	6 mm	0.24 mm/s
Online	3U$\underline{P}$S+R$\underline{P}$U	3.86	7 mm	0.28 mm/s

The Type II singularity avoidance algorithm requires 1 ms in each iteration during offline trajectory planning of spatial case, see Table 4.8. The proposed algorithm was compared with a Constrained Multi-Objective algorithm and roadmap (C-space) algorithm for offline trajectory in planar PRs. The pro-

posed avoidance algorithm applied to a 4-DOF PR is faster than CMO and C-space algorithms applied to planar cases. Thus, the low computational cost of the Type II singularity avoidance algorithm is verified. During the online trajectory planning for a 3UPS+RPU PR, the Type II avoidance algorithm requires 3.86 ms for execution. Considering that the controller is executed at every 10ms and the PID law takes 2 ms, there is 4.41 ms free at each iteration. Therefore, the Type II singularity avoidance algorithm is suitable for online applications in the 3UPS+RPU PR.

In offline trajectory planning with a 5R mechanism, the proposed avoidance algorithm introduced a maximum deviation of 2 ° that is imperceptible for the planar PR under study. The velocity trajectory was modified 0.58 °/s, i.e., 2 % of the working velocity.

In offline trajectory planning with the 3UPS+RPU PR, the trajectories of the two actuators were modified by a maximum of 6 mm, and the velocity profile changed on average 0.24 mm/s (2.4 % of the working velocity). Considering that the 3UPS+RPU PR is applied for knee rehabilitation, 6 mm is a minimum deviation compared with the range of movement of the human leg. In addition, the proposed algorithm modifies the trajectory of two actuators with a maximum deviation of 7 mm during the online trajectory planning in the 3UPS+RPU PR. Thereby, the proposed algorithm requires a minimum deviation on two actuators to avoid a Type II singularity during offline and online trajectory planning for the 5R and 3UPS+RPU PRs.

The minimum deviation on the original trajectory and the low computation cost make the Type II singularity avoidance algorithm suitable for knee rehabilitation assisted by the 3UPS+RPU PR. However, note that the online trajectory planning was analysed without human interaction to avoid risking the integrity of the patient. The next chapter combines the proposed singularity avoidance algorithm with a force controller for human-robot interaction.

Chapter 5

Compliant control and Type II singularity avoidance for knee rehabilitation

This chapter first introduces the fundamental control strategies employed for lower-limb rehabilitation, where admittance control is the most suitable for patient-active rehabilitation. Next, the drawbacks of conventional admittance control in the proximity to a Type II singularity are exposed. Subsequently, the conventional admittance controller is combined with the singularity avoidance algorithm proposed in the previous chapter to overcome the control issues in proximity to a Type II singularity. The complemented admittance controller is implemented in a Parallel Robot (PR) with four degrees of freedom (DOFs) for knee rehabilitation. The inability of conventional control to prevent Type II singularities is shown by experimentation over a mannequin leg. Finally, the performance of the complemented admittance controller is evaluated by executing a patient-active knee rotation in the actual 4-DOF PR by using a mannequin and human lower-limb.

5.1 Force/position control strategies

Motion rehabilitation therapies can be divided into patient-passive and patient-active exercises. In the patient-passive exercise, the robot follows a position and orientation (pose) reference defined by the therapist without considering the patient interaction. In this case, the robot requires a pose trajectory-tracking controller (Saglia et al., 2013). In patient-active exercise, the forces and moments exerted by the patient are able to modify the motion predefined by the therapist (Meng et al., 2015). For this kind of rehabilitation therapy, the robot requires a force/position controller with compliance behaviour.

Several force/position control strategies have been developed for rehabilitation robots based on force signals and bio-signals measured in the human limb (Ju et al., 2005; Fan and Yin, 2013; Wu et al., 2018). These approaches are based on four fundamental control strategies:

- Hybrid force/position
- Parallel force/position
- Impedance
- Admittance

These control strategies are explained below.

5.1.1 Hybrid force/position control

Raibert and Craig (1981) divided the workspace into two complementary orthogonal subspaces to apply a force and a position controller. Figure 5.1 shows the hybrid force/position control scheme with the Laplace variable s.

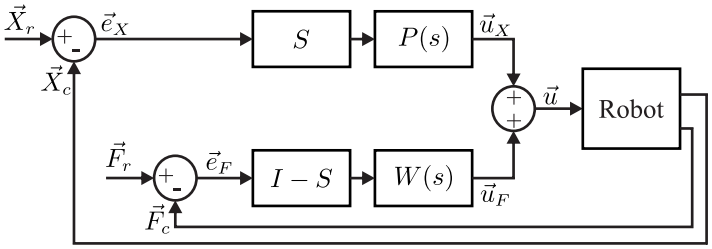

Figure 5.1: Block diagram of the hybrid force/position controller.

The position controller $P(s)$ works in the subspace defined by the matrix S to generate the control actions $\vec{u}_X$ for tracking the reference pose of the end-effector $\vec{X}_r$. $P(s)$ aims to minimise the error in pose tracking $\vec{e}_X$ defined as:

$$\vec{e}_X = \vec{X}_r - \vec{X}_c \tag{5.1}$$

where $\vec{X}_c$ stands for the pose measured in the F DOFs of the mobile platform and $\vec{X}_r$ is the target reference in the same DOFs.

The force controller $W(s)$ generates the control actions $\vec{u}_F$ in the subspace $I - S$ to minimise the error in force and moment tracking $\vec{e}_F$, where I is an identity matrix. The error $\vec{e}_F$ is calculated as:

$$\vec{e}_F = \vec{F}_r - \vec{F}_c \tag{5.2}$$

with $\vec{F}_r$ represents the reference forces and moments for rehabilitation in the F DOFs of the robot. $\vec{F}_c$ stands for forces and moments measured on the human limb in the same F DOFs of end-effector.

The robot is driven to a desired pose with a specific force and moment exerted by the patient using $\vec{u}$ that is calculated by adding $\vec{u}_X$ and $\vec{u}_F$. S is a diagonal matrix with dimension $F \times F$ where only the DOFs that require free motion control are equal to 1. The hybrid force/position control provides individual pose control over a defined subset of DOFs while the rest has individual force control. Therefore, a detailed environment model is required. In contrast, $P(s)$ and $W(s)$ are arbitrary control laws selected based on the application requirements.

5.1.2 Parallel force/position control

Chiaverini and Sciavicco (1988) propose a controller able to track the reference motion trajectory and control the contact forces in the F DOFs at the same time. Thus, the parallel force/position control avoids dividing the workspace into two subspaces, see Figure 5.2. In contrast to the hybrid force/position control, the parallel force/position control $\vec{u}_X$ and $\vec{u}_F$ are superimposed in all DOFs. In this case, the model of the environment is not required. In the literature, $P(s)$ is a Proportional-Derivative (PD) control law and $W(s)$ is a Proportional-Integral (PI) control strategy. The use of PD control provides accurate pose tracking and the PD controller ensures driving the steady-state force error to zero.

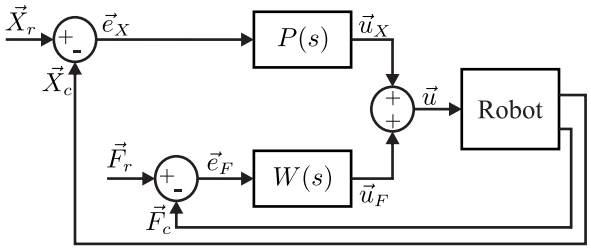

Figure 5.2: Block diagram of the parallel force/position controller.

The compliant control of lower-limb rehabilitative robot aims to provide safe, comfortable, and flexible equipment for treatment and healing, i.e., accurate force trace control is optional. Therefore, parallel and hybrid force/position control strategies are uncommonly used in compliant control for lower-limb rehabilitative robots (Zhang et al., 2017).

5.1.3 Impedance control

Hogan (1985) proposed the impedance control to achieve a suitable relationship between the pose and force tracking instead of tracking both individually. The impedance control has a double closed-loop architecture, with $W(s)$ in the inner loop and a mechanical impedance $I(s)$ in the outer loop, see Figure 5.3. In the outer loop, $I(s)$ modifies the reference $\vec{F}_r$ to generate a modified force reference $\vec{F}_i$ that is the set-point for the controller $W(s)$ in the inner loop.

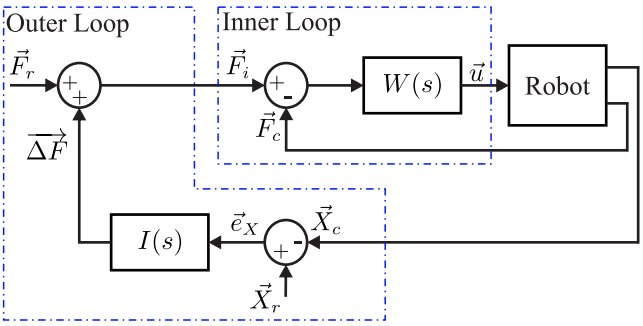

Figure 5.3: Block diagram of the impedance controller.

The function $I(s)$ relates the deviation on the force reference $\overrightarrow{\Delta F}$ with the error in pose tracking $\vec{e}_X$ according to:

$$\overrightarrow{\Delta F}(s) = I(s)\vec{e}_X(s) \tag{5.3}$$

Generally, $I(s)$ is a second order dynamic model:

$$I(s) = K + Ds + Ms^2 \tag{5.4}$$

where K, D and M are square matrices that represent the stiffness, the damping and the mass of the dynamic system, respectively.

The trade-off between the motion and force tracking is defined by the $I(s)$, thus the parameters K, D and M are set according to compliant requirements of the PR. For a compliant behaviour of the robot in response to a variation on $\vec{F}_c$, the K, D and M require low values and for a robust behaviour high values. However, $I(s)$ defined simultaneously the accuracy of the pose tracking and the effective dynamic disturbance rejection, hereby the control setting is not trivial. Moreover, if $I(s)$ is set with high values, the controller could have stability issues because the $\overrightarrow{\Delta F}$ experiences huge changes. These sudden changes could be dangerous for the patient.

5.1.4 Admittance control

The admittance control has a double closed-loop architecture, see Figure 5.4. In this case, the inner loop implements a pose controller in which the $\vec{X}_r$ is modified by the mechanical admittance $A(s)$ to achieve the force reference $\vec{F}_r$ in the outer loop.

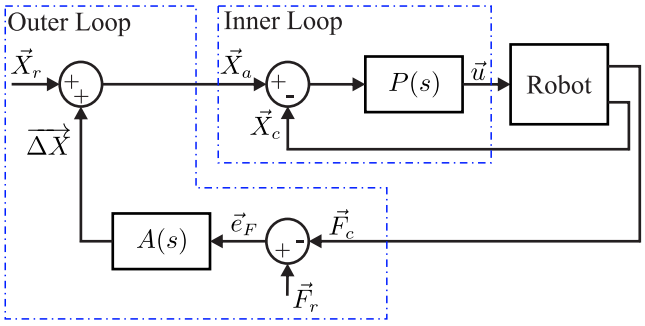

Figure 5.4: Block diagram of the conventional admittance controller.

The relation between the deviation on the pose reference $\overrightarrow{\Delta X}$ and the force error $\vec{e}_F(s)$ is:

$$\overrightarrow{\Delta X}(s) = A(s)\vec{e}_F(s) \tag{5.5}$$

with

$$A(s) = \frac{1}{I(s)} = \frac{1}{K + Ds + Ms^2} \tag{5.6}$$

In this case, the problem of stability in the outer loop appears for low values in the gains of $A(s)$. However, $A(s)$ is set to minimise $\vec{e}_F(s)$ without concern about the pose tracking. It is because the pose controller $P(s)$ in the inner loop is a control law stable with the feature of suppressing non-modelling dynamic disturbance such as friction in the joints. This makes the admittance controller the most appropriate strategy for rehabilitation because it allows an appropriate dynamic relationship between the pose of the robot and the patient effort (Meng et al., 2015; Kim et al., 2019). In addition, the control law of the inner loop could be selected arbitrarily allowing the incorporation of sophisticated techniques (Schumacher et al., 2019).

For patient-active knee rehabilitation based on the 3U$\underline{\text{P}}$S+ R$\underline{\text{P}}$U PR, the patient modifies a predefined movement according to the pain limitation of the limb in rehabilitation. Hence, the 3U$\underline{\text{P}}$S+ R$\underline{\text{P}}$U PR requires an admittance control.

If $\vec{F}_c < \vec{F}_r$, the deviation pose $\overrightarrow{\Delta X}$, calculated by (5.5), moves the PR against the human limb and increase the $\vec{F}_c$. When $\vec{F}_c > \vec{F}_r$, the $\overrightarrow{\Delta X}$ varies $\vec{X}_r$ to move the PR away from the limb under rehabilitation and reduce the $\vec{F}_c$. Thus, the $\overrightarrow{\Delta X}$ enables the patient to drive the PR to an arbitrary pose within the workspace. However, if a Type II singularity arises, the PR loses control of the end-effector motion and could hurt the limb in rehabilitation. For example, if the patient flexes the knee because of pain, and the PR extends the knee due to loss of control, that could damage the human leg. Consequently, the conventional admittance controller is unsuitable for PR-assisted lower limb rehabilitation. Therefore, the conventional admittance controller must be improved using online avoidance of Type II singularities.

5.2 Control unit and sensors

5.2.1 *Hardware and software control architecture*

For the 3UPS+ RPU PR, a force/position controller is executed in an industrial computer connected to a 3D Tracking System (3DTS) and an FTN-Delta force/torque sensor with six degrees of freedom. Figure 5.5 shows the overview of the control architecture that uses the equipment shown in Figure 5.6. The industrial computer (PR control computer) is equipped with a PCI 1784 Advantech card connected to four quadruple AB phase encoder counters with a resolution of 500 counts per turn to measure the length of the linear actuators. The linear actuators were driven using four ESCON 50/5 servo controllers, where the $\vec{u}$ was sent through a 12-bit, 4-channel PCI 1720 Advantech card at a rate of 100 Hz.

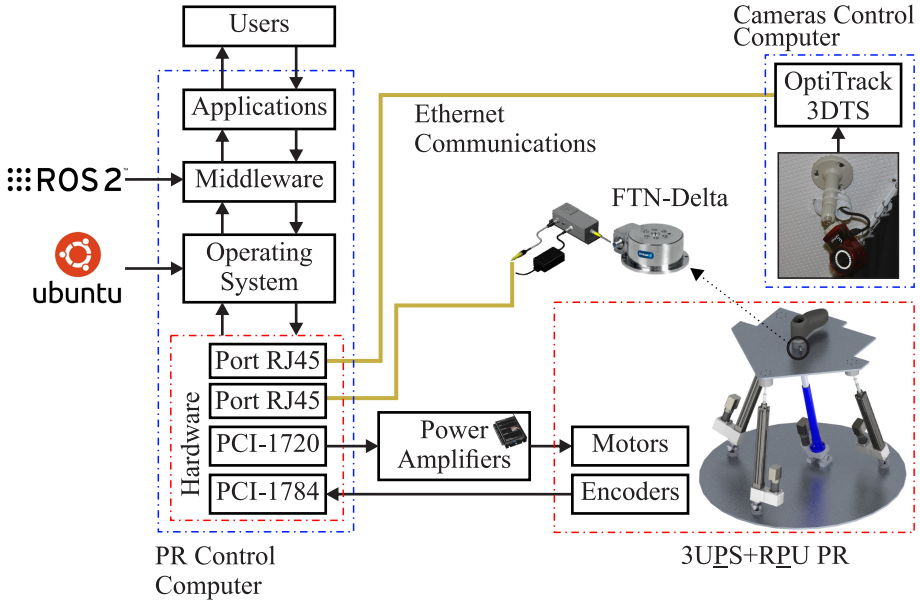

Figure 5.5: Overview of the control architecture for the 3UPS+ RPU PR.

The actual pose of the 3UPS+ RPU PR is measured by 3DTS in the cameras control computer and sent in streaming by Ethernet communications. The data from the FTN-Delta force/torque is also sent by Ethernet communications in a different physical port of the PR control computer.

A force/position control law is implemented in the PR control computer using a modular structure using the real-time middleware Robot Operating System 2 (ROS2) and the C++ programming language. Each element of the block diagram of an arbitrary controller is implemented as a node of ROS2, including the sensors and actuators. The nodes in ROS2 use DDS communication to exchange messages under the publisher/subscribe system. A publisher node could send a string message in a specific channel of communication (topic) and only the nodes subscribed to the topic receive the topic. This architecture makes ROS2 a suitable middleware for real-time tasks. The nodes for receiving the actual pose of the PR and the force exerted by a patient are explained in Sections 5.2.2 and 5.2.3. The PR control computer runs a force/position controller with at a rate of 100 Hz using a processor Core i7 3.4 GHz with Ubuntu 18.04.5 and ROS2 Eloquent distribution.

5.2.2 Vision-based tracking sensor

A 3D Tracking System (3DTS) was implemented as a vision-based sensor to track the location and orientation of the knee rehabilitation PR. The 3DTS allows an accurate avoidance of Type II singularities, increasing the safety of the patient. In particular, the 3DTS consists of 10 infrared cameras (Flex 13) manufactured by OptiTrack, see Figure 5.6. The cameras can achieve an average accuracy greater than 0.1 mm. Moreover, the cameras have a resolution of 1.3 Megapixels at 120 Hz, i.e., 8.3 ms between two subsequent captures.

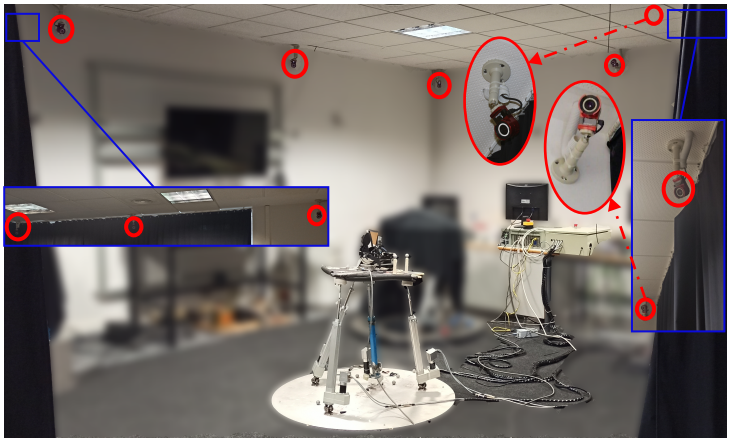

Figure 5.6: Overall view of the OptiTrack 3DTS.

In the architecture of the 3DTS (see Figure 5.7a), the cameras are connected to two OptiHub2 devices to record the captured images. The OptiHub2 devices send the image data through a high-speed USB to the camera control computer. Finally, the location data are sent to the PR control computer via an Ethernet connection.

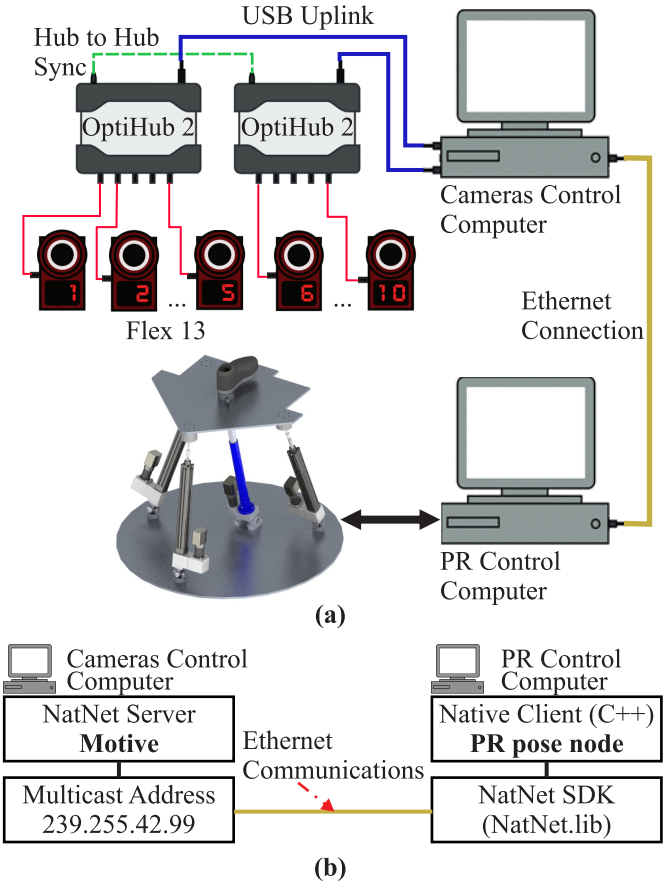

Figure 5.7: Architecture of OptiTrack 3DTS (a) hardware (b) software.

In the camera control computer, the software Motive, provided by OptiTrack, processes the 2D camera images in the 3D location of markers inside the tracking area. In particular, the software Motive can associate a custom set of markers in a virtual object defined as a rigid body that can be set with 3 to 20 markers. A marker is a sphere covered with a reflective material. Motive can perform a real-time stream of the location and orientation of all rigid bodies,

including the location of each marker, via Ethernet using unicast or multicast protocols. The streaming data are accessed by a client/server architecture based on the NatNet software development kit (NatNet SDK).

This thesis implemented a NatNet client/server architecture where the server could be run in the camera control computer, and a native client could be executed in the PR control computer (see Figure 5.7b). The native client had attached to a C++ handler named ***PR pose node*** that was executed when a new frame of data was available.

The actual pose of the 3UPS+RPU PR was retrieved by measuring the 3D location of six markers. Three markers were placed on the mobile platform while the other three were attached to the fixed platform, where both sets were elements of two different rigid bodies. Given the location of the six markers, the actual position and orientation of the mobile platform were calculated with respect to the fixed frame $\{O_f - X_f Y_f Z_f\}$. The actual position and orientation of the mobile platform were represented by $\vec{X}_c$ and sorted as $[x_m \; z_m \; \theta \; \psi]^T$, analogous to $\vec{X}_r$.

All cameras required calibration to ensure a correct reconstruction of the 3D location provided by the 3DTS. The calibration process is:

1. Set the orientation of the cameras so that they focus on the centre of the tracking area.
2. Adjust the brightness and illumination of the cameras to avoid the detection of unwanted objects.
3. Adjust the relative position of the cameras by moving the calibration wand provided by OptiTrack. An empty tracking area is required.
4. Set the ground plane for the tracking area with a calibration square provided by OptiTrack.

Steps 2-4 of the calibration process were executed in Motive, consuming less than five minutes.

5.2.3 Force/torque sensor

The admittance control requires an accurate measurement of the external force applied to the PR. The proposed system measures the forces and moments exerted by the patient's foot on the mobile platform using an FTN-Delta sensor. The FTN-Deltas sensor is a six-axis force/torque sensor from Schunk. For the knee rehabilitation PR, the FTN-Delta sensor was installed at O_m on the mobile platform, see Figure 5.8a. The forces measured in the x, y, and z axes of the sensor reference frame can be represented by F_x, F_y, and F_z, respectively. Similarly, M_x, M_y, and M_z stand for the moments measured by the FTN-Delta sensor in the reference frame $\{O - xyz\}$, see Figure 5.8a. The FTN-Delta sensor measures force with a resolution of 0.065 N for F_x, F_y, and 0.125 N for F_z. The moments M_x, M_y, and M_z are measured with a resolution of 0.004 N·m. The FTN-Delta sensor has a measuring range of ±330 N for F_x, F_y and ±990 N for F_z. The measuring range for the moments M_x, M_y, and M_z is ±30 N·m. The data from the FTN-Delta sensor were amplified, filtered, and transmitted by a Netbox NETB that supports CAN bus, DeviceNet, PROFINET, and UDP interface protocols at up to 7 Mhz.

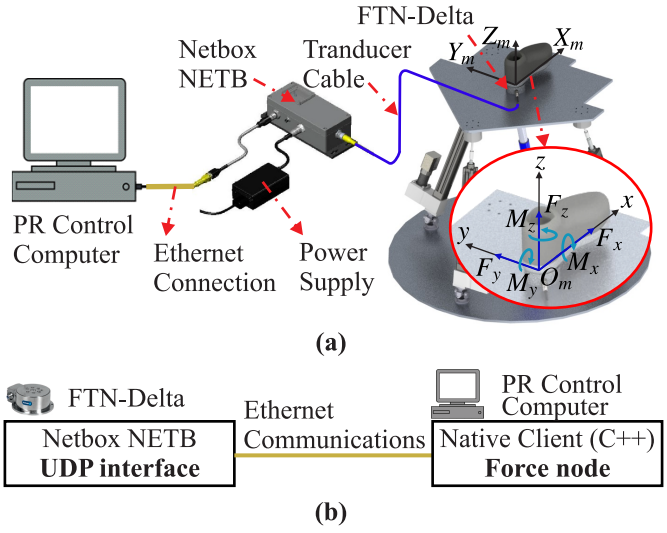

Figure 5.8: Architecture of FTN-Delta sensor (a) hardware (b) software.

The Netbox NETB was connected to the PR control computer as a single client using a UDP interface on the Ethernet protocol, see Figure 5.8a. The single client had a C++ handler named ***Force node*** attached, which was executed when the admittance controller required a new frame of data, see Figure 5.8b.

The force node provided the measurements of force and moments in the 4-DOF of the knee rehabilitation PR in the vector $\vec{F}_c$ as follows:

$$\vec{F}_c = \begin{bmatrix} F_x & F_z & M_y & M_z \end{bmatrix}^T \tag{5.7}$$

where the F_x stands for the force exerted by the patient on the axis X_m, and the F_z is the force exerted on the axis Z_m. The M_y and M_z are the moments exerted by the patient around the tibiofemoral and coronal planes, respectively. The reference frame of the FTN-Delta sensor matches the mobile reference frame, see Figure 5.8a.

The zero adjustments of forces and moments were performed considering no load on the mobile platform. Moreover, a death zone was defined as three times the standard deviation of data measured with the sensor unloaded to account for the noise.

5.3 Admittance controller complemented with singularity avoidance algorithm

The architecture of the admittance controller complemented with the Type II singularity avoidance algorithm for the 3UPS+ RPU PR is shown in Figure 5.9. Taking advantage of the cascade architecture of conventional admittance controllers, the outer loop is divided into two layers. In the first layer, an admittance model $A(s)$ modifies the reference $\vec{X}_r$ by adding $\overrightarrow{\Delta X}$ to achieve the reference efforts $\vec{F}_r$ using the measurement $\vec{F}_c$ as feedback. In the second layer, the Type II singularity avoidance algorithm collects the modified pose reference $\vec{X}_a$ and generates a singularity-free trajectory $\vec{q}_{ind_d}$ in the joint space. The avoidance algorithm keeps $\vec{q}_{ind_d} = \vec{q}_{ind_a}$ as long as $\vec{X}_a$ is not singular. The $\vec{q}_{ind_a}$ stands for the inverse kinematic solution of $\vec{X}_a$.

The Type II singularity algorithm for the 3UPS+ RPU PR uses the spatial case of the algorithm introduced in Section 4.2. If the reference $\vec{X}_a$ or the actual pose of the PR $\vec{X}_c$ is singular, the avoidance algorithm modifies $\vec{q}_{ind_a}$ to generate the singularity-free trajectory $\vec{q}_{ind_d}$. The proposed avoidance algorithm modifies the trajectory of the two actuators identified by the $\alpha_c = min(\overrightarrow{V\Omega}_c)$. The $\overrightarrow{V\Omega}_c$ is calculated based on the measurement of the actual pose of the PR $\vec{X}_c$. As soon as $\vec{X}_c$ becomes non-singular, the modification in the actuators identified by α_c vanishes.

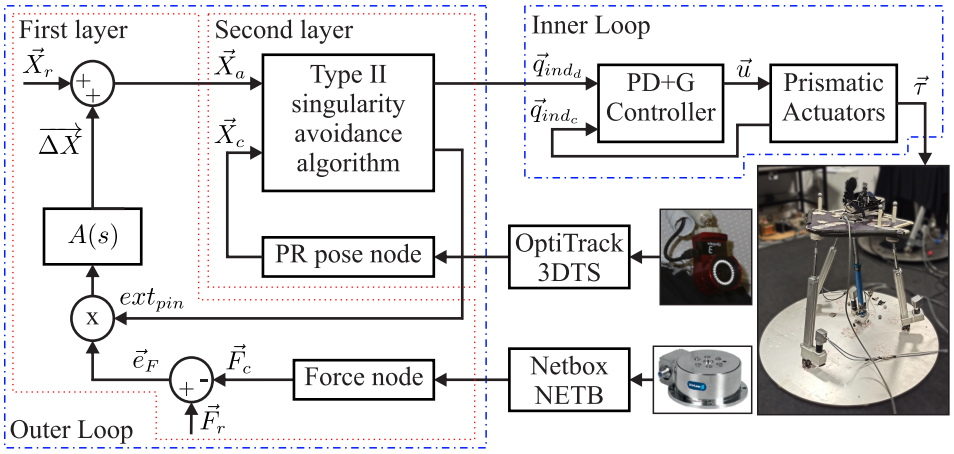

Figure 5.9: Architecture of the admittance controller complemented with the Type II singularity avoidance algorithm.

When the reference $\vec{X}_r$ is non-singular, the trajectory $\vec{X}_a$ becomes singular due to the output $\overrightarrow{\Delta X}$ from the $A(s)$, see the outer loop in Figure 5.9. Thus, the admittance control must temporally be deactivated to prevent conflict during the Type II singularity avoidance developed by the proposed algorithm. The admittance control could be deactivated by setting $\overrightarrow{\Delta X}$ to zero, see (5.5). However, if $\overrightarrow{\Delta X}$ is suddenly set to $\vec{0}$, the $\vec{X}_a$ presents random discontinuities that could hurt the human limb. In contrast, if $\vec{e}_F$ immediately changes to $\vec{0}$, the admittance control is gradually deactivated, i.e., the $\overrightarrow{\Delta X}$ decreases smoothly according to the dynamics of the second-order model $A(s)$, see (5.6).

The proposed Type II singularity avoidance algorithm multiplies the unitary gain ext_{pin} by the $\vec{e}_F$ to deactivate the admittance controller in the first layer of the outer loop (Figure 5.9). In the proximity to a Type II singularity, the avoidance algorithm sets $ext_{pin} = 0$ to decrease $\overrightarrow{\Delta X}$. As soon as the trajectory $\vec{X}_a$ becomes non-singular, the admittance controller is reactivated by setting $ext_{pin} = 1$. It is important to note that this mechanism enables the admittance control and the avoidance algorithm to coexist to ensure the safety of the limb under rehabilitation.

The scheme of the Type II singularity avoidance, after adding the gain ext_{pin} to activate/deactivate the admittance control, is shown in Figure 5.10. In this

figure, the pair of actuators identified by α_c are stored at $\vec{i}_{av}$. The procedure to modify the $\vec{\Delta}\iota$ and its return to zero is detailed in Section 4.2.

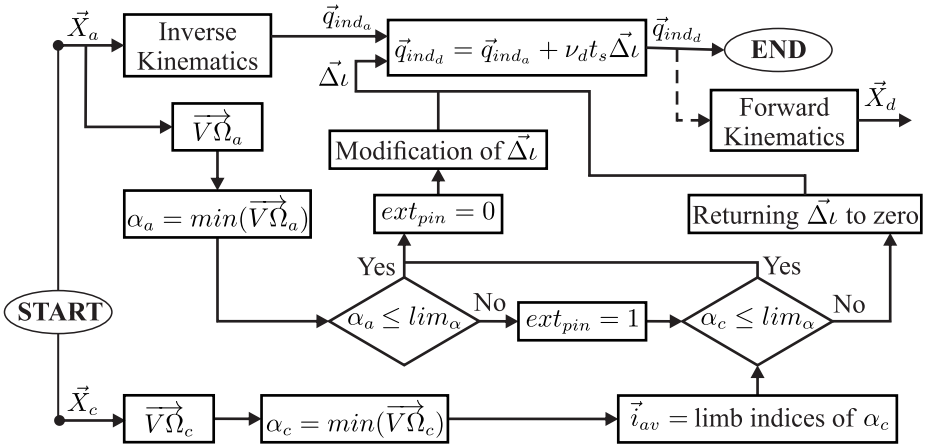

Figure 5.10: Type II singularity avoidance algorithm for admittance control in the knee rehabilitation PR.

In the PR under analysis, the $\vec{F}_c$ is measured using a six-axis force/torque sensor, specifically an FTN-Delta sensor. The specifications of the FTN-Delta sensor and the C++ handler ***Force node*** for reading the force and moment measurements are detailed in Section 5.2.3.

The actual pose $\vec{X}_c$ required by the Type II singularity avoidance algorithm could be determined by solving the Forward Kinematic Problem (FKP) or by an external measure on the end-effector. The calculation of $\vec{X}_c$ by solving FKP could be inaccurate near a Type II singularity. Hereby, the 3DTS is a solid option to ensure accurate singularity avoidance during a robotic rehabilitation procedure and ensure the integrity of the constrained mobility limb. The actual pose $\vec{X}_c$ of 3U$\underline{\text{P}}$S+ R$\underline{\text{P}}$U PR is measured by a 3DTS from OptiTrack ®. The features of the 3DTS and its data stream processing in the C++ handler named ***PR pose node*** are presented in Section 5.2.2.

In the inner loop of the scheme Figure 5.9, a trajectory controller takes $\vec{q}_{ind_d}$ as a set point. For the 3U$\underline{\text{P}}$S+ R$\underline{\text{P}}$U PR, the trajectory controller is a Proportional-Derivative control with Gravitational compensation (PD+G). The PD+G calculates the control actions $\vec{u}$ to track the location in joint space $\vec{q}_{ind_d}$ while the gravitational term of the dynamic model of the PR is compensated. The location reached by the actuators $\vec{q}_{ind_c}$ is provided by a set of incremental encoders

on the motors. The PD+G controller was selected because the 3UPS+RPU PR works at low velocity making unnecessary the compensation of the inertial, centrifugal, and Coriolis forces.

Note that identifying a proper set of dynamic parameters of the admittance model for each user remains open. Nevertheless, this thesis aims to prove that the admittance controller complemented with the proposed Type II singularity avoidance algorithm ensures the integrity of the patient even in the closeness to a singular configuration.

5.3.1 Experimental setup

A patient-active exercise close to a Type II singularity was designed to compare the performance of the complemented admittance controller with that of the conventional admittance controller. The patient-active exercise comprised an internal-external knee rotation with the 3UPS+RPU PR. During the internal-external knee rotation, the reference $\vec{X}_r$ is constant and equal to the starting pose of the human limb and the patient had a zero-effort trajectory ($\vec{F}_r = \vec{0}$). Thus, the patient had complete control over the PR movements, i.e., the PR was completely compliant. The starting pose for the knee rotation exercise was set close to a Type II singularity by experimentally searching on the actual 3UPS+RPU PR based on the angle α_c.

Before implementing the proposed complemented admittance controller on the actual PR, several simulations were executed using a virtual model of the human leg. Here, only the experiments with the actual robot are presented.

The experiments have two phases designed to prioritise patient safety:

> Phase I: A mannequin leg is considered to mimic an internal-external knee rotation, see Figure 5.11a.
>
> Phase II: An uninjured and unrestricted human knee performs the same internal-external knee rotation, see Figure 5.11b.

The experiment in Phase II was approved by the Ethics Committee of the Universitat Politècnica de València, and the patient signed an informed consent document.

(a) **(b)**

Figure 5.11: Experimental setup using (a) Mannequin leg and (b) Human limb.

The conventional admittance controller was applied to Phase I to expose the risk of the straightforward application to a PR. The complemented admittance controller is applied in Phases I and II to verify that PR could overcome the singular configurations. In both phases, the admittance model was set experimentally to provide minimum resistance to the limb of the patient. It is because our purpose is to verify that the proposed controller can overcome Type II singularities during patient-active knee exercise.

Table 5.1: Parameters settings for the admittance model for the 3U$\underline{P}$S+R$\underline{P}$U PR.

Parameter	Value
K	$\begin{bmatrix} 250 & 0 & 0 & 0 \\ 0 & 500 & 0 & 0 \\ 0 & 0 & 25 & 0 \\ 0 & 0 & 0 & 25 \end{bmatrix}$
D	$\begin{bmatrix} 894 & 0 & 0 & 0 \\ 0 & 894 & 0 & 0 \\ 0 & 0 & 89.4 & 0 \\ 0 & 0 & 0 & 89.4 \end{bmatrix}$
M	$\begin{bmatrix} 200 & 0 & 0 & 0 \\ 0 & 200 & 0 & 0 \\ 0 & 0 & 20 & 0 \\ 0 & 0 & 0 & 20 \end{bmatrix}$

Table 5.1 lists the parameters of the admittance model. Columns one and two of matrix K are defined in N/m while columns three and four are defined in $N \cdot m$. In matrix D, columns one and two are defined in $N \cdot s/m$ and columns

three and four in $N \cdot m \cdot s$. The matrix M defines the first two columns in kg and the last two columns in $kg \cdot m^2$.

The parameters of the Type II avoidance algorithm are $\nu_d = 0.01\ m/s$ and $t_s = 0.01\ s$ to fit the maximum working velocity of the actuators and the control unit sample rate, see Section 4.2.2. The limit $lim_\Omega = 2°$ according to the experimental procedure presented in Section 3.4.

5.3.2 Performance evaluation

In Phase I, the conventional admittance controller drives the PR to a Type II singularity. In this case, the PR falls due to the gravity effect, and then the mannequin leg was extended abruptly. A recording of this experiment is available in `http://roboprop.ai2.upv.es/admittance_without_evader`.

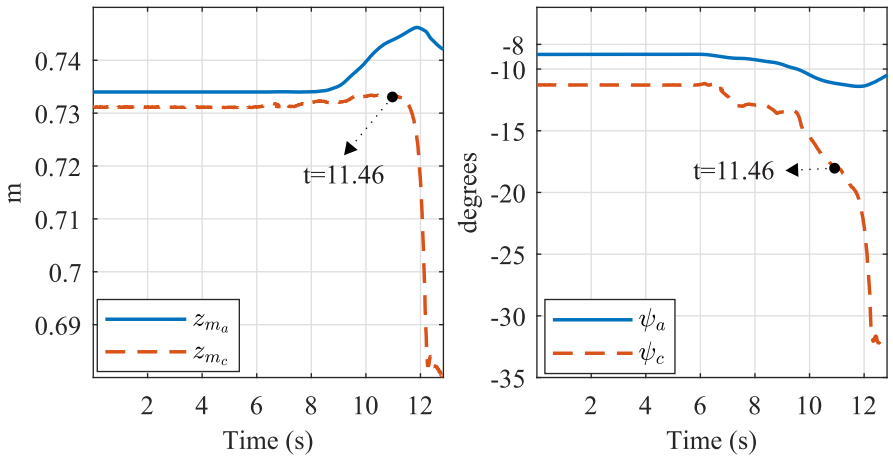

Figure 5.12: (a) Location on z_m (b) Rotation around ψ during knee rotation with a mannequin leg using the conventional admittance controller.

Figure 5.12 shows the tracking of z_m and ψ from the 3DTS during the knee rotation in Phase I. The variables z_m and ψ stand for the height and the orientation around the coronal plane for the actual 3UPS+RPU PR, respectively. In this figure, $*_a$ stands for the reference calculated by the conventional admittance controller, and $*_c$ is the measurement in the actual PR. The signals z_{m_c} and ψ_c show the loss of control on the PR from $t = 11.46\ s$, and the subsequent fall because the conventional admittance controller reaches a Type II

singularity. Thus, the risk of directly implementing a conventional admittance controller in a non-redundant PR is showcased.

Figure 5.13 shows the proximity detection of the Type II singularity based on α. In this case, $\alpha = \Omega_{2,4}$ during the entire experiment of the internal-external knee rotation. The signal α_a represents the closeness to a singular configuration in the reference calculated for the conventional admittance controller. The singularity proximity measurement for the actual pose of the PR is plotted as α_c. At $t = 11.46\ s$, $\alpha_c < lim_\Omega$ verifies that the 3UPS+RPU PR reaches a Type II singularity, see Figure 5.13. The index α_c detects the proximity to a Type II singularity at $t = 9.77\ s$, i.e., $1.69\ s$ before the PR falls. Thus, the α_c is a feasible option to prevent the PR from reaching a Type II singularity.

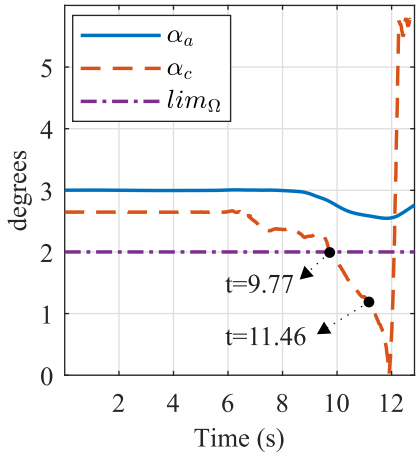

Figure 5.13: Index α during knee rotation with a mannequin leg using the conventional admittance controller.

The admittance controller complemented with the Type II singularity avoidance algorithm completes the two experimental phases without losing control. The execution of the complemented admittance controller during Phases I and Phase II are available in `http://roboprop.ai2.upv.es/admittance_with_evader_vf/` and `http://roboprop.ai2.upv.es/admittance_with_evader_pierna_humana_vf/`, respectively.

Figure 5.14 shows the proximity detection to a Type II singularity based on α for the complemented admittance controller during Phase II. In this figure, three periods arise where the patient tries to drive the PR to a Type II singularity ($\alpha_a < lim_\Omega$), and the complemented controller avoids that singularity.

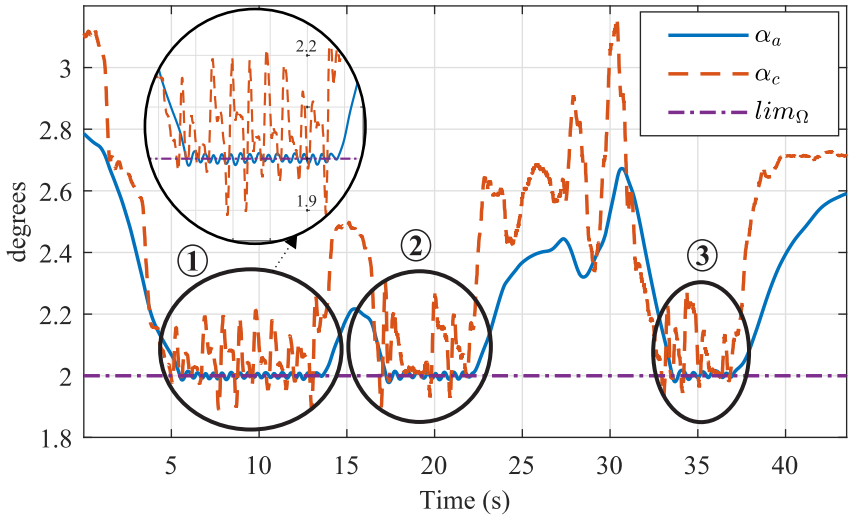

Figure 5.14: Index α during knee rotation with a human limb using the complemented admittance controller.

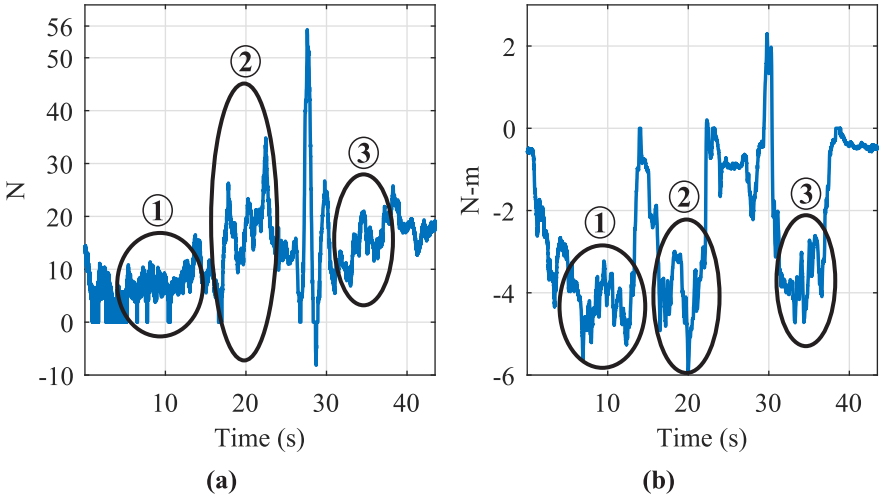

Figure 5.15: Knee rotation with a human limb using the complemented admittance controller: (a) force and (b) moment exerted by the patient in z_m and ψ, respectively.

Figure 5.15 shows the force in z_m and the moment around in the DOF ψ measured during the internal-external knee rotation in Phase II. Figure 5.15

reflects that no discontinuities or sudden changes arise in the patient's foot during the three periods of Type II singularity avoidance. Note that during these three periods of Type II singularity avoidance, the patient did not perceive the deactivation of the admittance control. The non-perception of the deactivation of the admittance control was qualitatively verified by asking the patient. Therefore, the proposed complemented admittance controller overcomes the limitation of the Type II singularities in PRs, making it a safe option for knee rehabilitation.

The deviation from the prescribed trajectory due to Type II singularity avoidance was quantified using the Mean Absolute Error (MAE) between the $\vec{q}_{ind_d}$ and $\vec{q}_{ind_a}$. This deviation could also be represented by the Mean Absolute Percentage Error (MAPE) between the same variables. The MAE and MAPE are calculated as follows:

$$MAE = \frac{1}{F}\sum_{i=1}^{F}\left\{\sum_{k=1}^{n_{av}}\left(\frac{1}{n_s}\sum_{j=h}^{n_s}|q_{ind_a}(i,j) - q_{ind_c}(i,j)|\right)\right\} \tag{5.8}$$

$$MAPE = \frac{100}{F}\sum_{i=1}^{F}\left\{\sum_{k=1}^{n_{av}}\left(\frac{1}{n_s}\sum_{j=h}^{n_s}\left|\frac{q_{ind_a}(i,j) - q_{ind_c}(i,j)}{q_{ind_a}(i,j)}\right|\right)\right\} \tag{5.9}$$

where n_{av} is the number of periods of activation of the Type II singularity avoidance algorithm. n_s is the number of samples in each k period. h is the initial instant of each period of activation of the singularity avoidance algorithm. i and j identify the actuator and the time instant analysed, respectively.

The absence of discontinuities or sudden changes in forces applied by the PR to the patient is verified by the Absolute Variation Rate (AVR) of the actions τ. For the complemented admittance controller, the AVR control actions during the singularity avoidance periods is:

$$AVR = \frac{1}{F}\sum_{i=1}^{F}\left\{\sum_{k=1}^{n_{av}}\left(\frac{1}{n_s}\sum_{j=h}^{n_s}|\tau(i,j) - \tau(i,j-1)|\right)\right\} \tag{5.10}$$

Table 5.2 lists the performance results of the complemented admittance controller during the two experimental Phases. This table shows that the deviation on the q_{ind_a} during a Type II singularity avoidance was lower than 2.5 mm (0.4 %) with an AVR lower than 5 N. This variation in the forces exerted by the PR is negligible because during human walking the leg could exert 500 N on

Table 5.2: Performance of the complemented admittance controller in the 3UPS+RPU PR.

	Phase I	Phase II
MAE (mm)	2.30	1.02
MAPE (%)	0.31	0.12
AVR (N)	3.42	3.83

average, Racic et al. (2009). Thus, the proposed combined admittance controller ensures a smooth behaviour of the 3UPS+RPU PR with a minimum deviation of the rehabilitation trajectory.

The proposed Type II singularity only deviates the trajectory of the actuators on limbs 2 and 4 (q_{23} and q_{42}) because they were identified by $\alpha_c = \Omega_{2,4}$. Figure 5.16a and Figure 5.17a show the location of the actuator on limbs 2 and 4 during the experiment during Phase II, respectively. The signals $*_a$ represent the trajectory defined by the admittance model. The plots $*_d$ are the singularity-free trajectory generated by the singularity avoidance algorithm, and the curves $*_c$ are the actual location reached by the actuator. Figure 5.16b and Figure 5.17b verify that the deviation on the trajectory of the two actuators is less than 2.5 mm during the three periods of Type II singularity avoidance.

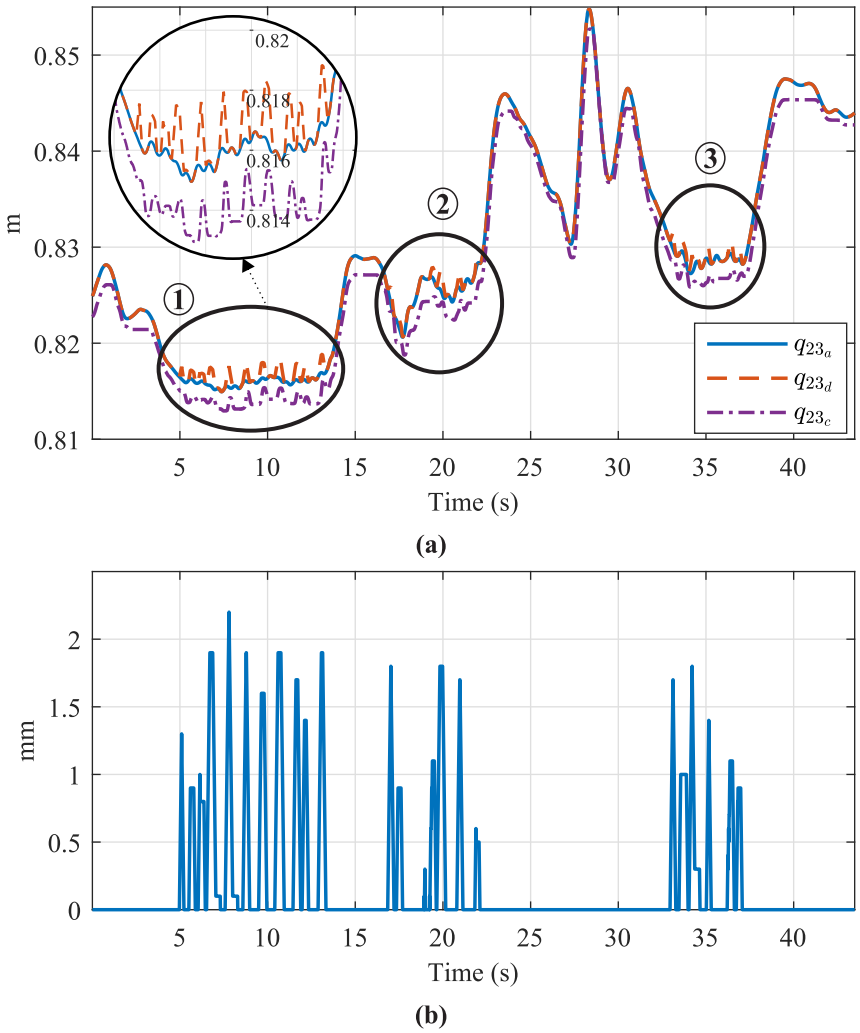

Figure 5.16: Limb 2: (a) tracking of the location of the actuator (b) absolute deviation introduced by the singularity avoidance algorithm, during knee rotation with a human limb.

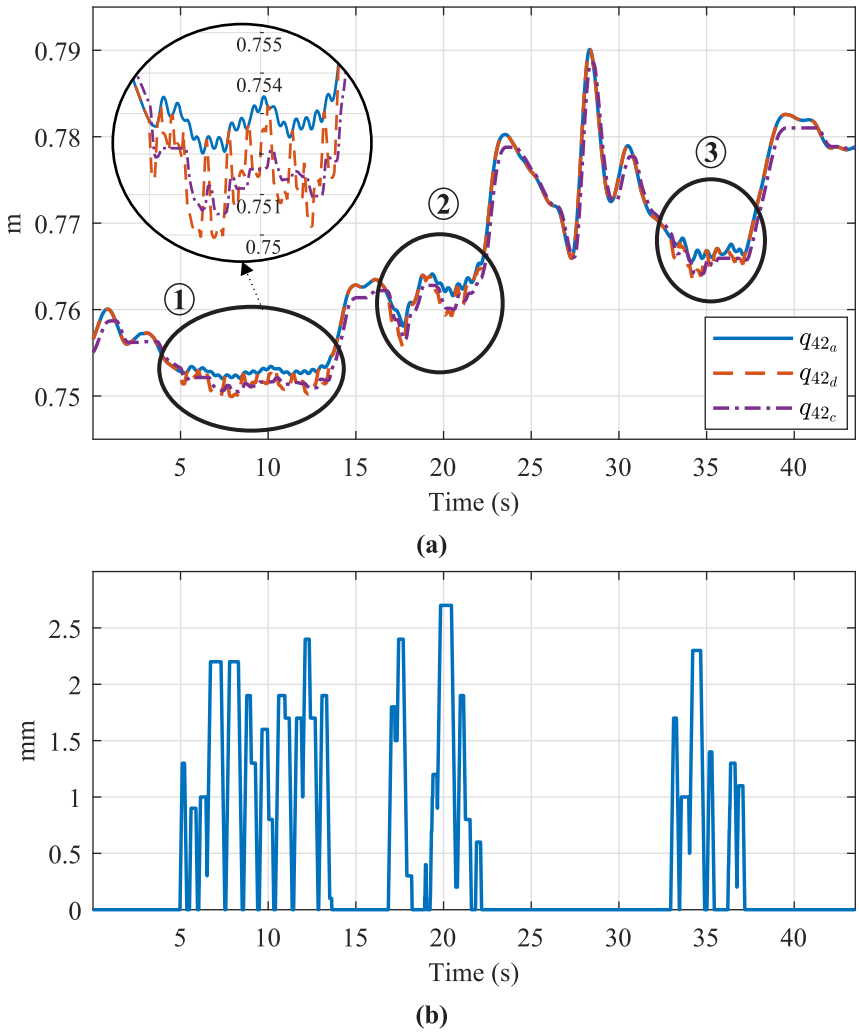

Figure 5.17: Limb 4: (a) tracking of the location of the actuator (b) absolute deviation introduced by the singularity avoidance algorithm, during knee rotation with a human limb.

5.4 Discussion and Conclusions

Conventional admittance control is a suitable strategy for rehabilitation based on PR in a non-singular workspace. In a patient-active exercise, the admittance control lets the patient to modify the movement of the original trajectory according to the pain limit on the human limb. However, in the closeness to a Type II singularity, a non-redundant PR cannot maintain its stiffness, this was verified by experimentation in the 3U$\underline{P}$S+R$\underline{P}$U PR. This limitation makes the conventional admittance controller an unsafe option for human interaction using a PR for knee rehabilitation.

The limitation of the Type II singularities was overcome by complementing the admittance controller with a real-time singularity avoidance algorithm. The proposed complemented admittance controller was successfully applied to a 3U$\underline{P}$S+R$\underline{P}$U PR designed for knee rehabilitation. The completed admittance controller provided complete control over the mobile platform during an internal-external knee rotation performed by an uninjured and unrestricted patient. The real-time avoidance algorithm required a maximum deviation of 2.5 mm in the two actuators identified by α_c to avoid a Type II singularity.

Despite the temporary deactivation of the admittance model during the Type II singularity avoidance, the patient feels no deactivation of the force control. This is because the singularity avoidance algorithm introduces a smooth mechanism taking advantage of the second-order admittance model. Thus, during a Type II singularity avoidance, the complemented admittance controller generated control signals within a 5 N rate of change.

The deterministic strategy of the proposed algorithm for Type II singularity avoidance enables real-time implementation with low computational cost. The effectiveness of the proposed singularity avoidance algorithm depends on measuring the pose reached by the PR with accuracy. The actual pose of the PR could be estimated by solving the FKP based on the feedback of the actuators because the trajectory in joint space is always non-singular. However, for the 3U$\underline{P}$S+R$\underline{P}$U PR the human leg in rehabilitation is injured or has a restriction of motion. For this reason, a pose sensor based on a 3DTS was implemented to increase the safety of the patient. A 3DTS could be expensive for a single rehabilitation PR. However, a single 3DTS is able to measure the location of several PRs at the same time. This feature lets execute several rehabilitation exercises in different rehabilitation robots supervised by the same physiotherapist.

Chapter 6

Conclusions and future research

This chapter reflects the general conclusions of the thesis and proposes lines for future work. The contributions of the thesis were listed in Chapter 1, and the particular discussion and conclusions were presented at the end of each chapter.

6.1 Conclusions

From the results obtained in this thesis, the main conclusions are grouped as follows:

Detecting and measuring the proximity to a Type II singularity

The angles between the linear ($\Theta_{i,j}$) and angular ($\Omega_{i,j}$) components between two i, j normalised Output Twist Screws (OTSs) are able to detect Type II singularities in non-redundant Parallel Robots (PRs). From a theoretical perspective, a Type II singularity appears when $\Theta_{i,j}$ and $\Omega_{i,j}$ are zero. The singularity detection based on $\Theta_{i,j}$ and $\Omega_{i,j}$ was contrasted with respect to the determinant of the forward Jacobian $\|J_D\|$. A planar five bars mechanism for pick and place tasks and a PR with four degrees of freedom (DOFs) for knee rehabilitation were used as case studies in Chapter 3. The 4-DOF PR is named 3UPS+RPU because of its architecture. Note that the PRs under study have no constrained singularities. Thus, these singular configurations are not analysed in this thesis.

The proximity to a Type II singularity is measured with accuracy by the minimum angles $\Theta_{i,j}$ ($min\Theta$) and $\Omega_{i,j}$ ($min\Omega$). This is because if at least two actuators are contributing to the motion of the end-effector in the same direction, two normalised OTSs become parallel, the complete control over the mobile platform is lost. Thus, the indices $min\Theta$ and $min\Omega$ provide a physical meaning of the closeness to a Type II singularity. Moreover, the angular scale of both indices facilitates measuring how close is a singular configuration. The closeness to a Type II singularity is measured by $min\Theta$ in planar robots. In spatial case, the proximity to a singular configuration is measured by $min\Omega$ because the linear component could vanish in non-singular configurations. In Chapter 3, the angle $min\Omega$ was applied to a 4-DOF PR for knee rehabilitation and verified its effectiveness of detecting the closeness to a Type II singularity. The proximity detection to a singular configuration based on $min\Theta$ was evaluated by offline trajectory planning in a symmetrical five mechanism in Chapter 4. The detection and the proximity measure to Type II singularities based on the angles $min\Theta$ and $min\Omega$ are the first contributions of this thesis. The results of this approach were reflected in the papers J2, J4, C2, C4 and C6, see Section 6.3.

Limit of the closeness to a Type II singularity

An experimental procedure for setting a proper limit of closeness to a Type II singularity was successfully developed. The proposed experimental procedure could be applied to arbitrary indices for detecting singularities in non-redundant PRs with different purposes. This procedure requires a proper identification of the common movement developed for a PR and an accurate external measure of the location and orientation (pose) of the mobile platform. The experimental procedure for setting the limit of closeness to a singular configuration for an arbitrary index ι_a is summarised in the following steps:

1. Identification of the fundamental movements according to the application of the PR.

2. Generate a set of test trajectories that approach a Type II singularity from different non-singular.

3. Execute the set of test trajectories on the actual PR under analysis while the actual pose reached by the mobile platform is measured.

4. Define the limit of closeness to a Type II singularity (lim_{ι_a}) averaging the minimum values of the index under analysis where the PR is still in control.

5. Generate a set of verification trajectories considering that the 50 % has a final configuration that $\iota_a < lim_{\iota_a}$ and the rest has a non-singular pose at the end with $\iota_a > lim_{\iota_a}$.

6. Execute the verification trajectories on the actual PR.

7. If the actual PR loses control in the non-singular poses ($\iota_a > lim_{\iota_a}$) the procedure restarts enlarging the number of test trajectories.

The experimental procedure for setting a proper limit of closeness to a Type II singularity was applied to the indices $min\Omega$ and $\|J_D\|$ in the 4-DOF PR for knee rehabilitation. For this purpose, an experimental setup that uses an industrial computer-based control system in conjunction with a 3D Tracking System (3DTS) to measure the pose of the actual 3UPS+RPU PR was applied. The experimental limits lim_Ω and lim_{J_D} determined for the $min\Omega$ and $\|J_D\|$ guarantee that the actual 4-DOF PR does not reach a Type II singularity. Moreover, the procedure needed no model for the errors produced by clearances in the PR joints. This thesis was not intended to establish a direct relation between Type II singularities and manufacturing errors such as joint clearances. The proposed experimental procedure for setting a proper limit of closeness to Type II singularities is the second contribution of this research and it is detailed in Chapter 3. This approach produces the following publications: J4, J6, J8, J9.

Algorithm to release a PR from singular configurations

Based on the angle $min\Omega$ an algorithm to release a non-redundant PR from a Type II singularity was developed. In this novel strategy, the angle $min\Omega$ identifies the pair of limbs that contributes to the motion of the mobile platform in the same direction. Then, the two actuators in the pair of limbs identified by $min\Omega$ are moved to achieve that $min\Omega > lim_\Omega$. The proposed strategy could be combined with different pose control laws and only requires an accurate measure of the actual pose reached by the PR.

In Chapter 4, the algorithm to escape from a Type II singularity was effectively applied in the 3UPS+RPU PR. In this case, the algorithm to release the 4-DOF PR from a singular configuration was combined with a linear algebra-base LAB controller into a two closed-loop controller. The pose of the actual PR was provided by a 3DTS from OptiTrack® because the solution of Forward Kinematic Problem (FKP) is inaccurate in the proximity to a singular configuration. Several simulations and experiments have been conducted with

trajectories that leave the 4-DOF PR in distinct singular configurations, where the releasing algorithm is activated.

Two versions of the singular release algorithm were developed. The version SRA-V1 moves the limbs identified by the angle $min\Omega$ while the second version SRA-V2 moves the limbs not identified by $min\Omega$. The results in simulation, see Section 4.1.1, clearly show that SRA-V1 requires less trajectory deviation to release the PR from the singularity, with respect to SRA-V2. During the experimental evaluation, the SRA-V1 requires an average deviation of 0.54 % (4.09 mm) in the actuator's trajectory to escape from the Type II singularity. Thus, SRA-V1 verified that moving the actuators identified by $min\Omega$ is the best option to release the 3U$\underline{P}$S+R$\underline{P}$U PR from a Type II singularity. The proposed algorithm to release a non-redundant PR was not evaluated in the planar case. However, the block diagram of the singularity release algorithm includes the case of planar PRs. The proposed algorithm to release a general non-redundant PR from a singular configuration represents another contribution of this thesis. The results of the implementation of the proposed algorithm in the 3U$\underline{P}$S+R$\underline{P}$U PR were reflected in the paper J3.

Algorithm to avoid singular configurations

Subsequently, the fourth contribution of this thesis, a novel Type II singularity avoidance algorithm for general purposes based on the angle α was presented in Chapter 4. The avoidance algorithm uses $\alpha = min\Theta$ to detect the proximity to a singularity in the planar PR and $\alpha = min\Omega$ for the spatial case. The proposed avoidance algorithm could be combined with different pose control laws and only requires an accurate measure of the actual pose reached by the PR. However, contrary to the singularity release algorithm the actual pose of the mobile platform can be found by solving Forward Kinematic Problem. It is because the avoidance algorithm ensures a non-singular trajectory at every time.

The parameters for setting the Type II singularity avoidance algorithm are the sample time of the control unit and the average velocity of the PR under analysis. The proposed Type II avoidance algorithm using the solutions of the FKP as feedback was applied for offline trajectory planning in a five bars mechanism (planar case) and in the 3U$\underline{P}$S+R$\underline{P}$U PR (spatial case).

In the planar case, the Type II avoidance algorithm has been successfully applied in offline trajectory planning for a symmetrical 5R mechanism. In the spatial case, the proposed singularity avoidance is implemented for offline and

online trajectory planning for a 3UPS+RPU PR. In the five bars mechanism, the proposed avoidance algorithm introduced a maximum deviation of 2 ° that is imperceptible for the planar PR under study. The velocity trajectory was modified 2 % of the working velocity. In the 3UPS+RPU PR, the trajectories of the two actuators were modified by a maximum of 6 mm, and the velocity profile changed on average 2.4 % of the working velocity. In the 4-DOF PR the avoidance algorithm requires 1 ms in each iteration, which is less than other algorithms for offline trajectory planning for planar PRs, see Table 4.5. Therefore, the proposed algorithm requires a minimum modification on the trajectory of the actuators to avoid a Type II singularity with a low computation cost. The publication C3 derives from the offline trajectory planning results.

The proposed Type II avoidance algorithm, in combination with a Proportional-Integral-Derivative (PID) position controller, was applied for online trajectory planning in the 4-DOF PR for knee rehabilitation. The experimental results show a maximum deviation of 7 mm in the actuators' trajectory with an average elapsed time of 3.86 ms. The minimum movement in a human lower limb is measured in centimetres and the sample time for the control unit in 3UPS+RPU PR is 10 ms. Therefore, the proposed Type II singularity algorithm is suitable for knee rehabilitation purposes. The proposed Type II singularity avoidance algorithm was published in J2. In addition, J1, J5, J7, C1 and C5 were derived form the same approach.

Force position/control complemented with real-time Type II singularity avoidance

Admittance control is the most common strategy for force/position control in patient-active rehabilitation of human limbs. However, in a PR with singularities within its workspace, the admittance control could accidentally drive the end-effector to a Type II singularity. It is because the admittance control provides compliant behaviour in response to the force and moments exerted by a patient. Reaching a Type II singularity during a patient-active exercise is risky to the patient due to the loss of control over the mobile platform. This fact was verified by performing an internal-external knee rotation with a mannequin leg in the actual 3UPS+RPU PR.

In Chapter 5 an admittance control is complemented with the proposed Type II singularity avoidance algorithm to enable the 4-DOF PR for safety human-robot interaction. The real-time application of the proposed avoidance algorithm overcomes the limitation of the Type II singularities. The proposed

complemented admittance controller was successfully applied to a 3UPS+RPU PR. The novel controller provided complete control over the mobile platform during an internal-external knee rotation with a maximum deviation of 2.5 mm in the joint space trajectory during a Type II singularity avoidance. The knee rotation exercise is performed by an uninjured and unrestricted patient. It is important to mention that the proposed avoidance algorithm modifies the trajectory of two actuators because in the proximity to a Type II singularity, at least two actuators transmit motion in the same direction. However, the case of three actuators contributing in the same direction is coped by pairs at each iteration.

In the proximity to a Type II singularity, the real-time avoidance algorithm temporarily deactivated the admittance control. The deactivation of the force control was not perceived by the patient because this study introduced a smooth mechanism that takes advantage of the second-order admittance model. Although the real-time singularity avoidance algorithm could use the solution of the FKP as pose feedback, in the 3UPS+RPU PR, the pose is measured by an OptiTrack® 3DTS. The actual pose of the end-effector is measured by the OptiTrack® 3DTS because the limb in rehabilitation is injured or has a restriction of motion and the safety of the process is essential. Hence, the final contribution of this thesis is the proposed admittance control complemented with the real-time Type II singularity avoidance algorithm because it provides complete control over the 3UPS+RPU PR even in the closeness to singular configurations.

On the other hand, for applications where the safety of patients or objects is not at risk, the actual pose could be estimated by solving the forward kinematics based on the feedback of the actuators. Furthermore, if the application requires high velocities, the singularity avoidance algorithm allows to combine the admittance model with a model-based controller without problems. This is because the location reached by the PR keeps non-singular, avoiding the degeneration of the dynamic model.

6.2 Future research

Based on the results presented in this thesis, the angles between the linear ($\Theta_{i,j}$) and angular ($\Omega_{i,j}$) components between two i, j normalised OTSs may serve for future research in the following lines:

- Knee rehabilitation and diagnosis based on 3UPS+RPU PR.

- Optimisation of the non-singular workspace in non-redundant PR.
- Analyse the relation between singular configurations and the pose errors due to joint clearances.
- Analyse the closeness to a constraint singularities in non-redundant PR.
- Combination of the Type II singularity avoidance algorithm with hybrid and parallel force/position controllers.

The proposed future research lines are detailed below.

Knee rehabilitation and diagnosis based on 3U$\underline{P}$S+R$\underline{P}$U PR

This thesis concludes by enabling the 3U$\underline{P}$S+R$\underline{P}$U PR to develop safe active and passive rehabilitation of the knee. Hence, assisted by expert physiotherapists, the authors were able to carry out knee rehabilitation in patients with real limitations of movement in the lower limb. The measures of the motion of the lower limb in rehabilitation and the forces exerted by the patient could be used to quantify the progress of the rehabilitation procedure. Moreover, the 3U$\underline{P}$S+R$\underline{P}$U PR could be used for non-invasive diagnosis of deficiencies in the knee ligaments.

Optimisation of the non-singular workspace in non-redundant PR

The experimental limit established for the $\|J_D\|$ and the minimum angle $\Theta_{i,j}$ ($min\Omega$) was used for optimising the workspace of the 3U$\underline{P}$S+R$\underline{P}$U PR. The results of the optimisation were combined with spherical rolling joints to build a new prototype of the 3U$\underline{P}$S+R$\underline{P}$U PR, see Figure 6.1.

This new prototype minimises the presence of Type II singularities and the errors in position and orientation due to joint clearances. However, the optimisation based on the angle $min\Omega$ has not been evaluated in detail. In addition, the $min\Theta$ was not used for optimisation purposes. Thus, the optimal design of general non-redundant parallel robots could be developed based on the angles $min\Omega$ and $min\Theta$.

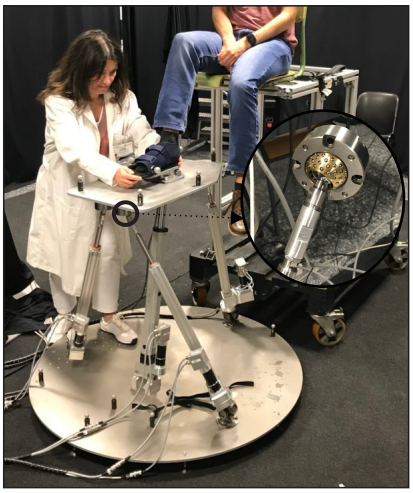

Figure 6.1: Prototype of the 3UPS+RPU PR with spherical rolling joints, after optimisation of the workspace.

Analyse the relation between singular configurations and the pose errors due to joint clearances

The error due to joint clearances was indirectly incorporated in the proposed experimental procedure for setting a proper limit of closeness to a Type II singularity. In addition, to date modelling the error due to the join clearances is still a challenging problem. Hence, this study could be a starting point for researching the relation between Type II singularities and errors from the joint clearances.

Analyse the closeness to a constraint singularities in non-redundant PR

The singularity analysis based on $min\Omega$ and $min\Theta$ was limited to non-redundant PRs where the unused DOFs are constrained by mechanical limitations. Thus, the singular configurations that appear only in PRs with the unused DOFs constrained by the disposition of the limbs have not been analysed. The constraints due to the distribution of the limbs could be added to the formulation of the normalised Output Twist Screws (OTSs). Therefore, constraint singularities could be analysed by the angles $\Theta_{i,j}$ and $\Omega_{i,j}$ after modifying the procedure to calculate the OTSs.

Combination of the Type II singularity avoidance algorithm with hybrid and parallel force/position controllers

The proposed Type II singularity avoidance algorithm was applied in combination with the admittance model for a specific knee rehabilitation robot. The possibility of combining the proposed singularity avoidance algorithm with other strategies for force/position control has not been analysed. Moreover, due to the low dynamic of knee rehabilitation, the position controllers have no compensation for dynamic components such as inertial forces, and centrifugal and Coriolis effects.

Hereby, in future works, the Type II singularity could be implemented in combination with another force/position controller in the outer loop, and model-based controllers in the inner loop. The combination of the proposed avoidance algorithm with force/position strategies could be extended to different PR fields, such as ankle rehabilitation, upper-limb rehabilitation and collaborative robotics.

6.3 Publications

Journal papers with Impact Factor

J1 Escarabajal, R. J., **Pulloquinga, J. L.**, Valera, Á., Mata, V., Vallés, M., and Castillo, F. (2023). Combined Admittance Control With Type II Singularity Evasion for Parallel Robots Using Dynamic Movement Primitives. *IEEE Transactions on Robotics*. DOI: 10.1109/TRO.2023.3238136. **Q1** in ROBOTICS.

J2 **Pulloquinga, J. L.**, Escarabajal, R. J., Valera, Á., Vallés, M., and Mata, V. (2023). A Type II singularity avoidance algorithm for parallel manipulators using output twist screws. *Mechanism and Machine Theory*, 183:105282. DOI: 10.1016/j.mechmachtheory.2023.105282. **Q1** in ENGINEERING, MECHANICAL.

J3 **Pulloquinga, J. L.**, Escarabajal, R. J., Ferrándiz, J., Vallés, M., Mata, V., and Urízar, M. (2021). Vision-Based Hybrid Controller to Release a 4-DOF Parallel Robot from a Type II Singularity. *Sensors*, 21(12). DOI: 10.3390/S21124080. **Q2** in INSTRUMENTS & INSTRUMENTATION.

J4 **Pulloquinga, J. L.**, Mata, V., Valera, Á., Zamora-Ortiz, P., Díaz-Rodríguez, M., and Zambrano, I. (2021). Experimental analysis of Type

II singularities and assembly change points in a 3UPS+RPU parallel robot. *Mechanism and Machine Theory*, 158. DOI: 10.1016/j.mechmachtheory.2020.104242. **Q1** in ENGINEERING, MECHANICAL.

J5 Zamora-Ortiz, P., Carral-Alvaro, J., Valera, Á., **Pulloquinga, J. L.**, Escarabajal, R. J., and Mata, V. (2021). Identification of Inertial Parameters for Position and Force Control of Surgical Assistance Robots. *Mathematics*, 9:773. DOI: 10.3390/math9070773. **Q1** in MATHEMATICS.

J6 Llopis-Albert, C., Valero, F., Mata, V., **Pulloquinga, J. L.**, Zamora-Ortiz, P., and Escarabajal, R. J. (2020). Optimal Reconfiguration of a Parallel Robot for Forward Singularities Avoidance in Rehabilitation Therapies. A Comparison via Different Optimization Methods. *Sustainability*, 12:5803. DOI: 10.3390/su12145803. **Q3** in GREEN & SUSTAINABLE SCIENCE & TECHNOLOGY.

Journal papers indexed

J7 **Pulloquinga, J. L.**, Escarabajal, R. J., Mata, V., Valera, A., Zambrano, I., and Rosales, A. (2022). Gravitational Base Parameters Identification for a Knee Rehabilitation Parallel Robot. *International Journal on Advanced Science, Engineering and Information Technology*, 12:501. DOI: 10.18517/ijaseit.12.2.15289.

J8 Llopis-Albert, C., Valero, F., Mata, V., Escarabajal, R. J., Zamora-Ortiz, P., and **Pulloquinga, J. L.** (2020). Optimal Reconfiguration of a Limited Parallel Robot for Forward Singularities Avoidance. *Multidisciplinary Journal for Education, Social and Technological Sciences*, 7:113. DOI: 10.4995/muse.2020.13352.

J9 Escarabajal, R. J., Abu-Dakka, F. J., **Pulloquinga, J. L.**, Mata, V., Vallés, M., and Valera, Á. (2020). Development of lower-limb rehabilitation exercises using 3-PRS Parallel Robot and Dynamic Movement Primitives. *Multidisciplinary Journal for Education, Social and Technological Sciences*, 7:30. DOI: 10.4995/muse.2020.13907.

Conference papers

C1 **Pulloquinga, J. L.**, Altuzarra, O., Petuya, V., Hernandez, A., Mata, V., and Valera, Á. (2022). Estudio Del Contacto Cuasi-Estático De

Un Robot Paralelo Flexible En Tareas Colaborativas. In *XV Congreso Iberoamericano de Ingeniería Mecánica 2022*, volume 1. URL: https://cibim2022.com/CIBIM2022.

C2 **Pulloquinga, J. L.**, Ceccarelli, M., Mata, V., and Valera, Á. (2022). Experimental Identification of Singularities in Parallel Manipulators. In *SYROM & ROBOTICS 2022 Joint International Conference of the 13th IFToMM International Symposium on Science of Mechanisms and Machines*, volume 1. URL: https://syrom-robot.upt.ro/.

C3 **Pulloquinga, J. L.**, Escarabajal, R. J., Vallés, M., Valera, Á., and Mata, V. (2022). Trajectory Planner for Type II Singularities Avoidance Based on Output Twist Screws. In *Advances in Robot Kinematics 2022*, volume 24, pages 445–452. Springer International Publishing. URL: https://link.springer.com/10.1007/978-3-031-08140-8_48.

C4 **Pulloquinga, J. L.**, Mata, V., Valera, Á., Vallés, M., Escarabajal, R. J., and Zamora-Ortiz, P. (2021). Performance analysis in a 3UPS+RPU parallel robot of controllers designed using co-simulation. In *International Symposium on Co-Simulation and Solver Coupling in Dynamics 2021*, volume 1. URL: http://lim.ii.udc.es/events/cosim2020/. Online.

C5 **Pulloquinga, J. L.**, Escarabajal, R. J., Mata, V., Valera, Á., Iván, Z., and Andres, R. (2021). Gravitational Base Parameters Identification for a Knee Rehabilitation Parallel Robot. In *Mechanical Engineering Trends 2021*, volume 1. URL: https://met.epn.edu.ec/index.php/es/. Online.

C6 **Pulloquinga, J. L.**, Mata, V., Valera, Á., Díaz-Rodríguez, M., and Zambrano, I. (2019). Evaluación de la Cercanía a Singularidades Mediante Índices de Transmisión de Salida en Un Robot Paralelo 3UPS + RPU. In *XIV Congreso Iberoamericano de Ingeniería Mecánica 2019*, volume 1.URL: https://feibim.org/cibim-descarga/.

References

ABB Group (2022). Delicious pastries with your coffee courtesy of ABB robots. https://new.abb.com/news/detail/71261/delicious-pastries-with-your-coffee-courtesy-of-abb-robots. Accessed 2022-12-15. (cit. on p. xvii, 15, 16).

Agarwal, A., Nasa, C., and Bandyopadhyay, S. (2016). Dynamic singularity avoidance for parallel manipulators using a task-priority based control scheme. *Mechanism and Machine Theory*, 96:107–126. (cit. on p. 5, 6, 31).

Aginaga, J., Iriarte, X., Plaza, A., and Mata, V. (2018). Kinematic Design of a New Four Degree-of-Freedom Parallel Robot for Knee Rehabilitation. *Journal of Mechanical Design*, 140. (cit. on p. 4).

Altuzarra, O., Pinto, C., Aviles, R., and Hernandez, A. (2004). *A Practical Procedure to Analyze Singular Configurations in Closed Kinematic Chains*, volume 20. Institute of Electrical and Electronics Engineers Inc. (cit. on p. 4).

Amine, S., Masouleh, M. T., Caro, S., Wenger, P., and Gosselin, C. (2012). Singularity analysis of 3T2R parallel mechanisms using Grassmann–Cayley algebra and Grassmann geometry. *Mechanism and Machine Theory*, 52:326–340. (cit. on p. 6).

Arakelian, V., Briot, S., and Glazunov, V. (2008). Increase of singularity-free zones in the workspace of parallel manipulators using mechanisms of variable structure. *Mechanism and Machine Theory*, 43:1129–1140. (cit. on p. 5, 28).

Araujo-Gómez, P., Díaz-Rodríguez, M., Mata, V., and González-Estrada, O. A. (2019). Kinematic analysis and dimensional optimization of a 2R2T parallel manipulator. *Journal of the Brazilian Society of Mechanical Sciences and Engineering*, 41:425. (cit. on p. 5, 29, 46).

Araujo-Gómez, P., Mata, V., Díaz-Rodríguez, M., Valera, A., and Page, A. (2017). Design and Kinematic Analysis of a Novel 3UPS/RPU Parallel Kinematic Mechanism With 2T2R Motion for Knee Diagnosis and Rehabilitation Tasks. *Journal of Mechanisms and Robotics*, 9:061004. (cit. on p. 46, 50, 86).

Banala, S. K., Kim, S. H., Agrawal, S. K., and Scholz, J. P. (2009). Robot Assisted Gait Training With Active Leg Exoskeleton (ALEX). *IEEE Transactions on Neural Systems and Rehabilitation Engineering*, 17:2–8. (cit. on p. 2).

Baron, N., Philippides, A., and Rojas, N. (2020). A robust geometric method of singularity avoidance for kinematically redundant planar parallel robot manipulators. *Mechanism and Machine Theory*, 151:103863. (cit. on p. xvii, 28).

Ben-Horin, P. and Shoham, M. (2006). Singularity condition of six-degree-of-freedom three-legged parallel robots based on Grassmann - Cayley Algebra. *IEEE Transactions on Robotics*, 22:577–590. (cit. on p. xvii, 6, 23).

Blaya, J. and Herr, H. (2004). Adaptive control of a variable-impedance ankle-foot orthosis to assist drop-foot gait. *IEEE Transactions on Neural Systems and Rehabilitation Engineering*, 12:24–31. (cit. on p. 2).

Block, D. J., Michelotti, M. B., and Sreenivas, R. S. (2013). Application of the Novint Falcon haptic device as an actuator in real-time control. *Paladyn, Journal of Behavioral Robotics*, 4:182–193. (cit. on p. xvii, 16).

Bohigas, O., Henderson, M. E., Ros, L., Manubens, M., and Porta, J. M. (2013). Planning Singularity-Free Paths on Closed-Chain Manipulators. *IEEE Transactions on Robotics*, 29:888–898. (cit. on p. 30, 84).

Bourbonnais, F., Bigras, P., and Bonev, I. A. (2015). Minimum-Time Trajectory Planning and Control of a Pick-and-Place Five-Bar Parallel Robot. *IEEE/ASME Transactions on Mechatronics*, 20:740–749. (cit. on p. 30).

Briot, S. and Arakelian, V. (2008). Optimal Force Generation in Parallel Manipulators for Passing through the Singular Positions. *The International Journal of Robotics Research*, 27:967–983. (cit. on p. 5, 31).

Briot, S. and Khalil, W. (2015). *Dynamics of Parallel Robots*, volume 35. Springer International Publishing, 1 edition. (cit. on p. 6, 14, 15).

Bu, W. (2016). Closeness to singularities of robotic manipulators measured by characteristic angles. *Robotica*, 34:2105–2115. (cit. on p. 24, 27).

Caro, S., Wenger, P., and Chablat, D. (2012). Non-Singular Assembly Mode Changing Trajectories of a 6-DOF Parallel Robot. In *ASME 2012 International Design Engineering Technical Conferences and Computers and Information in Engineering Conference*, volume 4, pages 1245–1254. American Society of Mechanical Engineers. (cit. on p. 29).

Chiaverini, S. and Sciavicco, L. (1988). Force/Position Control of Manipulators in Task Space with Dominance in Force. *IFAC Proceedings Volumes*, 21:137–143. (cit. on p. 95).

Choudhury, P. and Ghosal, A. (2000). Singularity and controllability analysis of parallel manipulators and closed-loop mechanisms. *Mechanism and Machine Theory*, 35:1455–1479. (cit. on p. 22).

Cieza, A., Causey, K., Kamenov, K., Hanson, S. W., Chatterji, S., and Vos, T. (2020). Global estimates of the need for rehabilitation based on the Global Burden of Disease study 2019: a systematic analysis for the Global Burden of Disease Study 2019. *The Lancet*, 396:2006–2017. (cit. on p. 1).

Clavel, R. (1988). A fast robot with parallel geometry. In *Proc. Int. Symposium on Industrial Robots*, pages 91–100. (cit. on p. 16).

Cleveland, W. S. and Loader, C. (1996). Smoothing by Local Regression: Principles and Methods. In *Statistical Theory and Computational Aspects of Smoothing*, pages 10–49. (cit. on p. 51).

Colombo, G., Joerg, M., Schreier, R., and Dietz, V. (2000). Treadmill training of paraplegic patients using a robotic orthosis. *Journal of rehabilitation research and development*, 37(6):693–700. (cit. on p. 2).

Conconi, M. and Carricato, M. (2009). A New Assessment of Singularities of Parallel Kinematic Chains. *IEEE Transactions on Robotics*, 25:757–770. (cit. on p. 22).

Corinaldi, D., Callegari, M., and Angeles, J. (2018). Singularity-free path-planning of dexterous pointing tasks for a class of spherical parallel mechanisms. *Mechanism and Machine Theory*, 128:47–57. (cit. on p. 5).

Dalvand, M. M. and Shirinzadeh, B. (2012). Remote centre-of-motion control algorithms of 6-RRCRR parallel robot assisted surgery system (PRAMiSS). In *2012 IEEE International Conference on Robotics and Automation*, pages 3401–3406. IEEE. (cit. on p. xvii, 16, 17).

Dash, A. K., Chen, I.-M., Yeo, S. H., and Yang, G. (2005). Workspace generation and planning singularity-free path for parallel manipulators. *Mechanism and Machine Theory*, 40:776–805. (cit. on p. 5).

Davidson, J. K., Hunt, K. H., and Pennock, G. R. (2004). Robots and Screw Theory: Applications of Kinematics and Statics to Robotics. *Journal of Mechanical Design*, 126:763–764. (cit. on p. 28).

di Gregorio, R. and Parenti-Castelli, V. (1999). Mobility analysis of the 3-UPU parallel mechanism assembled for a pure translational motion. In *1999 IEEE/ASME International Conference on Advanced Intelligent Mechatronics (Cat. No.99TH8399)*, pages 520–525. IEEE. (cit. on p. 22).

Dong, M., Fan, W., Li, J., Zhou, X., Rong, X., Kong, Y., and Zhou, Y. (2021). A New Ankle Robotic System Enabling Whole-Stage Compliance Rehabilitation Training. *IEEE/ASME Transactions on Mechatronics*, 26:1490–1500. (cit. on p. 4, 6).

Doty, K. L., Schwartz, E. M., Melchiorri, C., and Bonivento, C. (1995). Robot Manipulability. *IEEE Transactions on Robotics and Automation*, 11:462–468. (cit. on p. 25).

Díaz, I., Gil, J. J., and Sánchez, E. (2011). Lower-Limb Robotic Rehabilitation: Literature Review and Challenges. *Journal of Robotics*, 2011:1–11. (cit. on p. xvii, 2, 3).

Fan, Y. and Yin, Y. (2013). Active and Progressive Exoskeleton Rehabilitation Using Multisource Information Fusion From EMG and Force-Position EPP. *IEEE Transactions on Biomedical Engineering*, 60:3314–3321. (cit. on p. 4, 94).

Freivogel, S., Mehrholz, J., Husak-Sotomayor, T., and Schmalohr, D. (2008). Gait training with the newly developed 'LokoHelp'-system is feasible for non-ambulatory patients after stroke, spinal cord and brain injury. A feasibility study. *Brain Injury*, 22:625–632. (cit. on p. xvii, 2, 3).

Gallardo-Alvarado, J., Rodríguez-Castro, R., and Delossantos-Lara, P. J. (2018). Kinematics and dynamics of a 4-PRUR Schönflies parallel manipulator by means of screw theory and the principle of virtual work. *Mechanism and Machine Theory*, 122:347–360. (cit. on p. 22).

Gasparetto, A., Boscariol, P., Lanzutti, A., and Vidoni, R. (2015). Path Planning and Trajectory Planning Algorithms: A General Overview. In *Mechanisms and Machine Science*, volume 29, pages 3–27. Springer International Publishing. (cit. on p. 29).

Girone, M., Burdea, G., Bouzit, M., Popescu, V., and Deutsch, J. E. (2001). Stewart platform-based system for ankle telerehabilitation. *Autonomous Robots*, 10:203–212. (cit. on p. xvii, 3, 16, 17).

Gosselin, C. (1988). *Kinematic Analysis, Optimization and Programming of Parallel Robotic Manipulators*. PhD thesis, McGill University. (cit. on p. 25).

Gosselin, C. and Angeles, J. (1990). Singularity analysis of closed-loop kinematic chains. *IEEE Transactions on Robotics and Automation*, 6:281–290. (cit. on p. 6, 19).

Heesbeen, B., Ruigrok, R., and Hoekstra, J. (2006). GRACE - a Versatile Simulator Architecture Making Simulation of Multiple Complex Aircraft Simple. In *AIAA Modeling and Simulation Technologies Conference and Exhibit*, volume 1, pages 643–656. American Institute of Aeronautics and Astronautics. (cit. on p. xvii, 16).

Hernandez, A., Altuzarra, O., Petuya, V., and Macho, E. (2009). Defining Conditions for Nonsingular Transitions Between Assembly Modes. *IEEE Transactions on Robotics*, 25:1438–1447. (cit. on p. 29).

Hesse, S. and Uhlenbrock, D. (2000). A mechanized gait trainer for restoration of gait. *Journal of rehabilitation research and development*, 37:701–708. (cit. on p. 2).

Hesselbach, J., Maaß, J., and Bier, C. (2005). Singularity Prediction for Parallel Robots for Improvement of Sensor-Integrated Assembly. *CIRP Annals*, 54:349–352. (cit. on p. 30).

Hill, R. B., Six, D., Chriette, A., Briot, S., and Martinet, P. (2017). Crossing type 2 singularities of parallel robots without pre-planned trajectory with a virtual-constraint-based controller. In *IEEE International Conference on Robotics and Automation*, pages 6080–6085. Institute of Electrical and Electronics Engineers Inc. (cit. on p. 6, 30).

Hogan, N. (1985). Impedance Control: An Approach to Manipulation: Part II—Implementation. *Journal of Dynamic Systems, Measurement, and Control*, 107:8–16. (cit. on p. 96).

Hubert, J. and Merlet, J.-P. (2009). Static of Parallel Manipulators and Closeness to Singularity. *Journal of Mechanisms and Robotics*, 1:1–6. (cit. on p. 26, 28).

IHME (2021). WHO Rehabilitation Need Estimator. `https://www.healthdata.org/data-visualization/who-rehabilitation-need-estimator`. Accessed 2022-12-09. (cit. on p. 1).

Innocenti, C. and Parenti-Castelli, V. (1998). Singularity-Free Evolution From One Configuration to Another in Serial and Fully-Parallel Manipulators. *Journal of Mechanical Design*, 120:73–79. (cit. on p. 29).

Iqbal, A., Iqbal, K., Ali, S. A., Azim, D., Farid, E., Baig, M. D., Arif, T. B., and Raza, M. (2021). The COVID-19 Sequelae: A Cross-Sectional Evaluation of Post-recovery Symptoms and the Need for Rehabilitation of COVID-19 Survivors. *Cureus*, 13. (cit. on p. 1).

Joshi, S. A. and Tsai, L.-W. (2002). Jacobian Analysis of Limited-DOF Parallel Manipulators. *Journal of Mechanical Design*, 124:254–258. (cit. on p. 6, 22).

Ju, M.-S., Lin, C.-C., Lin, D.-H., Hwang, I.-S., and Chen, S.-M. (2005). A rehabilitation robot with force-position hybrid fuzzy controller: hybrid fuzzy control of rehabilitation robot. *IEEE Transactions on Neural Systems and Rehabilitation Engineering*, 13:349–358. (cit. on p. 4, 94).

Khoukhi, A., Baron, L., and Balazinski, M. (2009). Constrained multi-objective trajectory planning of parallel kinematic machines. *Robotics and Computer-Integrated Manufacturing*, 25:756–769. (cit. on p. 5, 30, 84).

Kim, M. J., Lee, W., Choi, J. Y., Chung, G., Han, K. L., Choi, I. S., Ott, C., and Chung, W. K. (2019). A passivity-based nonlinear admittance control with application to powered upper-limb control under unknown environmental interactions. *IEEE/ASME Transactions on Mechatronics*, 24:1473–1484. (cit. on p. 4, 98).

Kim, S.-G. and Ryu, J. (2003). New dimensionally homogeneous jacobian matrix formulation by three end-effector points for optimal design of parallel manipulators. *IEEE Transactions on Robotics and Automation*, 19:731–737. (cit. on p. 23).

Kolpashchikov, D., Gerget, O., and Meshcheryakov, R. (2022). Robotics in Healthcare. In Lim, C., Chen, Y., Vaidya, A., Mahorkar, C., and Jain, L., editors, *Handbook of Artificial Intelligence in Healthcare*, volume 212, pages 281–306. Springer International Publishing, 1 edition. (cit. on p. 2).

Leinonen, T. (1991). Terminology for the theory of machines and mechanisms. *Mechanism and Machine Theory*, 26(5):435–539. (cit. on p. 13).

Li, Y., Huang, T., and Chetwynd, D. G. (2018). An approach for smooth trajectory planning of high-speed pick-and-place parallel robots using quintic B-splines. *Mechanism and Machine Theory*, 126:479–490. (cit. on p. 30).

Liu, G., Lou, Y., and Li, Z. (2003). Singularities of parallel manipulators: a geometric treatment. *IEEE Transactions on Robotics and Automation*, 19:579–594. (cit. on p. 22).

Liu, X.-J. and Wang, J. (2014). *Parallel Kinematics*. Springer Berlin Heidelberg. (cit. on p. 4, 14).

Liu, X.-J., Wang, J., and Pritschow, G. (2006). Performance atlases and optimum design of planar 5R symmetrical parallel mechanisms. *Mechanism and Machine Theory*, 41:119–144. (cit. on p. 28, 41).

Liu, X.-J., Wu, C., and Wang, J. (2012). A New Approach for Singularity Analysis and Closeness Measurement to Singularities of Parallel Manipulators. *Journal of Mechanisms and Robotics*, 4:041001. (cit. on p. 6, 24, 25, 27).

Maruyama, Y., Kato, S., and Azumi, T. (2016). Exploring the performance of ROS2. In *Proceedings of the 13th International Conference on Embedded Software*, pages 1–10. ACM. (cit. on p. 75).

McAree, P. R. and Daniel, R. W. (1999). An Explanation of Never-Special Assembly Changing Motions for 3–3 Parallel Manipulators. *The International Journal of Robotics Research*, 18:556–574. (cit. on p. 20).

McDaid, A., Tsoi, Y. H., and Xie, S. (2013). MIMO Actuator Force Control of a Parallel Robot for Ankle Rehabilitation. In *Interdisciplinary Mechatronics*, pages 163–208. John Wiley and Sons, Inc., 1 edition. (cit. on p. 4, 6).

MECADEMIC (2022). Affordable dual-arm SCARA academic robot. `https://www.mecademic.com/en/products`. Accessed 2022-12-15. (cit. on p. xvii, 15, 16).

Meng, W., Liu, Q., Zhou, Z., Ai, Q., Sheng, B., and Xie, S. S. (2015). Recent development of mechanisms and control strategies for robot-assisted lower limb rehabilitation. *Mechatronics*, 31:132–145. (cit. on p. 4, 94, 98).

Merlet, J.-P. (1989). Singular Configurations of Parallel Manipulators and Grassmann Geometry. *The International Journal of Robotics Research*, 8:45–56. (cit. on p. xvii, 6, 23).

Merlet, J. P. (2006). Jacobian, Manipulability, Condition Number, and Accuracy of Parallel Robots. *Journal of Mechanical Design*, 128:199–206. (cit. on p. 6, 22, 25).

Monsarrat, B. and Gosselin, C. M. (2001). Singularity Analysis of a Three-Leg Six-Degree-of-Freedom Parallel Platform Mechanism Based on Grassmann Line Geometry. *The International Journal of Robotics Research*, 20:312–328. (cit. on p. 6, 23).

Morell, A., Tarokh, M., and Acosta, L. (2013). Solving the forward kinematics problem in parallel robots using Support Vector Regression. *Engineering Applications of Artificial Intelligence*, 26:1698–1706. (cit. on p. 10).

Neumann, D. A. (2016). *Kinesiology of the Musculoskeletal System: Foundations for Rehabilitation*. Elsevier Health Sciences, 3 edition. (cit. on p. 53).

Nouri Rahmat Abadi, B. and Carretero, J. A. (2022). Modeling and Real-Time Motion Planning of a Class of Kinematically Redundant Parallel Mechanisms With Reconfigurable Platform. *Journal of Mechanisms and Robotics*, 15. (cit. on p. 5, 28, 31).

Pagis, G., Bouton, N., Briot, S., and Martinet, P. (2015). Enlarging parallel robot workspace through Type-2 singularity crossing. *Control Engineering Practice*, 39:1–11. (cit. on p. 31).

Park, F. C. and Kim, J. W. (1999). Singularity Analysis of Closed Kinematic Chains. *Journal of Mechanical Design*, 121:32–38. (cit. on p. 20).

Patel, Y. D. and George, P. M. (2012). Parallel Manipulators Applications—A Survey. *Modern Mechanical Engineering*, 02:57–64. (cit. on p. 15).

Rabischong, P. and Bel, J.-P. (1976). Orthopaedic appliances. Patent US3993056A. (cit. on p. 2).

Racic, V., Pavic, A., and Brownjohn, J. (2009). Experimental identification and analytical modelling of human walking forces: Literature review. *Journal of Sound and Vibration*, 326:1–49. (cit. on p. 113).

Raibert, M. H. and Craig, J. J. (1981). Hybrid Position/Force Control of Manipulators. *Journal of Dynamic Systems, Measurement, and Control*, 103:126–133. (cit. on p. 94).

Rastegarpanah, A., Saadat, M., and Borboni, A. (2016). Parallel Robot for Lower Limb Rehabilitation Exercises. *Applied Bionics and Biomechanics*, 2016:1–10. (cit. on p. 4).

Russo, M., Herrero, S., Altuzarra, O., and Ceccarelli, M. (2018). Kinematic analysis and multi-objective optimization of a 3-UPR parallel mechanism for a robotic leg. *Mechanism and Machine Theory*, 120:192–202. (cit. on p. 5).

Saafi, H., Laribi, M. A., and Zeghloul, S. (2015). Redundantly actuated 3-RRR spherical parallel manipulator used as a haptic device: improving dexterity and eliminating singularity. *Robotica*, 33:1113–1130. (cit. on p. xvii, 5, 27, 28).

Saglia, J., Tsagarakis, N., Dai, J., and Caldwell, D. (2009). A High-performance Redundantly Actuated Parallel Mechanism for Ankle Rehabilitation. *The International Journal of Robotics Research*, 28:1216–1227. (cit. on p. 4).

Saglia, J. A., Tsagarakis, N. G., Dai, J. S., and Caldwell, D. G. (2013). Control Strategies for Patient-Assisted Training Using the Ankle Rehabilitation Robot (ARBOT). *IEEE/ASME Transactions on Mechatronics*, 18:1799–1808. (cit. on p. 4, 94).

Sawicki, G. S. and Ferris, D. P. (2009). A pneumatically powered knee-ankle-foot orthosis (KAFO) with myoelectric activation and inhibition. *Journal of NeuroEngineering and Rehabilitation*, 6:23. (cit. on p. 2).

Schmidt, H., Hesse, S., Bernhardt, R., and Krüger, J. (2005). HapticWalker—a novel haptic foot device. *ACM Transactions on Applied Perception*, 2:166–180. (cit. on p. xvii, 3).

Schumacher, M., Wojtusch, J., Beckerle, P., and von Stryk, O. (2019). An introductory review of active compliant control. *Robotics and Autonomous Systems*, 119:185–200. (cit. on p. 98).

Sen, S., Dasgupta, B., and Mallik, A. K. (2003). Variational approach for singularity-free path-planning of parallel manipulators. *Mechanism and Machine Theory*, 38:1165–1183. (cit. on p. 29).

Shiller, Z. (2015). Off-Line and On-Line Trajectory Planning. In *Mechanisms and Machine Science*, volume 29, pages 29–62. Springer International Publishing. (cit. on p. 5, 29).

Six, D., Briot, S., Chriette, A., and Martinet, P. (2017). A controller for avoiding dynamic model degeneracy of parallel robots during type 2 singularity crossing. In *New Trends in Mechanism and Machine Science*, volume 43, pages 589–597. Kluwer Academic Publishers. (cit. on p. 31).

Slavutin, M., Shai, O., Sheffer, A., and Reich, Y. (2019). A novel criterion for singularity analysis of parallel mechanisms. *Mechanism and Machine Theory*, 137:459–475. (cit. on p. 24).

Sosa-Lopez, E. D., Arias-Montiel, M., and Lugo-Gonzalez, E. (2017). A numerical approach for the inverse and forward kinematic analysis of 5R parallel manipulator. In *2017 14th International Conference on Electrical Engineering, Computing Science and Automatic Control (CCE)*, pages 1–6. Institute of Electrical and Electronics Engineers. (cit. on p. 43, 83).

Staicu, S. (2019). *Dynamics of Parallel Robots*. Springer International Publishing, 1 edition. (cit. on p. 15).

Stewart, D. (1965). A Platform with Six Degrees of Freedom. *Proceedings of the Institution of Mechanical Engineers*, 180(1):371–386. (cit. on p. 16).

Taghirad, H. D. (2013). *Parallel Robots*. CRC Press, 1 edition. (cit. on p. 4, 15).

Takeda, Y. and Funabashi, H. (1995). Motion Transmissibility of In-Parallel Actuated Manipulators. *JSME international journal. Ser. C, Dynamics, control, robotics, design and manufacturing*, 38:749–755. (cit. on p. 8, 24, 34).

Tufekciler, N., van Asseldonk, E. H. F., and van der Kooij, H. (2011). Velocity-dependent reference trajectory generation for the LOPES gait training robot. In *2011 IEEE International Conference on Rehabilitation Robotics*, pages 1–5. IEEE. (cit. on p. 2).

Urízar, M. (2012). *Methology to enlarge the workspace of parallel manipulators by means of non-singular transitions*. PhD thesis, University of the Basque Country (UPV/EHU). (cit. on p. 29).

Valero, F., Díaz-Rodríguez, M., Vallés, M., Besa, A., Bernabéu, E., and Ángel Valera (2020). Reconfiguration of a parallel kinematic manipulator with 2T2R motions for avoiding singularities through minimizing actuator forces. *Mechatronics*, 69:102382. (cit. on p. 5, 29, 46).

Vallés, M., Araujo-Gómez, P., Mata, V., Valera, A., Díaz-Rodríguez, M., Álvaro Page, and Farhat, N. M. (2018). Mechatronic design, experimental setup, and control architecture design of a novel 4 DoF parallel manipulator. *Mechanics Based Design of Structures and Machines*, 46:425–439. (cit. on p. 5, 46).

Vallés, M., Cazalilla, J., Ángel Valera, Mata, V., Álvaro Page, and DIáz-Rodríguez, M. (2017). A 3-PRS parallel manipulator for ankle rehabilitation: Towards a low-cost robotic rehabilitation. *Robotica*, 35:1939–1957. (cit. on p. 4).

Van der Loos, H. M., Reinkensmeyer, D. J., and Guglielmelli, E. (2016). Rehabilitation and Health Care Robotics. In Siciliano, B. and Khatib, O., editors, *Springer Handbook of Robotics*, pages 1685–1728. Springer International Publishing, 2 edition. (cit. on p. 1, 2).

Voglewede, P. and Ebert-Uphoff, I. (2004). Measuring "closeness" to singularities for parallel manipulators. In *IEEE International Conference on Robotics and Automation, 2004. Proceedings. ICRA '04. 2004*, pages 4539–4544 Vol.5. IEEE. (cit. on p. 6, 25).

Voglewede, P. and Ebert-Uphoff, I. (2005). Overarching framework for measuring closeness to singularities of parallel manipulators. *IEEE Transactions on Robotics*, 21:1037–1045. (cit. on p. 25).

Wang, J., Wu, C., and Liu, X. J. (2010). Performance evaluation of parallel manipulators: Motion/force transmissibility and its index. *Mechanism and Machine Theory*, 45:1462–1476. (cit. on p. 5, 8, 26, 28, 36).

Wen, H., Cong, M., Wang, G., Qin, W., Xu, W., and Zhang, Z. (2019). Dynamics and Optimized Torque Distribution Based Force/position Hybrid Control of a 4-DOF Redundantly Actuated Parallel Robot with Two Point-contact Constraints. *International Journal of Control, Automation and Systems*, 17:1293–1303. (cit. on p. 5, 27).

Wenger, P. and Chablat, D. (1998). Workspace and Assembly Modes in Fully-Parallel Manipulators: A Descriptive Study. In *Advances in Robot Kinematics: Analysis and Control*, pages 117–126. Springer Netherlands. (cit. on p. 18).

WHO (2022). Disability. `https://www.who.int/news-room/fact-sheets/detail/disability-and-health`. Accessed 2022-12-09. (cit. on p. 1).

Wu, C., Liu, X.-J., and Wang, J. (2009a). Force Transmission Analysis of Spherical 5R Parallel Manipulators. In *2009 ASME/IFToMM International Conference on Reconfigurable Mechanisms and Robots*, pages 331–336. IEEE. (cit. on p. 28).

Wu, C., Liu, X.-J., Xie, F., and Wang, J. (2011). New measure for 'Closeness' to singularities of parallel robots. In *2011 IEEE International Conference on Robotics and Automation*, pages 5135–5140. IEEE. (cit. on p. 22, 26).

Wu, J., Chen, X., Li, T., and Wang, L. (2013). Optimal design of a 2-DOF parallel manipulator with actuation redundancy considering kinematics and natural frequency. *Robotics and Computer-Integrated Manufacturing*, 29:80–85. (cit. on p. 5, 28).

Wu, J., Gao, J., Song, R., Li, R., Li, Y., and Jiang, L. (2016). The design and control of a 3dof lower limb rehabilitation robot. *Mechatronics*, 33:13–22. (cit. on p. 3).

Wu, J., Wang, J., Wang, L., and Li, T. (2009b). Dynamics and control of a planar 3-DOF parallel manipulator with actuation redundancy. *Mechanism and Machine Theory*, 44:835–849. (cit. on p. 27).

Wu, Q., Wang, X., Chen, B., and Wu, H. (2018). Development of an RBFN-based neural-fuzzy adaptive control strategy for an upper limb rehabilitation exoskeleton. *Mechatronics*, 53:85–94. (cit. on p. 4, 94).

Xie, F. and Liu, X.-J. (2016). Analysis of the kinematic characteristics of a high-speed parallel robot with Schönflies motion: Mobility, kinematics, and singularity. *Frontiers of Mechanical Engineering*, 11:135–143. (cit. on p. 8, 24).

Xie, F., Liu, X.-J., Wang, J., and Wabner, M. (2017). Kinematic Optimization of a Five Degrees-of-Freedom Spatial Parallel Mechanism With Large Orientational Workspace. *Journal of Mechanisms and Robotics*, 9. (cit. on p. 29).

Xie, S. (2016). *Advanced Robotics for Medical Rehabilitation*, volume 108. Springer International Publishing, 1 edition. (cit. on p. 2).

Yano, H., Tamefusa, S., Tanaka, N., Saitou, H., and Iwata, H. (2010). Gait rehabilitation system for stair climbing and descending. In *2010 IEEE Haptics Symposium*, pages 393–400. IEEE. (cit. on p. 3).

Yoshikawa, T. (1985). Manipulability of Robotic Mechanisms. *The International Journal of Robotics Research*, 4:3–9. (cit. on p. 25).

Zhang, X., Yue, Z., and Wang, J. (2017). Robotics in Lower-Limb Rehabilitation after Stroke. *Behavioural Neurology*, 2017:1–13. (cit. on p. 96).

Zhao, R. and Ratchev, S. (2017). On-line trajectory planning with time-variant motion constraints for industrial robot manipulators. In *2017 IEEE International Conference on Robotics and Automation (ICRA)*, pages 3748–3753. Institute of Electrical and Electronics Engineers. (cit. on p. 29).

Zlatanov, D., Bonev, I., and Gosselin, C. (2002). Constraint singularities of parallel mechanisms. In *Proceedings 2002 IEEE International Conference on Robotics and Automation (Cat. No.02CH37292)*, volume 1, pages 496–502. IEEE. (cit. on p. 21).